NATIONAL COOPERATIVE HIGHWAY RESEARCH PROGRAM REPORT 15

IDENTIFICATION OF CONCRETE AGGREGATES EXHIBITING FROST SUSCEPTIBILITY

INTERIM REPORT

HIGHWAY RESEARCH BOARD NATIONAL ACADEMY OF SCIENCES - NATIONAL RESEARCH COUNCIL

NATIONAL COOPERATIVE HIGHWAY RESEARCH PROGRAM REPORT **15**

IDENTIFICATION OF CONCRETE AGGREGATES EXHIBITING FROST SUSCEPTIBILITY

INTERIM REPORT

BY T. D. LARSON, A. BOETTCHER, P. CADY, M. FRANZEN, AND J. REED
THE PENNSYLVANIA STATE UNIVERSITY
UNIVERSITY PARK, PENNSYLVANIA

RESEARCH SPONSORED BY THE AMERICAN ASSOCIATION
OF STATE HIGHWAY OFFICIALS IN COOPERATION
WITH THE BUREAU OF PUBLIC ROADS

SUBJECT CLASSIFICATION:
MINERAL AGGREGATES

HIGHWAY RESEARCH BOARD OF THE DIVISION OF ENGINEERING AND INDUSTRIAL RESEARCH
NATIONAL ACADEMY OF SCIENCES - NATIONAL RESEARCH COUNCIL 1965

NATIONAL COOPERATIVE HIGHWAY RESEARCH PROGRAM

Systematic, well-designed research provides the most effective approach to the solution of many problems facing highway administrators and engineers. Often, highway problems are of local interest and can best be studied by highway departments individually or in cooperation with their state universities and others. However, the accelerating growth of highway transportation develops increasingly complex problems of wide interest to highway authorities. These problems are best studied through a coordinated program of cooperative research.

In recognition of these needs, the highway administrators of the American Association of State Highway Officials initiated in 1962 an objective national highway research program employing modern scientific techniques. This program is supported on a continuing basis by funds from participating member states of the Association and it receives the full cooperation and support of the Bureau of Public Roads, United States Department of Commerce.

The Highway Research Board of the National Academy of Sciences-National Research Council was requested by the Association to administer the research program because of the Board's recognized objectivity and understanding of modern research practices. The Board is uniquely suited for this purpose as: it maintains an extensive committee structure from which authorities on any highway transportation subject may be drawn; it possesses avenues of communications and cooperation with federal, state, and local governmental agencies, universities, and industry; its relationship to its parent organization, the National Academy of Sciences, a private, nonprofit institution, is an insurance of objectivity; it maintains a full-time research correlation staff of specialists in highway transportation matters to bring the findings of research directly to those who are in a position to use them.

The program is developed on the basis of research needs identified by chief administrators of the highway departments and by committees of AASHO. Each year, specific areas of research needs to be included in the program are proposed to the Academy and the Board by the American Association of State Highway Officials. Research projects to fulfill these needs are defined by the Board, and qualified research agencies are selected from those that have submitted proposals. Administration and surveillance of research contracts are responsibilities of the Academy and its Highway Research Board.

The needs for highway research are many, and the National Cooperative Highway Research Program can make significant contributions to the solution of highway transportation problems of mutual concern to many responsible groups. The program, however, is intended to complement rather than to substitute for or duplicate other highway research programs.

This report is one of a series of reports issued from a continuing research program conducted under a three-way agreement entered into in June 1962 by and among the National Academy of Sciences-National Research Council, the American Association of State Highway Officials, and the U. S. Bureau of Public Roads. Individual fiscal agreements are executed annually by the Academy-Research Council, the Bureau of Public Roads, and participating state highway departments, members of the American Association of State Highway

NCHRP Project 4-3(2) FY '63
NAS-NRC Publication 1214
Library of Congress Catalog Card Number: 65-60085

FOREWORD

By Staff

Highway Research Board

This report will be of particular interest to highway and materials engineers as the research has been directed toward providing a means for solving a long-standing problem related to aggregate quality. Of the many factors affecting the durability of concrete exposed to alternate cycles of freezing and thawing, an important one is the ability of the coarse aggregate to sustain the forces tending to cause deterioration. The aggregate is known to experience volume change during freezing-and-thawing cycles, and this is considered a mechanical factor of major importance in regard to deterioration. The capability to determine aggregate resistance to this effect is, however, severely hampered by lack of a suitable test which not only will identify deleterious particles in a range of environments but which also embodies the attributes of reliability, rapidity, and economy. Establishment of such a test would provide for the beneficiation of aggregate by alleviating the detrimental effects through removal or treatment of those particles distinguished as being harmful. The several test methods investigated in the approach to this problem are described, the merits and demerits of the most promising are highlighted, and their potential on either an individual or a combined basis is stated. This knowledge provides the basis on which further research can be conducted in attempting to develop the best method, or methods, for positively identifying aggregate particles which undergo excessive volume change when frozen in concrete.

High-quality pavements require high-quality materials if optimum economic life is to be realized. A serious problem facing highway engineers in connection with the use of exposed concrete is that of providing sound materials conductive to durability under extremes of environment. There are many factors influential in this respect; however, the primary focus is on the quality of coarse aggregate. It is the predominant constituent of concrete, and its reaction to environmental effects largely determines the degree of durability that can be achieved. Experience has demonstrated the variation in mineralogical character with the wide geographic distribution of sources of supply and the associated variation in susceptibility to the various processes of deterioration. Theories have been established to explain the phenomena which have been observed in studies of concrete subjected to alternate cycles of freezing and thawing, and test methods have been devised for experimental means to identify aggregate particles which undergo excessive volume change.

However, none of these studies has been extended to the point of establishing a test method, or methods, by which the quality of aggregate particles can be determined on a positive, reliable, rapid, and economical basis. This need has always been urgent, but is particularly so today because of the rapid depletion of sources of supply from which aggregates of "known" performance have been obtained. It is purely conjectural as to how truly representative of aggregate quality this "known" performance is because of the inadequacy of currently specified experimental measures to provide data which could be correlated with field per-

formance. Consequently, such adverse effects as cracking, spalling, and pop-outs have undoubtedly occurred in instances where requirements of existing soundness tests have ostensibly been met. The research reported here, together with a parallel study conducted by the Virginia Polytechnic Institute under the same project title, "Development of Methods to Identify Aggregate Particles Which Undergo Destructive Volume Changes When Frozen in Concrete," is viewed as an effort from which improved quality tests for aggregates may be realized.

Initial work on this project by the Pennsylvania State University consisted of a critical literature review and preparation of an annotated bibliography of the significant material. This information was previously published by the Highway Research Board as *Special Report 80*. Experimental work consisted of investigating four test methods for identifying aggregates susceptible to damage from cycles of freezing and thawing. These were (a) the Powers slow freeze-thaw of concrete specimens, (b) aggregate pore system studies, (c) aggregate particle expansion studies, and (d) petrographic examination. Aggregates of known frost resistance and varying mineralogical type were obtained; separated into nearly homogeneous groups according to their size, specific gravity and petrography; and test fractions were submitted to physical analyses.

In general, it is reported that no one method satisfies the express objectives; however, the results are felt to be encouraging. Although the Powers test is time consuming, it demonstrated that the deleterious particles of aggregate masses could be evaluated by the test procedure but not identified. This test will also manifest the variations in mixture, curing, and environment. Meaningful data can be obtained from studies of the pore systems of aggregates. On the other hand, the particle expansion test, which is rapid and simple, does not yield other than qualitative data. Although petrographic analyses are somewhat detailed, the data obtained therefrom can be combined with already established relationships between mineralogical structures and frost behavior to reasonably predict frost susceptibility of untested aggregates. Data are also reported relative to time and cost factors involved in performing the promising tests.

This document constitutes an interim report on the first 18 months of study, and a request for continuation of the research has been approved. An appreciation has been gained for the many difficulties intrinsic to the problem of aggregate beneficiation. It is generally concluded that a single test procedure has not yet been indicated which combines the attributes of simplicity, rapidity, and the ability to classify deleterious particles on the basis of degree of exposure to environment. It is further concluded that each of the procedures investigated does, however, possess its own sphere of usefulness, and the merits and limitations have been indicated for utilizing the most promising tests, either individually or in combination. Recommendations have been made for additional laboratory evaluation of a wider range of aggregate types and the correlation of the resulting data with field performance.

CONTENTS

FIGURES

TABLES

ACKNOWLEDGMENTS

The assistance and cooperation of many persons and agencies are acknowledged. Test and control aggregates and cement were cheerfully furnished to the project by the producers or manufacturers. Inquiries to various highway departments, universities, and private and public research groups yielded much helpful information.

T. D. Larson, as Associate Professor of Civil Engineering at The Pennsylvania State University, was the project director for the work reported herein. The others involved in the research were, respectively, A. Boettcher, Graduate Assistant in Geology; P. Cady, Research Assistant; M. Franzen, Graduate Assistant in Civil Engineering; and J. Reed, Assistant Professor of Civil Engineering, all at The Pennsylvania State University.

The university's Civil Engineering Department and the office of the Assistant Dean for Research provided facilities and support conducive to the effective prosecution of the work.

IDENTIFICATION OF CONCRETE AGGREGATES EXHIBITING FROST SUSCEPTIBILITY

INTERIM REPORT

SUMMARY

A search was made for a test or tests that would rapidly and reliably identify aggregate particles subject to destructive volume change when frozen in concrete. The test methods investigated included evaluation of pore characteristics, aggregate particle expansion, petrographic examination, and the Powers freeze-thaw test.

The pore studies examined the porosity, permeability, and capillarity of a variety of aggregates and a hardened mortar. In the permeability experiments air was used as the permeating fluid. A special device was designed for this purpose. Although each of the test aggregates showed a wide range of permeability, a highly significant correlation was found between the ratio of porosity to average permeability coefficient and the rapid freeze-thaw durability factor. Capillarity data were inconclusive. Moisture movement via the pores in concrete could not be effectively traced with dyes, but radioactive tracing methods gave promising results.

Expansion of individual aggregate particles during freezing correlated significantly with rapid freeze-thaw durability factors and with dilation of concrete specimens containing the aggregates.

Petrographic analyses explained and predicted the behavior of the test aggregates in freeze-thaw testing. Petrography alone, however, cannot isolate all possible effects of the several potentially deleterious features in most aggregates.

The method proposed by Powers for predicting the frost resistance of concrete was found to explain the observed phenomena related to frost action in concrete. Results obtained with the Powers test are highly dependent on the sensitivity and dependability of the instrumentation. Dilation of specimens during cooling cycles is the most sensitive indicator of frost damage, and the logical end of the test is the point at which dilations become exponential with respect to number of cooling cycles completed.

Air-void spacing factors must be kept below 0.004 in. when effects of the coarse aggregate are studied. Ratios of 1:6 and 1:8 between coarse aggregate size and specimen length had no effect on test results. The same was true for water/cement ratios between 0.50 and 0.57. Specimens dried during the curing period showed a pronounced increase in frost resistance. Rate of saturation of air voids during progressive freezing cycles is related to the deterioration function of concrete and varies with the type of coarse aggregate. Microcracking in the paste phase increases exponentially with advancing freezing cycles and varies directly with the amount of dilation.

A single procedure that possesses all of the desired attributes of speed, simplicity, and ability to discriminate by degree was not discovered. The research described herein, however, clearly established the merits and limitations of the most promising tests. The optimum method or methods to use under specified conditions can now be selected on the basis of these determinations.

CHAPTER ONE

INTRODUCTION

The objective of this research was to develop a quick method of test to distinguish deleterious particles in aggregate and to predict their behavior under various degrees of exposure in concrete subjected to freezing and thawing.

The need for ample supplies of sound mineral aggregate is apparent, inasmuch as aggregate comprises about 70 percent by volume of all concrete, the most widely used construction material. Consumption of concrete in the United States is now approximately 250 million cubic yards per year, and in the world about 1½ billion cubic yards.

Concrete is most often manufactured from materials available at or near each construction site. It is, in fact, the global availability of its constituents that has led to the present widespread use of this material. With convenience, however, comes the hazard of utilizing unsound materials, and so producing unsound concrete. An unfortunately large amount of concrete produced in this day of advanced technology deteriorates long before the intended span of its useful life has been attained, and unsound aggregate is a major cause of its disintegration.

Beneficiation of aggregates to acceptable quality levels can often be accomplished by removing deleterious particles, but the first premise to this solution is that harmful particles can be recognized. Much of the research effort here reported was devoted to experiments in which single aggregate particles were tested to determine their basic pore characteristics and length stability, and were submitted to petrographic examination. Rock types from many sources were studied in an attempt to find readily identifiable characteristics or groups of characteristics that would define their probable performance.

In view of the need for a more realistic test environment for suspect particles, aggregates similar to those used in the individual-particle experiments were also studied for their performance in concrete.

The aims of this project, as defined by the problem statement and the research plan, have been met as follows:

1. *Prepare a review of the literature.* An intermediate report, "A Critical Review of Literature Treating Methods of Identifying Aggregates Subject to Destructive Volume Change When Frozen in Concrete, and a Proposed Program of Research," has been published as HRB Special Report 80 (1964).

2. *Collect and classify representative aggregate types.* Appendix B describes how the samples collected were processed; Appendix C gives a complete petrographic description of each aggregate studied.

3. *Make length-change measurements on individual aggregate particles.* Chapter Four treats linear expansion of single aggregate particles. The equipment developed for this purpose is described, and the technique employed is evaluated.

4. *Use the Powers method to examine small quantities of aggregates from particular sources.* Chapter Six deals with the Powers method for determining volume stability characteristics of aggregates. Facets of the problem studied included: test cycle, instrumentation, aggregate conditioning, concrete conditioning, deterioration measures, repeatability, and time and cost. The test method is evaluated, with recommendations and suggestions for its implementation.

5. *Study the alcohol test developed and reported by Brink (12).* By letter dated July 22, 1963, the NCHRP Program Engineer authorized investigation of test methods based on pore characteristics in lieu of the freezing-in-alcohol procedure. Chapters Two and Three of this report present permeability, porosity, capillarity, and water-tracer investigations of all the major aggregate types studied. An index of performance is developed, and recommendations are made concerning this approach to evaluating concrete aggregates.

6. *Use one or several methods outlined in existing specifications to test aggregates cast in concrete specimens.* Appendix D contains test results from rapid freeze-thaw tests (ASTM C-290) made on specimens incorporating the various test aggregates.

7. The general accomplishments of this effort "to develop a quick method to distinguish deleterious particles in aggregate" are summarized in Chapter Seven.

The ability to predict the performance of concrete in various environments can be achieved only by relating theoretical studies and tests performed on component materials, or the composite, to the field performance of concrete structures. Devising tests to facilitate general predictions regarding the field performance of concrete is difficult for the following reasons:

1. The many subtle variations in the component materials make unique resolution by general physical laws or empirical tests impossible.
2. Laboratory concretes are not precisely comparable to one another even under ideal conditions, and are much less likely to be comparable to any field concrete.
3. Variations in placing, curing, and finishing field or laboratory concrete are known to cause extreme variations in all properties.
4. Not all of the significant field environmental factors are known, and many of those long since identified have not been quantitatively evaluated.

An appreciation of these inherent difficulties is essential to any worker in the field of concrete durability, as it has been in this investigation of methods to identify aggregate particles which undergo destructive volume changes when frozen in concrete.

CHAPTER TWO

AGGREGATE PORE SYSTEMS

INTRODUCTION

The effect of pore system characteristics of the paste and aggregate phases on the freeze-thaw durability of concrete has been well established. A pore system that will make the paste phase virtually immune to frost action can be created by the proper proportioning of concrete. This chapter deals primarily with studies of pore system characteristics of various mineral aggregate types, but the pore characteristics of hardened mortar are also examined because interaction between aggregate and mortar is fundamental to the frost deterioration process.

The characteristic porosity, permeability, and capillarity were determined for a number of different aggregates and for one "standard" hardened mortar. The objective was to find that single pore characteristic, or some index based on several characteristics, which would permit the identification of aggregate particles subject to destructive volume changes under freezing conditions.

Background

Some data are available on the porosity and permeability of hardened paste at various ages and with various water/cement ratios (*56, 65;* see Bibliography, Appendix A). The porosity and permeability of many rock types have also been studied, but different investigators have employed different procedures and the results are generally not comparable (*55, 67, 21, 22*). Blanks (*9*) developed an apparatus to measure capillary forces in porous media. Few data have been obtained to substantiate that approach, even though the greatest amount of moisture movement in hardened mortar and in aggregate particles is by capillary attraction. None of these efforts has resulted in the long-sought correlation between easily measured pore characteristics and freeze-thaw durability.

Theory

Two theories have been set forth by Powers (*54*) and Powers and Helmuth (*60*) to explain the disruption of neat hardened paste by freeze-thaw cycles. The first relates to hydraulic pressure generated by water escaping from a frozen zone to a nonfrozen zone. The water migrates if the degree of saturation is sufficiently high to prevent the paste from accommodating approximately 9 percent increase in volume of freezing water. The second theory concerns the growth of ice lenses in the larger capillary voids by capillary attraction of available water. Presumably the gel pores are too small to permit ice formation (*60*).

The concepts of hydraulic pressure and ice growth in capillary pores of neat hardened paste are also applicable to mortar and aggregates. Verbeck and Landgren (*77*) argued that in the freezing of unconfined aggregates the magnitude of the hydraulic pressure is dependent on the rate of freezing and the porosity, permeability, and size of the aggregates. They also argued that in the freezing of aggregates confined by mortar the magnitude of the hydraulic pressure is dependent on the freezing rate, aggregate porosity and "critical size," and the permeability and air content of the surrounding mortar. The aggregate "critical size" is that size above which the tensile strength of the aggregate is exceeded by the hydraulic pressure generated as water escapes ahead of an advancing ice front, and is therefore a function of aggregate permeability and tensile strength, and the rate of advance of the ice front.

There are, then, several possible sources of disruptive hydraulic pressure: (a) from freezing water located in the mortar, (b) from freezing water located in the aggregates, (c) from water being expelled from the mortar into the aggregates, and (d) from water being expelled from the aggregates into the mortar. Because disruption of concrete in all of these cases involves movement of water, there is an inescapable relationship between the pore characteristics of the hardened mortar and the aggregate particles, inasmuch as they determine moisture movement.

AGGREGATE POROSITY

Method

Each of the test aggregates was separated into four size groups, two specific gravity groups, and the basic mineralogical types present. Porosity values were then obtained for selected aggregate fractions, in accordance with AASHO Specification T85-60 (ASTM C129-59). A complete description of the methods used in processing the aggregates and a sample calculation are given in Appendix B.

Results and Discussion

Examination of the aggregate porosity (voids ratio) determination results (Table 1) and the complete aggregate porosity data (Table E-1) reveals that the aggregate fractions with a specific gravity less than 2.50 had higher porosity values than the fractions with a specific gravity greater than 2.50. This is as expected, for the heavier aggregates of any type should have less void space.

The deterioration of aggregates by freeze-thaw action requires the presence of water, and porosity serves as a measure of the amount of water than can exist in any particle. Aggregates with very good freeze-thaw resistance, such as the Benner and Snyder limestone and the White Marsh gravel, have very low porosity. Inasmuch as other

TABLE 1

SUMMARY OF AGGREGATE POROSITY VALUES [a]

AGGREGATE [b]	POROSITY [c] SP GR [d] <2.50	POROSITY [c] SP GR [d] >2.50
Gilmore City limestone	0.1512	0.1127
Maynes Creek and Eagle City limestone	0.1896	0.0912
Paducah gravel	0.2243	0.0608
White Marsh gravel	—	0.0205
Benner and Snyder limestone	—	0.0101
Meramec gravel	0.1902	0.0682
Rapid and Coralville limestone	—	0.1634

[a] Averages of three samples.
[b] See Appendix C for petrographic descriptions.
[c] Voids ratio.
[d] Vacuum saturated apparent specific gravity.

TABLE 2

SUMMARY OF MORTAR POROSITY RESULTS

SPECIMEN	VOIDS RATIO AFTER SOAKING 14 DAYS	VOIDS RATIO AFTER SOAKING 76 DAYS
1	0.4044	0.4292
2	0.4393	0.4674
3	0.3872	0.4100
Avg.	0.4103	0.4356

pore characteristics affect the magnitude of the generated hydraulic pressure, a generally good correlation between porosity and freeze-thaw resistance was not found here and has not been found by previous investigators (*68, 91*).

MORTAR POROSITY

Procedure

The mortar used in this investigation was similar to that used to develop the freeze-thaw data for different aggregates (see Chapter Six). This was done so that data collected here could be used later in an attempt to formulate an index to predict the freeze-thaw resistance of those aggregates.

The mortar was removed from the mix by sieving over a No. 4 sieve. It was then molded into three cylinders 3 in. in diameter and 6 in. long. These were cured in the same manner as the Phase I specimens utilized in gathering freeze-thaw data.

The procedure for measuring the mortar porosity was based on theoretical considerations given by Copeland and Hayes (*19*) and practical considerations given by Axon (*7*). The voids ratio of a material is the ratio of the void volume to the solid volume; that is,

$$P_t / (V_p - P_t) \qquad (1)$$

in which P_t is the total pore volume of the hardened paste and V_p is the bulk volume of the paste. According to Copeland and Hayes, the total pore volume of a hardened paste may be calculated from

$$P_t = 0.99 W_e \qquad (2)$$

in which W_e is the weight of the evaporable water in the hardened paste and 0.99 is the specific volume of chemically free water, considered a constant. By combining Eqs. 1 and 2, the voids ratio is

$$0.99 W_e / (V_p - 0.99 W_e) \qquad (3)$$

According to Axon, the weight of the evaporable water is found by determining the amount of water a specimen absorbs under vacuum saturation plus soaking, after ovendrying to constant weight.

Cores to be used later for permeability tests were cut from the cylinders at the completion of the curing period. The remnants of the specimens were then utilized for porosity determinations. They were brought to constant weight by ovendrying at 150 F, weighed, allowed to cool to room temperature in a desiccator, and vacuum saturated according to the procedure described in Appendix B. The soaking period following vacuum saturation was extended to 14 days, as recommended by Axon. Finally, the specimens were weighed in air and in water in a vacuum-saturated condition. The weights of evaporable water and the volumes of the specimens determined by this procedure permitted the calculation of voids ratios, using Eq. 3.

Results and Discussion

The mortar porosity results (Table 2), are for a mortar with 0.55 water/cement ratio and approximately 5 percent entrained air. The values based on 14 days of soaking appeared low compared with the 4.08 percent average porosity reported by Powers et al. (*58*) for hardened paste with 0.50 water/cement ratio. After the porosity specimens had been soaked 76 days, the results appeared to be more realistic, because the porosity determined on this basis was higher than that reported for pastes. The higher water/cement ratio, the use of entrained air, and the inclusion of fine aggregate should increase mortar porosity. Complete results are given in Table E-2.

None of the aggregates studied had a porosity greater than that of the hardened mortar. On the basis of porosity data alone, however, no inference can be made about the movement of water from the aggregate to the mortar or in the reverse direction, nor is it possible to predict the soaking time necessary to produce saturation in the mortar or aggregate of a concrete. Permeability and pore size distribution are likely to exert an overshadowing influence.

AGGREGATE PERMEABILITY

Background

Dolch (*21*), in 1959, used air and a decay phenomenon to measure the permeability of four Indiana limestones. Because the vacuum apparatus he used was restricted to

a maximum pressure differential of 1 atm across the specimen, a single measurement could require an extended period of time for the more impermeable specimens. Other investigators have employed water as the measuring fluid, but water has the undesirable feature of reacting with many materials through which it passes, altering their characteristics.

Dry air has been used for some years in the petroleum and ceramic fields to measure the permeabilities of porous materials. It is superior to any other measuring fluid because it does not react with the material through which it passes (*48*). In this investigation permeability coefficients were obtained by using dry air as the permeating fluid.

Theory

The concepts applied in the aggregate permeability study are embodied in Darcy's law:

$$K_a = Q\,\mu\,L/(A\,\Delta P) \qquad (4a)$$

in which

K_a = permeability coefficient, in darcys;
Q = volume rate of flow, in ml per sec;
μ = viscosity of fluid, in centipoises;
L = length of porous medium, in cm;
A = area of porous medium, in sq cm; and
ΔP = pressure differential causing flow, in atm.

When a gas is used, the gas volume must be corrected to the volume corresponding to the average pressure during the period of flow. With P_1 and P_2 representing the upstream and downstream pressures, respectively (*3*),

$$Q_2\,P_2 = Q_m\,(P_1 + P_2)/2 \qquad (5)$$

in which Q_m is the volume rate of flow under average pressure and Q_2 is the volume rate measured at P_2. Utilizing this concept, Eq. 4*a* becomes

$$K_a = Q_m\,\mu\,L/(A\,\Delta P) \qquad (4b)$$

Combining Eqs. 4*b* and 5 permits the calculation of permeability coefficients corresponding to each of several upstream pressures.

Also, when a gas is used to measure the permeability, molecular slippage of the gas at the solid grain surfaces occurs according to an equation of the form (*39*):

$$K_a = K_0\,(1 + b/P_m) \qquad (6)$$

in which

K_a = permeability coefficient at some finite mean pressure;
K_0 = permeability coefficient corresponding to infinite mean pressure;
b = constant $= M/K_0$;
M = slope of K_a versus $1/P_m$;
P_m = mean pressure across specimen $= (P_1 + P_2)/2$.

This is the so-called Klinkenberg effect. The constant, K_0, which is the limiting value of K_a at infinite mean pressure, is found to be equal, within experimental error, to the permeability as measured with liquids (*39*).

To determine with gases a value of permeability completely equivalent to that which would be obtained with liquids, it is necessary to make measurements at several mean pressures. The permeability coefficients calculated by Eqs. 4*b* and 5 plotted against the reciprocal of the mean pressure give K_0 as the intercept on the vertical axis.

Equipment and Procedure

The apparatus used to measure permeability (Fig. 1) was similar in principle to that described by Muskat (*49*). Air was dried by passing it through a column containing anhydrous calcium sulfate. Because of the high pressure needed to produce measureable flows through some of the cores, a series of pressure gages was used to measure the upstream pressure. These gages were connected so that as the pressure exceeded the limit of one, the next higher gage could be actuated. A volumetric water-displacement apparatus measured the small quantities of air collected from the more impermeable specimens. Larger air flows were measured by a wet test meter having a minimum sensitivity of 2 ml per sec. Valve No. 1 (Fig. 1) instantly stopped the flow of air to permit a final reading on the scale at the tangent screw. Valve No. 2 adjusted the water level in the volumetric water-displacement apparatus at the beginning of each run. A thermocouple and recorder measured the temperature of the air passing through the system. The thermocouple was inserted in the tubing at the air outlet.

Specimens were disks ½ in. in diameter by 3/16 in. thick, sawed from cores of single aggregate particles and cemented into polyethylene mounting rings. Several stages of preparation are shown in Figure 2. The specimen holder is shown in Figure 3. The mounted disks were centered by placing them in a recess machined in one end of the holder. A raised ring was machined on the other end of the specimen holder to bear against the polyethylene sleeve, forming an airtight seal. Specimen preparation and operating procedures for this equipment are described in greater detail elsewhere (*27*).

Preliminary Studies

To gain some knowledge of the basic phenomena of permeability as measured with air, for both the laminar and turbulent flow regions, a sandstone specimen known to have rather high permeability was submitted to preliminary tests. Figures 4, 5, and 6 show the findings.

Darcy's basic equation (Eq. 4*a*) is valid only in the laminar flow region. Klinkenberg's equation (Eq. 6) extends the usefulness of Darcy's equation by permitting an extension into the turbulent flow region. Operation in the laminar flow region is verified by a linear relationship between the rate of flow and the differential pressure across the specimen (Fig. 4). A linear relationship between the rate of flow and the differential pressure will produce a constant value for the permeability coefficient in the laminar flow region (Fig. 5). Figures 4 and 5 reveal that the rate of flow is not a linear function of the differential

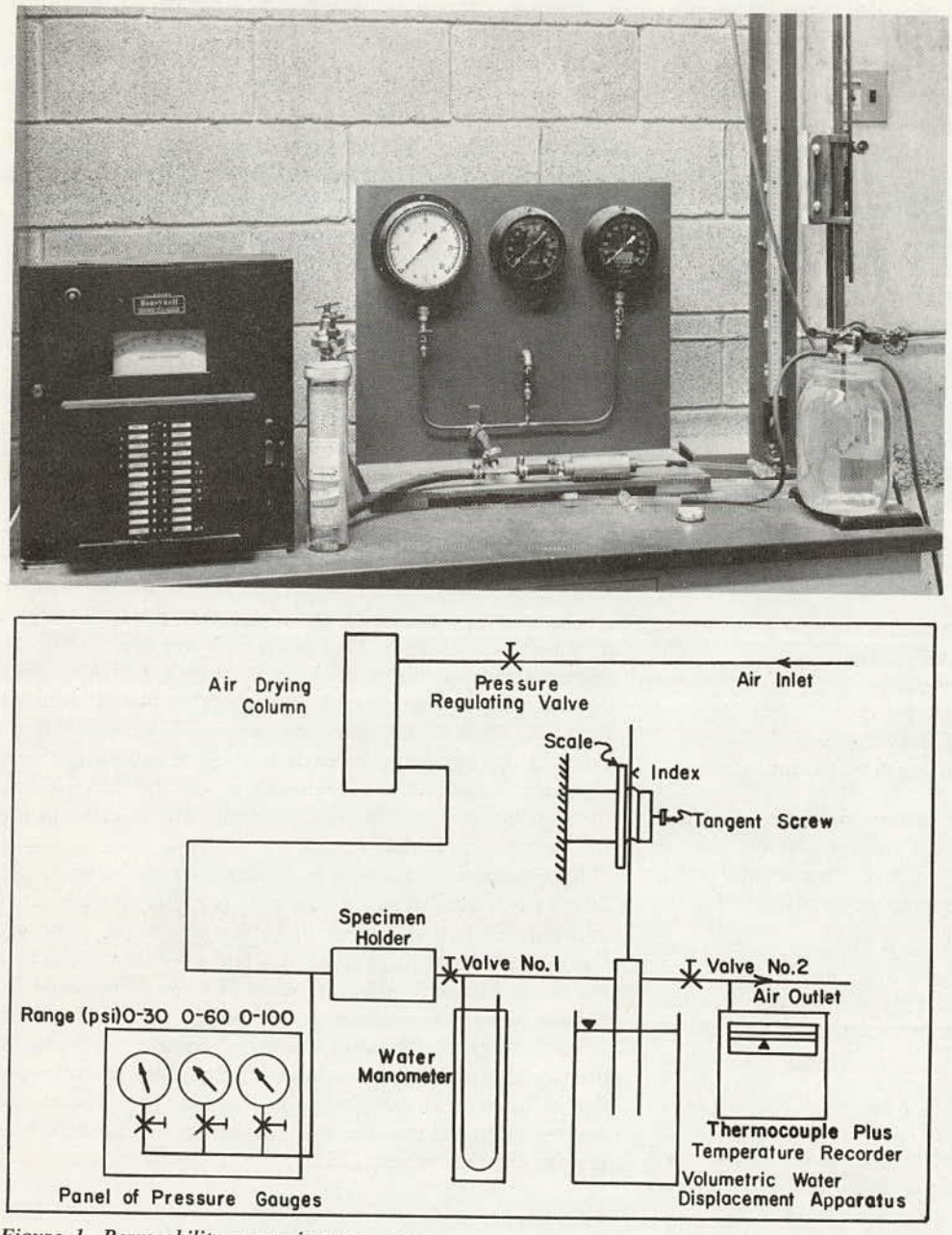

Figure 1. Permeability measuring apparatus.

pressure in the turbulent flow region. Consequently, as the differential pressure is increased, a decreasing permeability coefficient is obtained.

According to Klinkenberg (*39*), a linear relationship exists between the permeability coefficient and the reciprocal of the mean pressure in the turbulent flow region, as shown in Figure 6. The constancy of the permeability coefficient in the laminar flow region is again apparent here. For this specimen, the transition between the laminar and turbulent flow regions occurs from 0.55 to 0.6 of the reciprocal of the mean pressure. The extrapolated permeability coefficient is 1.92×10^{-2} darcys.

Results and Discussion

Permeability coefficients for the aggregates studied are summarized in Table 3. Detailed permeability results are given in Table E-3, and the individual aggregate particles tested are fully described by Franzen (*27*). The data were analyzed and the results plotted by programming them through an IBM 7074 electronic digital computer in the Computation Center at The Pennsylvania State University.

Table 3 indicates the wide range of permeability values that was characteristic of the aggregates; Figure 7 shows the overlap among their ranges. Figure 7 shows also that no differentiation between the two specific gravity fractions

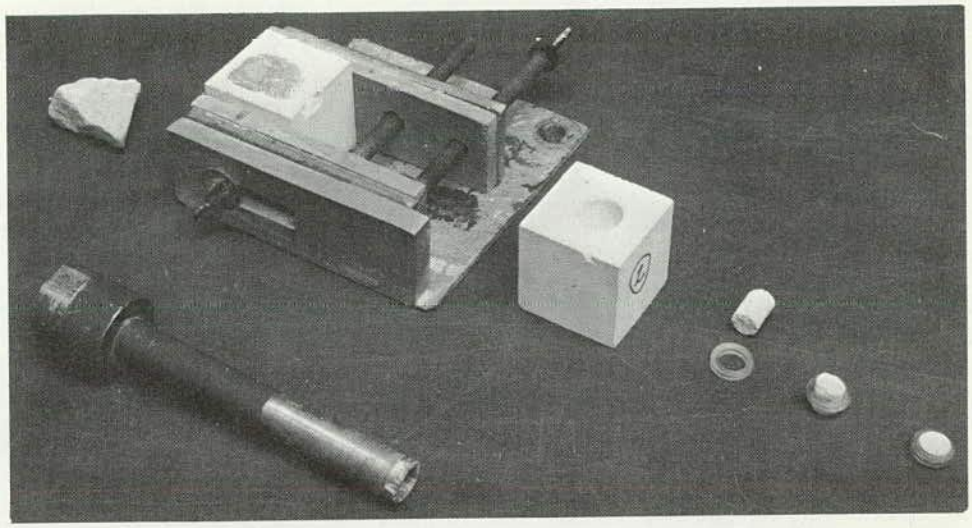

Figure 2. Preparation of specimens.

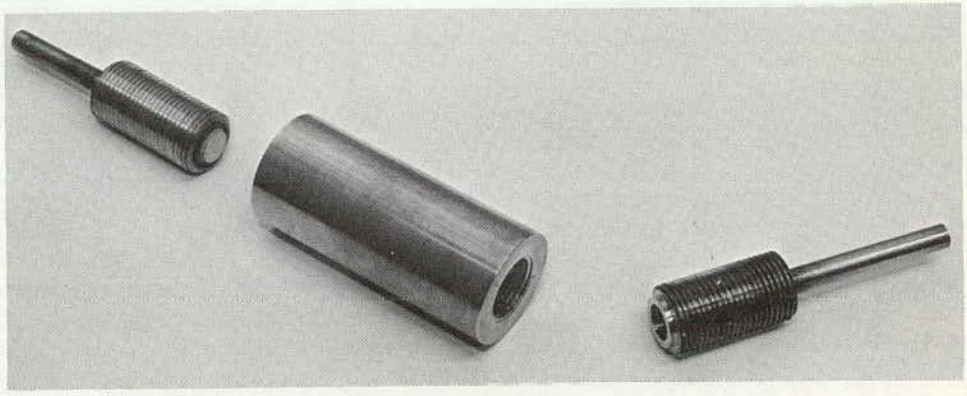

Figure 3. Specimen holder for permeability determinations.

TABLE 3

PERMEABILITY COEFFICIENTS

AGGREGATE	SPECIFIC GRAVITY	PERMEABILITY (DARCYS) RANGE	AVERAGE	NUMBER OF SPECIMENS AVERAGED
Gilmore City limestone	<2.50	1.908×10^{-4} to 2.926×10^{-3}	1.202×10^{-3}	6
	>2.50	3.105×10^{-5} to 1.941×10^{-3}	5.411×10^{-4}	6
Maynes Creek and Eagle City limestone	<2.50	3.065×10^{-5} to 2.881×10^{-3}	8.767×10^{-4}	6
	>2.50	7.952×10^{-6} to 3.507×10^{-3}	1.134×10^{-3}	5
Paducah gravel	<2.50	3.396×10^{-9} to 3.053×10^{-5}	7.581×10^{-6}	5
	>2.50	3.446×10^{-9} to 2.441×10^{-6}	1.222×10^{-6}	2
White Marsh gravel	>2.50	9.928×10^{-7} to 7.802×10^{-4}	2.786×10^{-4}	3
Benner and Snyder limestone	>2.50	Beyond limits of apparatus		
Meramec gravel	<2.50	4.829×10^{-7} to 5.443×10^{-4}	1.819×10^{-4}	3
	>2.50	1.191×10^{-7} to 8.751×10^{-5}	4.385×10^{-5}	2
Rapid and Coralville limestone	>2.50	9.138×10^{-7} to 1.416×10^{-4}	3.633×10^{-5}	6

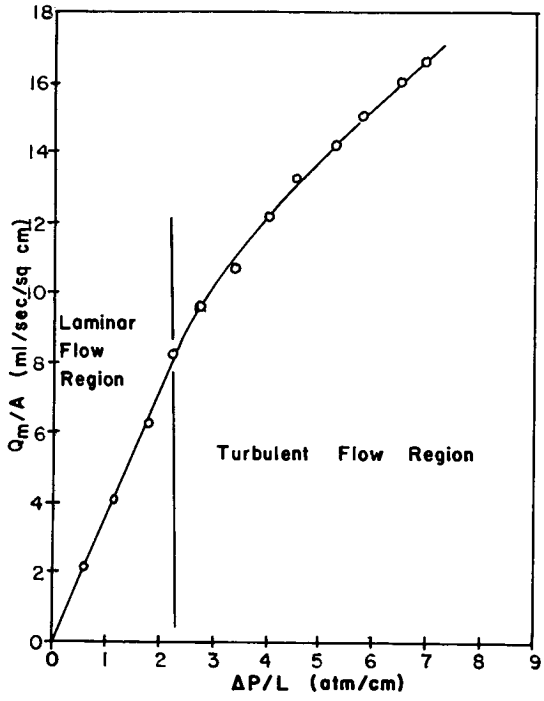

Figure 4. Mean flow rate vs differential pressure, sandstone specimen No. 1.

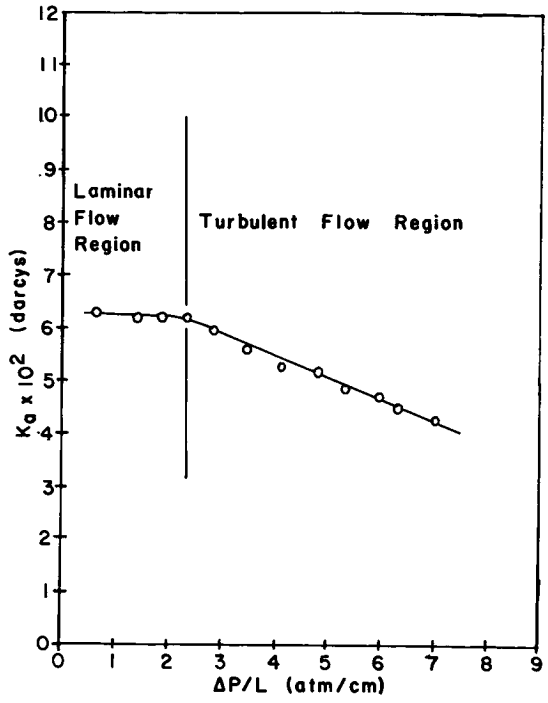

Figure 5. Permeability coefficient vs differential pressure, sandstone specimen No. 1.

of the various aggregate types can be made on the basis of permeability. The Gilmore City and the Maynes Creek and Eagle City limestones with less than 2.50 sp gr exhibit permeabilities within the ranges of the fractions having greater than 2.50 sp gr, and the reverse is true for the Meramec and Paducah gravels.

Specimen length has some effect on the permeability coefficients. Obviously, as the length is decreased the probability of bisecting continuous pores increases. McMahon (*47*), using oil-bearing sandstones, attempted to determine the effect of length of specimen on permeability. The heterogeneous nature of his specimens tended to mask true length effects, but he concluded that "statistical and sampling" errors are increased as the length of the specimen is decreased. Because of the difficulty of finding a homogeneous material, the effect of specimen

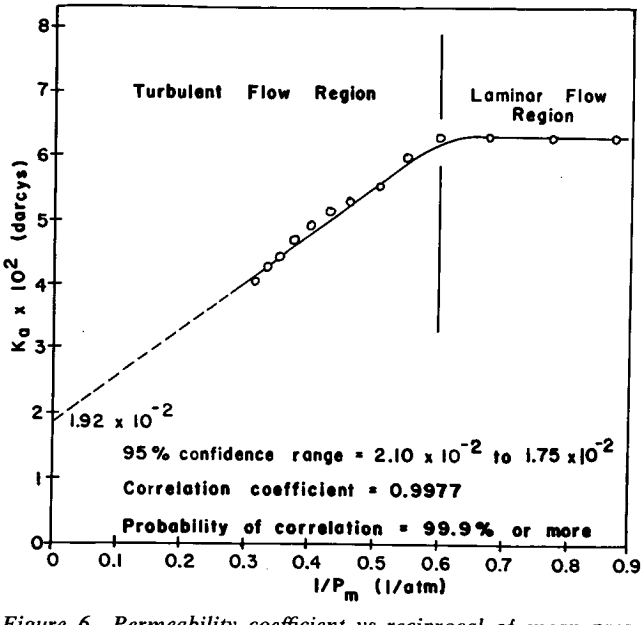

Figure 6. Permeability coefficient vs reciprocal of mean pressure, sandstone specimen No. 1.

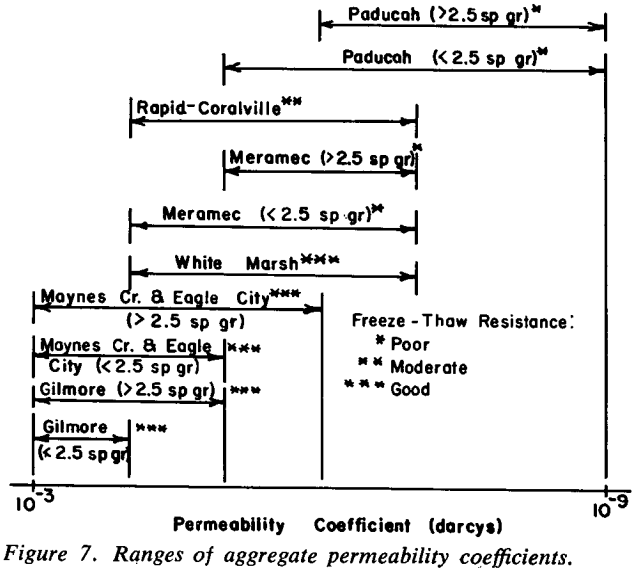

Figure 7. Ranges of aggregate permeability coefficients.

TABLE 4

EFFECTS OF BEDDING ON PERMEABILITY COEFFICIENTS, MAYNES CREEK AND EAGLE CITY LIMESTONE

SPECIMEN	ORIENTATION OF BEDDING	PERMEABILITY COEFFICIENT (DARCYS)	95 PERCENT CONFIDENCE RANGE (DARCYS)
1	Perpendicular to long axis of core	1.449×10^{-4}	1.569×10^{-4} to 1.330×10^{-4}
2		2.760×10^{-5}	2.938×10^{-5} to 2.582×10^{-5}
3	Parallel to long axis of core	9.262×10^{-4}	9.484×10^{-4} to 9.040×10^{-4}
4		2.653×10^{-4}	2.795×10^{-4} to 2.511×10^{-4}

length on the permeability coefficient was not evaluated in the present investigation.

Bedding planes in some of the aggregates could have accounted, in part, for the range of permeability values. Fancher, Lewis, and Barnes (*24*) found that both the permeability and the porosity of certain geological types varied from particle to particle, depending on the orientation of the bedding planes in relation to the long axis of the particle. In the work reported here, four permeability cores taken from a block of Maynes Creek and Eagle City limestone with visible bedding were studied in the light of this factor. Two of the cores were parallel and two were perpendicular to the bedding. As indicated in Table 4, the parallel specimens had higher permeability coefficients than the perpendicular. Although the importance of bedding was recognized, the small size of the aggregate particles from which permeability cores were taken at random for the general investigation prevented definite determination of its existence and orientation.

In calculating the permeability coefficients, isothermal conditions were assumed. Calhoun (*14*) investigated the effect of assuming adiabatic conditions and found this correction was insignificant. The difficulty of measuring the upstream and downstream temperatures with the necessary accuracy, and the overriding importance of other factors, precluded consideration of this correction.

Higher pressures reduced the distance that the least-squares line had to be extrapolated to infinite mean pressure, and therefore increased the reliability of the permeability coefficients. The results were also more reliable when the operating pressure range was very wide.

Reproducibility of the permeability measurements was good. Three repeat measurements on specimen No. 1 of the Maynes Creek and Eagle City limestone aggregate agreed within 2 to 6 percent. For the more impermeable specimens reproducibility tended to be less satisfactory, but two repeat measurements on Meramec gravel specimen No. 4 agreed within 6 percent.

Permeability measurements for two specimens from each of three pieces of Gilmore City limestone are given in Table 5. The coefficients for the specimens from core No. 3 were in good agreement, but the other two pairs show the heterogeneous nature of the aggregate particles. On this evidence, it cannot be expected that the permeability coefficients of aggregate particles of the same general geologic type will always be in good agreement.

Negative coefficients—a physical impossibility—were calculated for several extremely impermeable specimens. This may have been due to any one or a combination of the following factors: (a) The permeability apparatus was probably not sensitive enough for the small air volumes collected, with the consequence of large experimental error;

TABLE 5

PERMEABILITY COEFFICIENTS OF TWO SPECIMENS EACH FROM THREE PIECES OF GILMORE CITY LIMESTONE

SPECIMEN	SPECIFIC GRAVITY	LEAST-SQUARES PERMEABILITY (DARCYS)	95 PERCENT CONFIDENCE RANGE (DARCYS)
From core No. 3, spaced ½ in.			
3A	<2.50	2.888×10^{-3}	4.313×10^{-3} to 1.463×10^{-3}
3B	<2.50	2.926×10^{-3}	3.853×10^{-3} to 1.998×10^{-3}
From core No. 6, spaced ½ in.			
6A	<2.50	4.551×10^{-4}	4.740×10^{-4} to 4.363×10^{-4}
6B	<2.50	2.906×10^{-4}	3.169×10^{-4} to 2.643×10^{-4}
From cores drilled 1 in. c to c			
1A	>2.50	1.941×10^{-3}	2.049×10^{-3} to 1.833×10^{-3}
1B	>2.50	3.970×10^{-4}	4.071×10^{-4} to 3.869×10^{-4}

TABLE 6

COMPARATIVE PERMEABILITY VALUES

SPECIMEN	BEDDING	PERMEABILITY COEFFICIENT	
		WATER	AIR [a]
1A	Random	2.3×10^{-2}	1.7 to 2.1 $\times 10^{-2}$
1B	Random	1.4×10^{-2}	—
2A	Random	3.2×10^{-6}	8.9 to 9.7 $\times 10^{-5}$
2B	Random	5.1×10^{-6}	—
3A	Perpend.	2.7×10^{-5}	2.6 to 2.9 $\times 10^{-5}$
3B	Parallel	1.77×10^{-4}	2.5 to 2.8 $\times 10^{-4}$
5A	Perpend.	1.4×10^{-6}	1.2 to 3.1 $\times 10^{-6}$
5B	Parallel	4.1×10^{-7}	—

[a] 95 Percent confidence range.

(b) The pressure operating range may have been too narrow for these aggregates, producing the negative permeability coefficient when the least-squares line was extrapolated to infinite mean pressure; (c) The aggregates could have been reflecting some flow phenomenon that could not be identified in the narrow range of operating pressures. When negative permeability coefficients were obtained, repeat measurements were again negative in the majority of cases.

The magnitudes of the probable sources of error in using the volumetric water-displacement apparatus were estimated. Leakage in the inverted cylinders could produce an error of 3 percent. Errors in vernier reading could range from 0.2 percent for recording 60 ml of air to a maximum of 9 percent for 1 ml. Dissolution of air in water in the apparatus could cause an error of 4.5 percent when the flow was 1 ml during 10 min, or 0.08 percent for a flow of 60 ml in the same period. These probable sources of error may also have influenced the determinations of mortar permeability.

Water permeability measurements on four aggregate types having a range of permeability values were made with apparatus and methods similar to those used by Powers et al. (*PCA Bull.* 53). The results of these tests are compared with air permeability results in Table 6. The comparison is generally favorable, as only one water permeability coefficient is not within the 95 percent confidence range of the air permeability.

MORTAR PERMEABILITY

Method

The mortar permeability specimens were taken from the 3 x 6-in. cylinders described under "Mortar Porosity," and prepared in the same manner as the aggregate permeability specimens. Detailed descriptions of the specimens are given by Franzen (*27*).

Results

The mortar permeability coefficients are summarized in Table 7. The collected data were processed in the same manner as the data for the aggregate permeability study.

The cores were taken from the cylinders in such a way that the effect of location on permeability could be investigated. The permeability coefficients were higher at the top than at the bottom, those at the center being generally intermediate. The coefficients of specimens from cores taken at the center parallel to the long axis of the cylinders were generally higher than those from cores taken at the center perpendicular to the long axis. Powers et al. (*58*) found permeability to vary with depth in neat hardened paste specimens, and attributed this to the development of vertical channels during the bleeding period.

The mortar permeability coefficients were confined to a much narrower range than any determined for aggregate specimens in one geologic category.

The degree of mortar hydration is extremely important in relation to permeability. Powers et al. (*58*) found that the permeability of neat hardened paste specimens decreased approximately 700-fold from the age of five days to their ultimate values. Though ages are recorded for the specimens in Table 7, the exact effects of curing and pre-

TABLE 7

MORTAR PERMEABILITY COEFFICIENTS

SPECIMEN	PERMEABILITY COEFFICIENT (DARCYS)	95 PERCENT CONFIDENCE RANGE (DARCYS)	AGE AT TEST (DAYS)
1A	2.084×10^{-5}	2.278×10^{-5} to 1.889×10^{-5}	53
1B	1.509×10^{-5}	1.733×10^{-5} to 1.284×10^{-5}	49
1C	1.248×10^{-5}	1.410×10^{-5} to 1.086×10^{-5}	51
1D	1.340×10^{-5}	1.469×10^{-5} to 1.212×10^{-5}	51
2A	3.418×10^{-5}	3.573×10^{-5} to 3.263×10^{-5}	53
2B	1.958×10^{-5}	2.079×10^{-5} to 1.836×10^{-5}	56
2C	2.816×10^{-5}	3.200×10^{-5} to 2.431×10^{-5}	59
2D	2.606×10^{-5}	2.854×10^{-5} to 2.357×10^{-5}	60
3A	2.774×10^{-5}	2.986×10^{-5} to 2.563×10^{-5}	60
3B	2.967×10^{-5}	3.220×10^{-5} to 2.714×10^{-5}	62
3C	2.216×10^{-5}	2.511×10^{-5} to 1.992×10^{-5}	64
3D	2.833×10^{-5}	3.002×10^{-5} to 2.664×10^{-5}	64

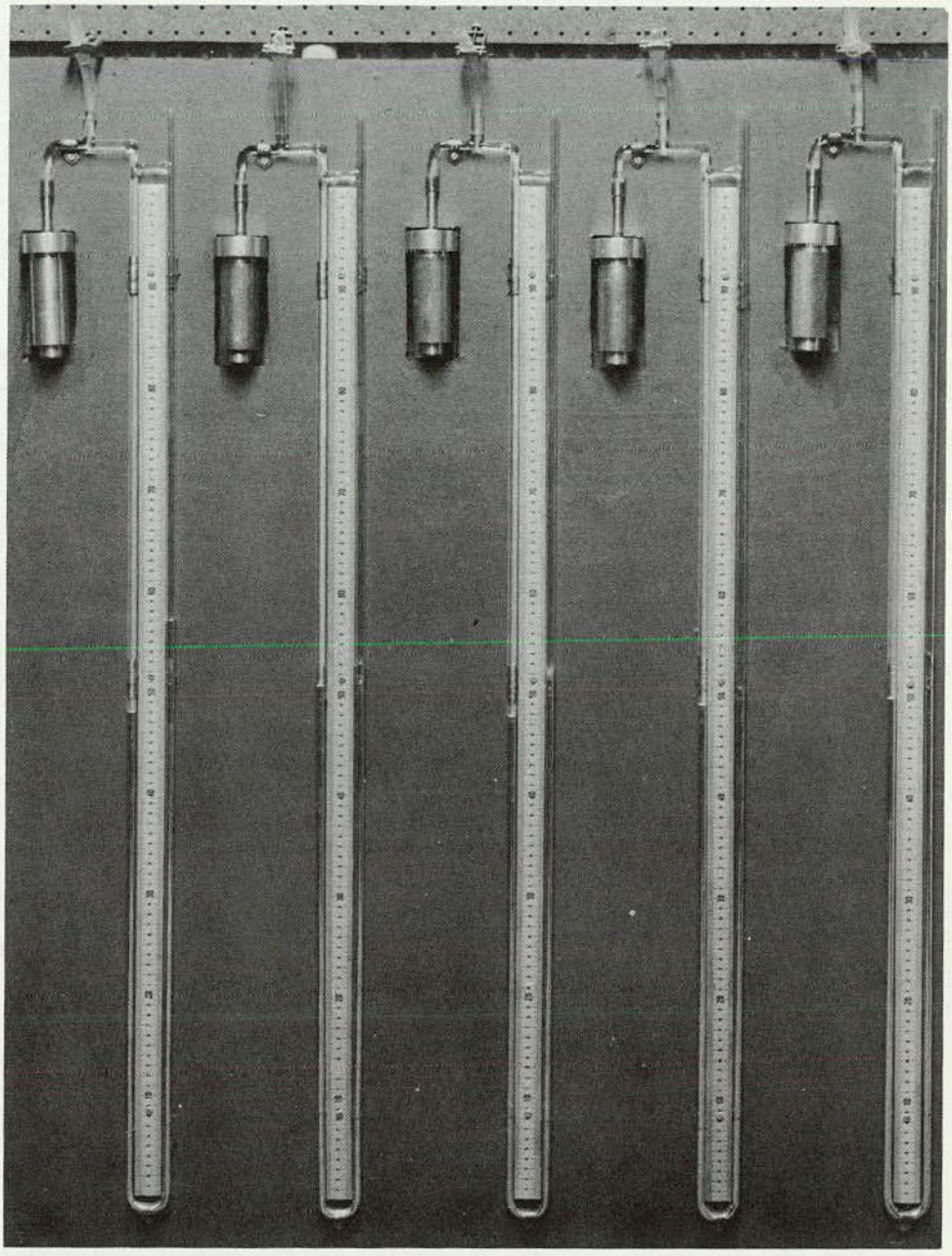

Figure 8. Capillarity test apparatus.

liminary treatment on the mortar permeability results were not ascertained in the tests conducted here.

AGGREGATE/MORTAR CAPILLARITY

Test Apparatus and Specimens

To test aggregate/mortar capillarity an apparatus was constructed that was identical in principle to one developed by Blanks (*9*). The specimen holder, a modified permeability-core holder, allowed the lower face of the specimen to be exposed to a controlled atmosphere and the upper face to a sealed water reservoir connected to a manometer. To minimize the chances of water leakage, all specimens were sealed in the holders with asphalt cement. A bank of capillary specimen holders and manometers was arranged to accommodate five specimens at a time (Fig. 8).

The same cores from which permeability coefficients were determined were used in this phase of the investigation. They were free of moisture, except for that absorbed from the atmosphere during storage.

Method

The rate of evaporation of water at the exposed face of a specimen was believed to be influenced by the relative

area of continuous capillaries exposed. Water that evaporated from the surface of the specimen was replaced with water from the reservoir by capillary attraction, producing a pressure decline in the reservoir. It was thought that the pressure declined either until it equaled the vapor pressure of water corresponding to the temperature at the exposed face, or until it equaled the capillary force. The range of vapor pressures corresponding to the operating temperature range of 76 F to 80 F is 22.9 cm Hg to 26.3 cm Hg (*29*). The maximum capillary force recorded was 14.4 cm Hg, suggesting that the pressure decline in the reservoir was controlled by the capillary force and not the vapor pressure.

The rate of evaporation of water at the exposed face of a specimen is mainly controlled by the relative humidity and temperature at the exposed face. To ensure a consistent environment for all tests, the relative humidity was maintained in the range from 44 to 46 percent and the temperature from 76 F to 80 F.

A pore diameter corresponding to the maximum capillary force measured for each specimen was computed, using (*8, 23*)

$$\tau = hDdg/(4\cos\theta) \qquad (7a)$$

in which

τ = surface tension, in dynes per cm;
h = height of capillary rise, in cm;
D = diameter of capillary pore, in cm;
g = acceleration of gravity, in cm per sec per sec;
d = density of liquid, in g per cc; and
θ = contact angle of liquid with walls of capillary pore, in deg.

Rearranged, Eq. 7*a* becomes

$$D = (4\tau\cos\theta)/h\,d\,g \qquad (7b)$$

To preclude any contamination of the permeability specimens, the capillarity tests were not started until the permeability tests were completed and the results analyzed. It was anticipated that the capillarity tests would take some time to complete, and it would not be possible to run all of the 73 specimens. On the basis of the permeability results, two specimens were selected from each of the 11 geologic categories and three specimens from the one mortar category.

Test Results

The results of these tests are given in Table 8. Because the time required for different specimens varied from 24 to more than 1,200 hr, the time factor appears to make this test impractical for some geologic types. Moreover, repeat measurements on several specimens produced results that differed by 25 to 400 percent, indicating poor reproducibility.

The ranges of pore diameters exposed at the surface of the capillarity specimens were also determined microscopically at 100 × magnification. In 14 of 25 cases, the calculated diameters fell within the range of the microscopic determinations.

TABLE 8

CALCULATED PORE DIAMETERS OF SELECTED SPECIMENS

AGGREGATE	SP. GR.	SPECIMEN	CALC. DIAM. (μ)
Gilmore City limestone	<2.50	2	16
		6A	155
	>2.50	1B	66
		5	29
Maynes Creek and Eagle City limestone	<2.50	3	155
		4	272
	>2.50	1	15
		3	99
Paducah river gravel	<2.50	1	310
		5	121
	>2.50	5	181
		6	362
White Marsh gravel	>2.50	2	46
		4	272
Benner and Snyder limestone	>2.50	2B	∞
		6	∞
Meramec gravel	<2.50	5	363
		6	128
	>2.50	2	∞
		7	78
Rapid and Coralville limestone	>2.50	4	242
		5	38
Mortar	—	1A	145
		2D	543
		3C	128

For three of the aggregate specimens zero capillary rise was recorded (Table 8). This resulted in pore diameters of infinity as calculated with Eq. 7*b*, but microscopic examination did not reveal a single capillary visible on the exposed surface. Although the calculated pore diameters are given as infinity in Table 8, they were considered to be zero in all analyses. A zero capillary rise will be recorded either when there is a lack of exposed capillaries or when a pore of infinite size occurs. The method of analysis used here lacks the ability to differentiate between those two extremes, producing a calculated pore diameter of infinity in either case.

The true nature of the pore diameters calculated in the capillarity studies is unknown. They may be diameters of the smallest continuous capillaries, the most abundant continuous capillaries, or some composite measure. No data are available to indicate their significance.

The calculated pore diameters were based on the maximum readings recorded on each of the manometers. Water taken up by wetting, in producing clay swelling, or in furthering hydration of the specimens, was not erroneously interpreted as the maximum capillary rise. Nevertheless, the occurrence of clay swelling or hydration, because it affects the size and number of pores, did affect the maximum capillary rise obtained.

The relatively small number of tests and the variation between the calculated pore diameters of the two specimens in each geological category preclude general conclusions based on capillarity. Ignoring the specimens with calculated pore diameters of infinity, the Gilmore City

TABLE 9

MEASURED PORE CHARACTERISTICS

AGGREGATE	SP. GR.	POROSITY: VOIDS RATIO	POROSITY: VOL. VOIDS/ BULK VOL.	PERMEABILITY (DARCYS): RANGE	PERMEABILITY (DARCYS): AVG.
Gilmore City limestone	<2.50	0.1521	0.0932	1.908×10^{-4} to 1.941×10^{-3}	1.202×10^{-3}
	>2.50	0.1127	0.0545	3.105×10^{-5} to 1.941×10^{-3}	5.411×10^{-4}
Maynes Creek and Eagle City limestone	<2.50	0.1896	0.1163	3.065×10^{-5} to 2.881×10^{-3}	8.767×10^{-4}
	>2.50	0.0912	0.0581	7.952×10^{-6} to 3.507×10^{-3}	1.134×10^{-3}
Paducah gravel	<2.50	0.2243	0.1166	3.396×10^{-6} to 3.053×10^{-5}	7.581×10^{-6}
	>2.50	0.0608	0.0339	3.446×10^{-6} to 2.441×10^{-6}	1.222×10^{-6}
White Marsh gravel	>2.50	0.0205	0.0070	9.928×10^{-7} to 7.802×10^{-4}	2.786×10^{-4}
Benner and Snyder limestone	>2.50	0.0101	0.0068	Beyond limits of apparatus	
Meramec gravel	<2.50	0.1902	0.0740	4.829×10^{-7} to 5.443×10^{-4}	1.819×10^{-4}
	>2.50	0.0682	0.0324	1.191×10^{-7} to 8.751×10^{-5}	4.385×10^{-5}
Rapid and Coralville limestone	>2.50	0.1634	0.0989	9.138×10^{-7} to 1.416×10^{-4}	3.633×10^{-5}
Mortar		0.4356	0.2937	3.573×10^{-6} to 1.086×10^{-5}	2.314×10^{-5}

limestone specimens have the smallest calculated pore diameters, the hardened mortar specimens the largest, and the remaining specimens fall between these two extremes.

POROSITY/PERMEABILITY INDEX

Index Development

The measured porosity and permeability values are summarized in Table 9. Durability factors for the eleven geologic categories are given in Table 10. Durability data were not available for hardened mortar specimens of the proportions used in these studies.

TABLE 10

RAPID FREEZE-THAW RESULTS (ASTM C290-61)

AGGREGATE	SP. GR.	DURABILITY FACTOR[a]: MEAN	DURABILITY FACTOR[a]: RANGE
Gilmore City limestone	<2.50	93[b]	—
	>2.50	93[b]	—
Maynes Creek and Eagle City limestone	<2.50	88.9	81.6 to 94.4
	>2.50	89.6	85.2 to 94.9
Paducah gravel	<2.50	0.7	0.7 to 0.8
	>2.50	0.7[c]	—
White Marsh gravel	>2.50	96.7	95.8 to 97.4
Benner and Snyder limestone	>2.50	98.1	95.4 to 99.5
Meramec gravel	<2.50	6.0	4.0 to 7.0
	>2.50	27.0	17.2 to 36.0
Rapid and Coralville limestone	>2.50	59.6	32.4 to 90.0

[a] Three specimens.

[b] From (25), obtained by ASTM C291-61T, "Tentative Method of Test for Resistance of Concrete Specimens to Rapid Freezing in Air and Thawing in Water." Durability factor of both specific gravity fractions assumed to be the same.

[c] Durability factor of both specific gravity fractions assumed to be the same.

Correlation analyses were performed on all possible combinations of pairs of the following variables: porosity (volume voids/bulk volume), log porosity, average permeability coefficient, log average permeability coefficient, average durability factor, and log average durability factor. The twelve possible combinations and a summary of the results of the correlation analyses are given in Table 11. Examination of these correlation coefficients suggested a possible further correlation between the logarithm of some combination of porosity and permeability, and the average durability factor or the logarithm of the average durability factor.

The combination of porosity and permeability was made in the following manner:

$$T = \frac{\text{Porosity}}{\text{Permeability coefficient}} \tag{8a}$$

That is to say,

$$T = \frac{\text{Volume voids/bulk volume}}{K_0} = \frac{V_v/AL}{Q_m \mu L/A(\Delta P)} = \frac{V_v(\Delta P)}{Q_m \mu L^2} \tag{8b}$$

in which

T = factor relating porosity and permeability;
V_v = volume of voids;
A = cross-sectional area of specimen;
L = length of specimen;
ΔP = pressure differential;
Q_m = volume of flow at average pressure; and
μ = viscosity of fluid.

Equation 8*a* can perhaps be thought of in terms of a volume of voids to be filled, divided by the rate of filling. The porosity is expressed in terms of the bulk volume. The specimen has a unit area exposed to flow, and a unit

TABLE 11

STATISTICAL ANALYSES OF PORE CHARACTERISTICS AND DURABILITY FACTOR

TEST	CORRELATION COEFF.	PROB. (%)
Porosity vs average permeability coefficient	0.2223	<90.0
Porosity vs log average permeability coefficient	—0.1209	<90.0
Porosity vs average durability factor	—0.0523	<90.0
Porosity vs log average durability factor	—0.0883	<90.0
Log porosity vs average permeability coefficient	—0.0087	<90.0
Log porosity vs log average permeability coefficient	—0.4983	<90.0
Log porosity vs average durability factor	—0.3163	<90.0
Log porosity vs log average durability factor	—0.4330	<90.0
Average permeability coefficient vs average durability factor	0.7381	≥98.0
Average permeability coefficient vs log average durability factor	0.5702	≥90.0
Log average permeability coefficient vs average durability factor	0.6719	≥95.0
Log average permeability coefficient vs log average durability factor	0.7040	≥95.0

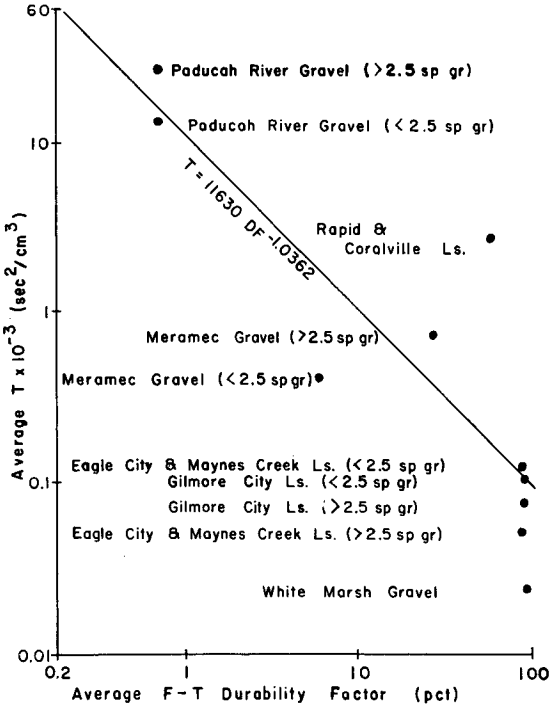

Figure 9. Relationship of T, *a combination of porosity and permeability coefficient, and the average freeze-thaw durability factor.*

length, and is acted upon by a fluid with a viscosity of 1 centipoise. (The viscosity of water varies from 1.145 centipoises at 59 F to 0.895 centipoises at 77 F (*3*), at a pressure differential of 1 atm.)

Correlation of Index with Freeze-Thaw Resistance

For the aggregates tested, correlation analyses were made of log T versus the average freeze-thaw durability factor, and of log T versus the logarithm of the average durability factor. The first analysis produced a correlation coefficient of —0.8433 and a probability of correlation of 99.6 percent or more. The second analysis produced a correlation coefficient of —0.8643 and a probability of correlation of 99.8 percent or more. The second analysis yielded a least-squares equation of

$$T = 11{,}630\mathrm{DF}^{-1.0362} \qquad (9)$$

in which DF is the average durability factor.

The plot of T versus the average freeze-thaw durability factor is shown in Figure 9.

EVALUATION

The porosity, permeability, and capillarity studies can be evaluated as follows:

1. Aggregate porosity values provide a sharp distinction between the two specific gravity fractions in any one geologic category (Table 1).
2. None of the aggregates studied had a porosity greater than that of the hardened mortar.
3. Each aggregate type was characterized by a wide range of permeability coefficients rather than a single coefficient (Fig. 7).
4. No differentiation between the two specific gravity fractions of the different aggregate types could be made on the basis of permeability (Fig. 7). The range of permeability coefficients of the specific gravity fractions overlap.
5. Mortar permeability coefficients were confined to a much narrower range than the permeability coefficients determined on aggregate specimens in any one geologic category (Table 7).
6. Significant correlation could not be found between porosity and permeability coefficient, nor between porosity and the average freeze-thaw durability factor (Table 11).
7. Aggregates with the poorest freeze-thaw resistance tended to have the lowest permeability coefficient ranges, and aggregates with the highest freeze-thaw resistance tended to have the highest permeability coefficient ranges (Fig. 7). Statistical analysis of average permeability coefficient versus average durability factor produced a correlation coefficient of 0.7381 and a probability of correlation of 98.0 percent or more (Table 11).
8. Strong correlation was found between a combination of porosity and permeability coefficient (factor T) and the average freeze-thaw durability factor. Statistical analysis of log T versus the logarithm of the average durability factor produced a correlation coefficient of —0.8643 and a probability of correlation of 99.8 percent or more (Fig. 9).

CHAPTER THREE

MOISTURE MOVEMENT BETWEEN AGGREGATES AND HARDENED MORTAR

Chapter One indicated that the relative size of pores in hardened mortar and in aggregate particles is an important factor in moisture movement between the two. Both the rate and the amount of moisture movement influence the susceptibility of aggregate and mortar to frost and general weathering.

Dye penetration and radioactive tracer studies were undertaken to evaluate their ability to detect moisture movement between certain types of aggregates and the mortar in which they were encased.

DYE PENETRATION STUDY

Using a water-soluble dye and the aggregates identified in Table 12, the movement of moisture was studied in two directions—that is, from the mortar into the aggregate when an external source of moisture was available, and from the aggregate into the surrounding mortar when drying began.

Dye Characteristics

After some preliminary tests, eosine dye was found to be suitable for detecting water movement in both the hardened mortar and the aggregate particles. The dye was prepared by mixing 0.2 percent by weight of eosine powder with distilled water. The resulting liquid had a specific gravity of 1.000 and a surface tension about equal to that of distilled water.

The performance of this dye was generally satisfactory. In a few cases, however, as it passed through the specimen the dye separated from the water with which it was mixed, and in several of the aggregate types the red eosine was indistinguishable because of the color of the aggregate particles.

Aggregate Preparation

After ovendrying at 212 to 230 F the particles were vacuum saturated with water. To evaluate the effect of specific gravity on the amount of water movement, they were then separated by heavy media (*79*), using trichloroethylene plus tetrabromoethane, into those particles above and below a specific gravity of 2.50. A specific gravity of 2.50 was selected because it had been reported (*41, 79*) as a dividing line for frost resistance in several types of aggregates. After separation the particles were again ovendried at 212 to 230 F to constant weight.

Specimen Preparation

All specimens for the studies of aggregate particles in hardened mortar were cast in 3-in. diameter cylindrical molds 3 in. long.

TABLE 12

DYE PENETRATION TEST RESULTS

			PENETRATION OF AGGREGATE PARTICLES (MM)						
			PLAIN SOAK, 5 DAYS			SOAKED AFTER 1-HR VAC. SAT.			SERIES 1, PENETR. THROUGH MORTAR
AGGREGATE	SP. GR.	MINERAL CLASS	PARTICLE 1	PARTICLE 2	PARTICLE 3	1 DAY	3 DAYS	5 DAYS	
H[a]	>2.5	Ool. LS	Total	Total	4.0	Total	Total	None[b]	No
	<2.5	Ool. LS	Total	Total	Total	Total	Total	None[b]	Yes
D	>2.5	Ool. and dolom. LS	2.8	2.0	3.0	1.0	Total	Slight[b]	Yes
	<2.5	Ool. and dolom. LS	Total	Total	Total	1.8	3.5	Total	Yes
E	>2.5	Dense chert	2.2	8.0	None	None	Total	3.0	Yes
	<2.5	Dense chert	None	1.0	None	Total	2.8	None	Yes
A	>2.5	Quartz	Total	None	None	Slight	None	None[b]	No
G	>2.5	Dense chert	1.0	Total	1.0	1.0	Total	None[b]	No
	>2.5	LS and dolom. LS	None	None	None	None	1.3	None	No
	>2.5	Granite		None	None	None	2.0	2.5	No
	<2.5	Soft shale	4.0			0.5	None	Total	Yes
	<2.5	Calc. and dolom. SS	4.0	0.5	1.0	Total	Total	Total	Yes
	<2.5	Silty LS	None	Total	1.0	4.0	Total	Total	Yes
	<2.5	Chert	Total	Slight	Total	8.5	Total	Total	Yes

[a] See Appendix C.
[b] Aggregates remaining from second and third series.

The mortar was prepared according to ASTM C109-58, "Standard Method of Test for Compressive Strength of Hydraulic Cement Mortars." A quartz sand of known high quality, graded to remove particles larger than the No. 4 sieve, was substituted for the standard Ottawa sand.

The mortar was placed in the molds in two layers, with a single piece of the desired aggregate positioned between the two layers.

Method of Opening Specimens

The cured cylindrical specimens were opened by the method prescribed in ASTM C496-62T, "Tentative Method of Test for Splitting Tensile Strength of Molded Concrete Cylinders." Regular clean breaks through the mortar and the embedded aggregate particle were usually achieved in one out of three specimens incorporating each of the aggregate types studied.

To improve the yield of good breaks, the particles should be larger or the molds smaller than those used here. The maximum mortar cover at any point should not exceed ¾ in., and the minimum cover should not be less than ½ in. This would facilitate opening the specimens, and would also decrease the dye ingression time.

Dye Penetration of Aggregate Particles

To determine the penetration of eosine dye into aggregate particles not protected by a mortar cover, representative samples of each of the aggregate types to be tested were soaked in the dye for approximately five days. The results for three particles of each aggregate are given in Table 12. The depth of penetration is an average across an exposed cross section.

Moisture Movement Between Aggregate and Hardened Mortar

Three series of specimens were prepared for this phase of the dye penetration experiments: Series 1, to study moisture movement through hardened mortar into various aggregate particles; Series 2, to study moisture movement from saturated aggregate particles through hardened mortar when drying started; and Series 3, to study the effects of relative humidity on moisture movement.

Ovendried aggregate particles were incorporated in Series 1 specimens, which were left in the molds 24 hr in a fog room, then removed from the molds and soaked in a water bath at 190 to 200 F for 3 days to accelerate strength development. After the water bath, the specimens were ovendried at 100 to 104 F to constant weight. Next they were subjected to a vacuum-saturating procedure in which eosine dye was substituted for water. After a 1-hr vacuum period, the specimens were soaked 24 hr in the eosine dye. (Some were soaked 48 hr, but no great difference in depth of dye penetration could be detected.) They were then broken open by the ASTM procedure.

Because capillary movement in a pore is a function of temperature, surface tension and density of the liquid, radius of the pore, and the acceleration of gravity, vacuum saturation affects the extent of dye or water movement per unit by removing entrapped air from the specimen but does not produce movement into those pores that would not be filled by prolonged soaking.

Vacuum dye-treated aggregate particles were incorporated in the Series 2 and Series 3 specimens, which were cured in the fog room 7 days. The cured Series 2 specimens were dried in an oven 3 days at 100 to 104 F, and were then split open. The Series 3 specimens were moved from the fog room (relative humidity approximately 100 percent) to a room maintained at 47 percent (± 2 percent) relative humidity. After 3 days in this room they were opened.

Because it was discovered that drying the split specimens made the red eosine dye more readily visible, all but the first few specimens were opened and allowed to dry overnight in laboratory air before they were examined.

Results

Test results for Series 1 are summarized in Table 12. In general, dye penetrated through the mortar into those aggregate particles with less than 2.50 sp gr and did not penetrate those with greater than 2.50 sp gr. The fractions of aggregates D and E with greater than 2.50 sp gr were exceptions to this generalization.

Examples of dye penetration may be seen in Figures 10 and 11. Figure 10 shows three split mortar specimens, each containing an aggregate H particle with less than 2.50 sp gr. Two of these experienced dye penetration, but it is visible here in only the bottom specimen, as the dark area adjacent to and within the particle. In Figure 11 each of the specimens contains an aggregate D limestone particle with less than 2.50 sp gr. All of them experienced dye penetration, but again it shows plainly in only the specimen at the bottom.

For Series 2 and Series 3 the results were inconclusive. After ovendrying for 3 days, Series 2 showed little or no dye in the aggregate particles or in the hardened mortar. Series 3 specimens yielded the same negative results after 3 days in an atmosphere of 47 percent relative humidity.

Figure 12, two Series 2 splits containing aggregate A, shows the ideal breaks obtainable by the ASTM splitting procedure.

Discussion

The results of the dye penetration tests were not conclusive. Evidence of penetration in one out of three cases does not prove that the dye will penetrate that class of aggregate particle. On the other hand, the absence of penetration in two out of three cases does not prove that dye penetration cannot occur in the aggregate types involved. A void in the mortar adjacent to the aggregate particle (Fig. 10, top) probably has a significant effect on dye movement and penetration. The dye sometimes did not penetrate the mortar a sufficient distance to reach the aggregate surface, and as mentioned earlier, the red eosine sometimes could not be detected because of the color of the aggregate particles. In compiling Table 12, questionable cases were regarded as lacking dye penetration.

When the various aggregate particles were soaked in

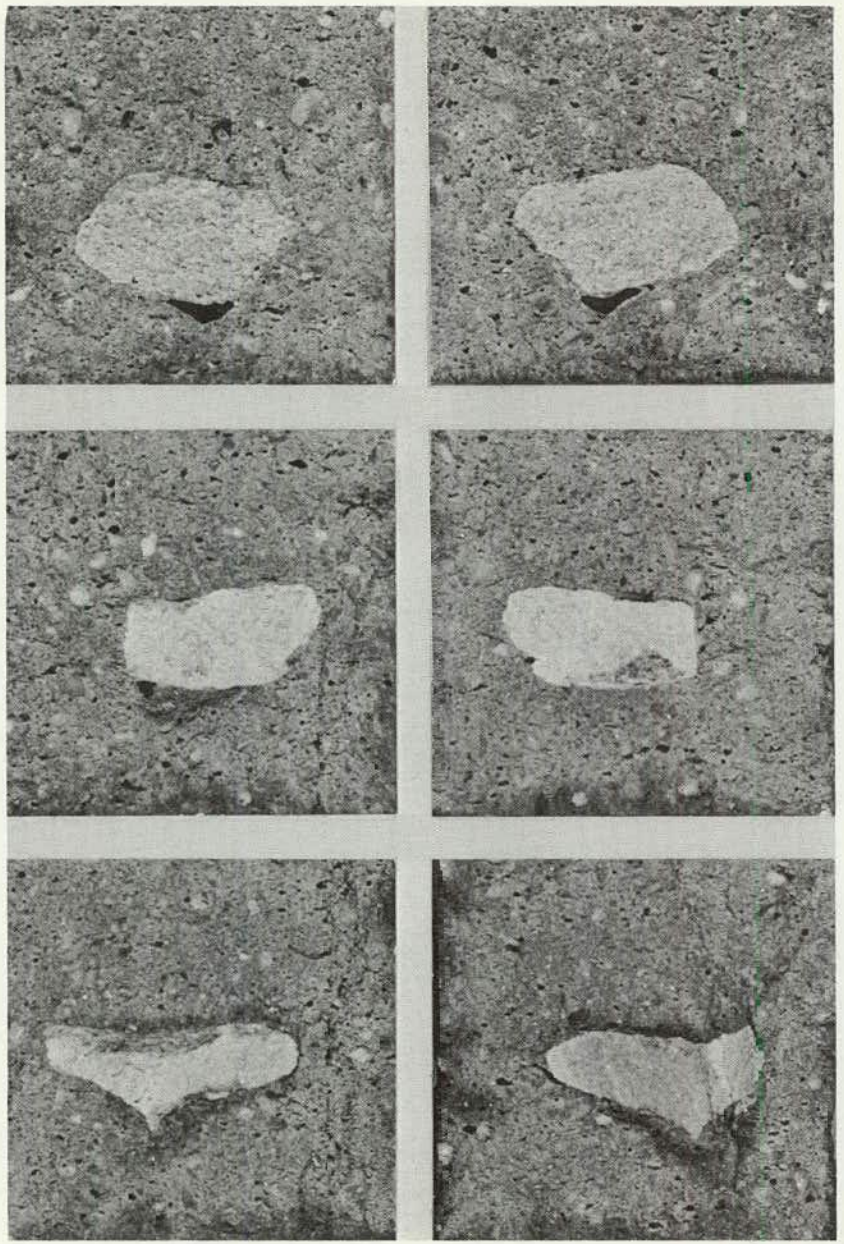

Figure 10. Series 1 specimens containing aggregate H, <2.5 sp gr.

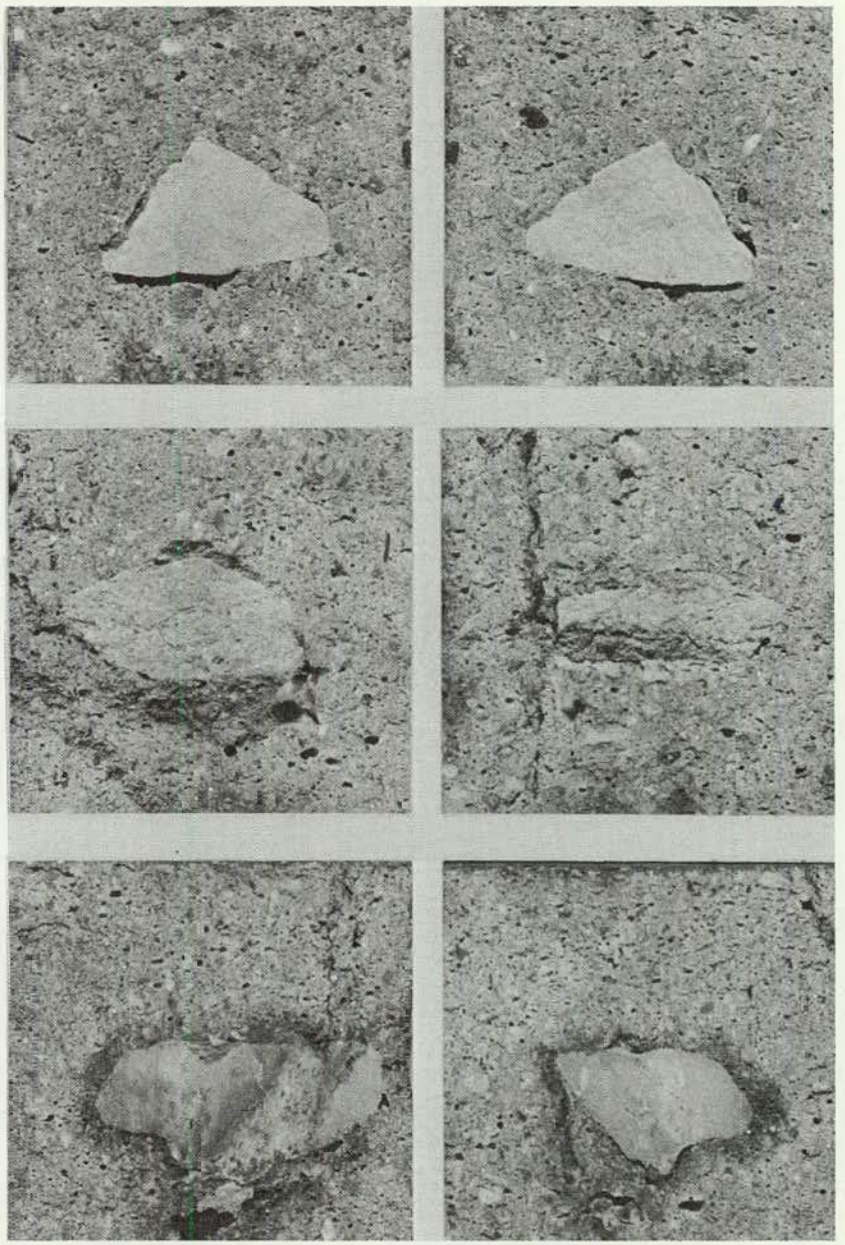

Figure 11. Series 1 specimens containing aggregate D, <2.5 sp gr.

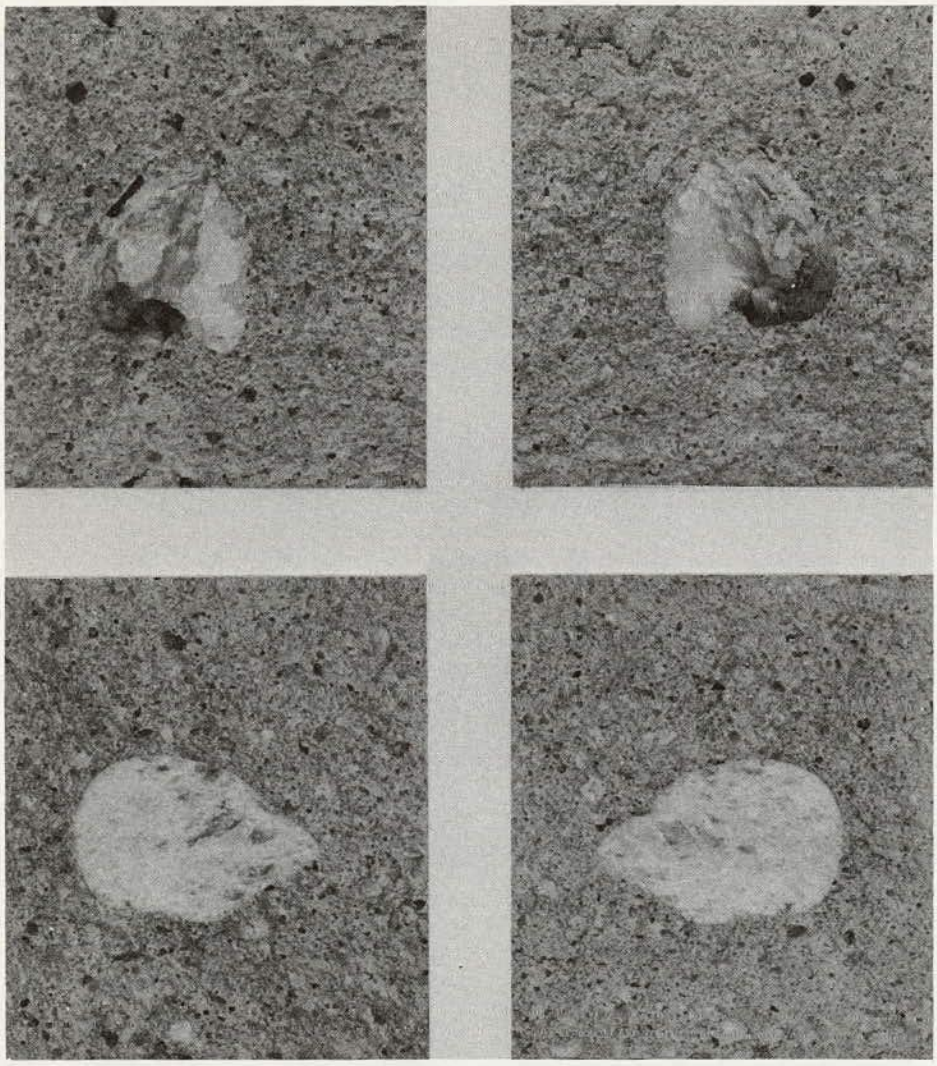

Figure 12. Series 2 specimens containing aggregate A.

dye for five days for the tests without mortar, the majority showed considerable dye penetration. It has been reported (*91*) that vacuum treatment produces higher degrees of saturation than plain soaking. The aggregate particles for Series 2 and Series 3 specimens were vacuum dye-treated, but no provision was made to determine the resulting degrees of saturation. Several vacuum-dyed particles remaining after these specimens were molded were split open and showed no penetration (Table 12). Additional particles were then vacuum dye-treated and analyzed, with the results indicated in Table 12.

Because of the heterogeneity and the consequent range of behaviors for any one mineralogical type, the results of these tests are difficult to compare. In a general way, however, Table 12 shows that vacuum treatment followed by soaking does not produce a noticeable increase in dye penetration over the results obtained by plain soaking without vacuum treatment. The length of the soaking period following the vacuum tends to overshadow any difference that might be produced by subjecting the aggregate particles to a vacuum before exposing them to moisture.

A time variable probably influenced the results for the Series 2 and Series 3 specimens. The vacuum-treated particles for Series 2 were soaked in dye various lengths of time before they were incorporated in mortar specimens: one-third for 24 hr, one-third for 2 days, and one-third for 3 days. The particles for Series 3 were vacuum treated and then soaked in dye for 4 days before they were incorporated in specimens. These short soaking periods and the consequent small total volumes of dye present in the aggregate particles may account for the failure of the specimens to produce meaningful results. It appears unlikely that a large enough volume of dye can be absorbed by aggregate particles to release noticeable traces into the surrounding mortar at the start of drying.

The effect of a mortar cover on dye movement into the aggregate particles is indicated in the last column of Table 12. In general, for all the mineralogical types with less than 2.50 sp gr the mortar cover had no effect on

moisture movement into the aggregate. For H, A, and G (chert) aggregates with greater than 2.50 sp gr, the mortar surrounding the particles did inhibit moisture movement into the aggregate, suggesting that the mortar around these aggregates increases the probability that they will survive cyclic freezing and thawing, cyclic wetting and drying, chemical attack, and thermal changes. But Table 12 shows that aggregates G (granite) and G (limestone) were not penetrated by dye even when a mortar cover was not provided. The other G aggregates experienced dye penetration whether or not they were encased in mortar and regardless of their specific gravity.

From the differences in dye penetration related to specific gravity, it can be conjectured that a difference exists between the pore structure of the hardened mortar used in this study and that of the aggregates of the two specific gravity fractions. This assumes, with reasonable confidence, that the pore structure of the hardened mortars from several mixes was fairly constant.

Thin-Section Analyses

Thin-section analyses completed after the dye tests confirm and explain some of the results of these tests. For example, aggregate H with less than 2.50 sp gr contains up to 10 percent voids, some as large as 0.5 mm in diameter; but in aggregate H with greater than 2.50 sp gr, all visible voids and fractures are healed with clear anhedral calcite. Dye penetration through the mortar into the former and not the latter might therefore be expected. Aggregate A is also characterized by few visible interstitial voids but contains 14 to 20 percent liquid inclusions by volume, and should resist dye penetration through the mortar.

Aggregate G (chert) with less than 2.50 sp gr contains numerous voids, apparently produced by weathering. These voids are up to 1 mm in diameter, some filled with and others only bordered by amorphous iron oxides. In aggregate G (dense chert), greater than 2.50 sp gr, all visible voids and fractures are healed with microcrystalline or cryptocrystalline quartz. Here again, preferential dye penetration would be likely. Both G (granite) and G (limestone) have very few or no visible voids or fractures; dye penetration should not occur, whether or not the particles are encased in mortar.

For the remaining aggregates, the thin-section analyses indicate characteristic visible voids or fractures in the particles of the following with less than 2.50 sp gr: aggregate D (limestone), aggregate E (dense chert), and aggregate G (soft shale).

RADIOACTIVE TRACER STUDY

The difficulties and anomalies of dye penetration as a means of tracing moisture movement in concrete prompted a search for a more positive technique. Photometry was eliminated when it was learned that Pflug and Crumpton (*20*), who have tried this method at Kansas State University, have not yet solved two problems: the reagent reacts with both bound water and free water, and the lacquer employed is itself a water emulsion.

Inasmuch as water movement was to be detected, the idea of using "radioactive water" was conceived. A small portion of the test water could easily be labeled with tritium, the radioisotope of hydrogen, but because the energy level of the beta radiation from tritium is very low, it is hard to detect by standard counting procedures. A means of circumventing that obstacle was suggested by the autoradiographic technique for examining tritium-labeled specimens, which is well established in the fields of medicine and metallurgy (*6, 26, 28, 38, 65*) and has also been used by General Foods Corporation to study redistribution of water in precooked rice (*52*). For this technique the low-energy beta radiation of tritium is an asset rather than a drawback.

The potentialities of autoradiography for the present study were therefore investigated.

Autoradiographic Process and the Artifact Problem

Autoradiography uses photographic emulsions to locate ionizing radiations. The method is simple and direct, requiring none of the expensive counting devices needed for ordinary radiotracer work, and is capable of very high resolution. Resolutions of the order of 10 microns are not uncommon, and 1 micron is attainable (*28*). Successfully applied, it produces a graphic portrait of the location of low-energy radiation that is easy to interpret.

To trace moisture movement in concrete by this process, a concrete specimen containing tritiated water would be subjected to the desired environmental conditions, then broken open, and the broken surfaces would be coated with a suitable photographic emulsion. After exposure for a sufficient length of time, the developed emulsion would reveal the location of the radioactive water, thus indicating the moisture migration patterns.

A problem arose, however, that was peculiar to the material to be tested. The emulsion supplier (Eastman Kodak Company) warned in correspondence (*71*) that false images, called "artifacts," might be caused by chemical action of alkalies in the concrete upon the photographic

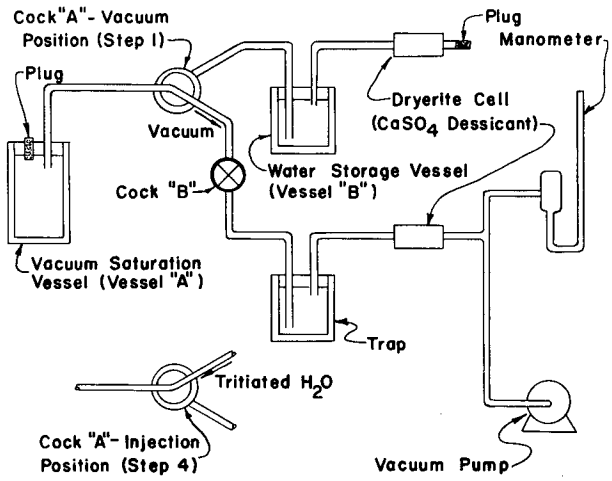

Figure 13. System for vacuum saturation of aggregates with tritiated water.

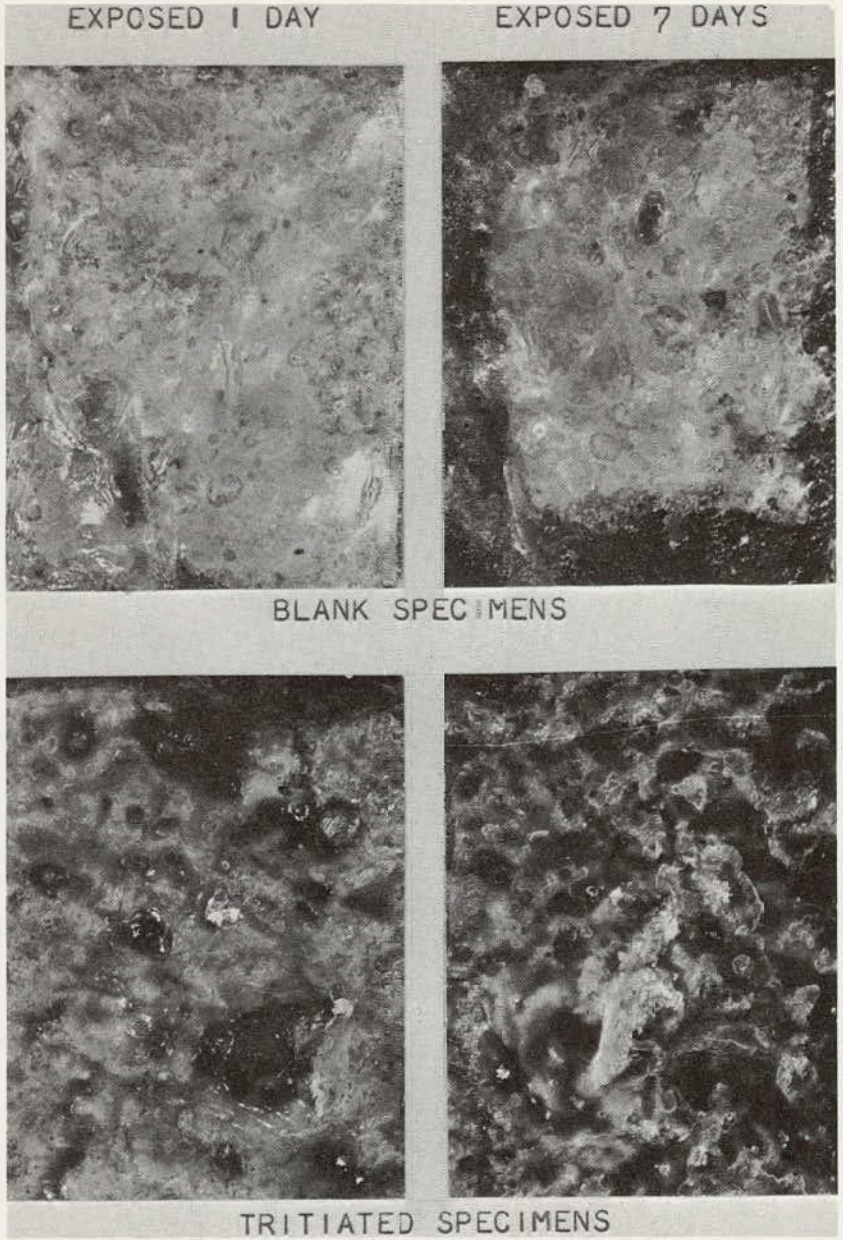

Figure 14. Specimens coated with melted naphthalene.

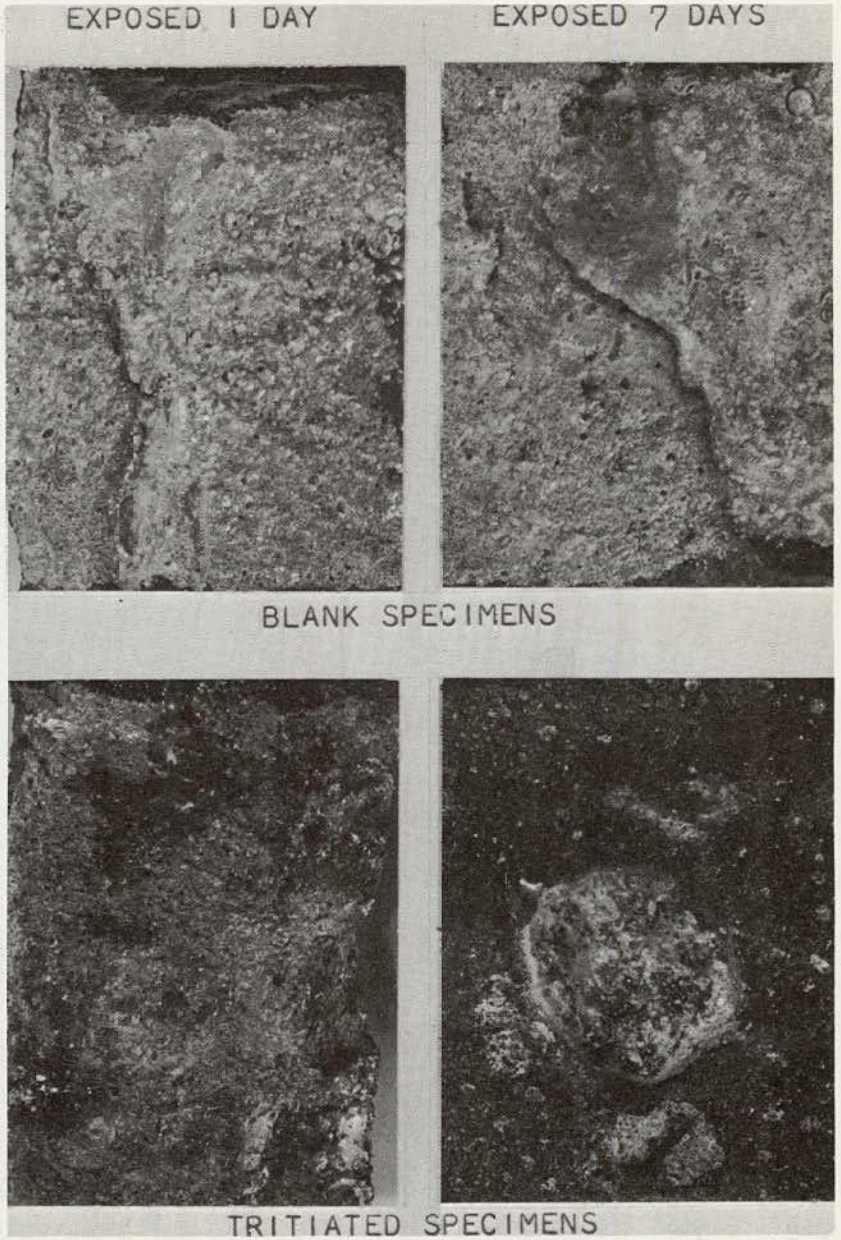

Figure 15. Specimens coated with naphthalene dissolved in chloroform.

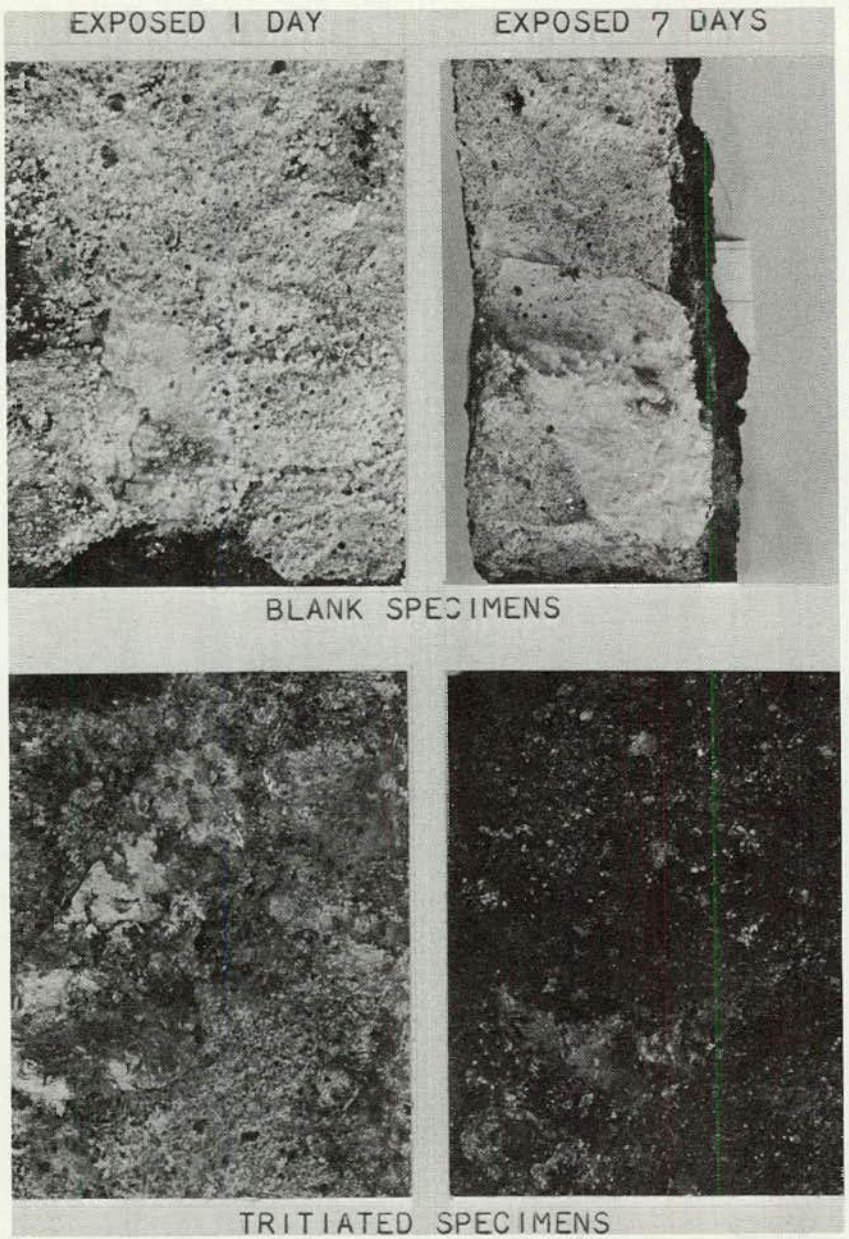

Figure 16. Specimens coated with naphthalene and anthracene dissolved in benzene.

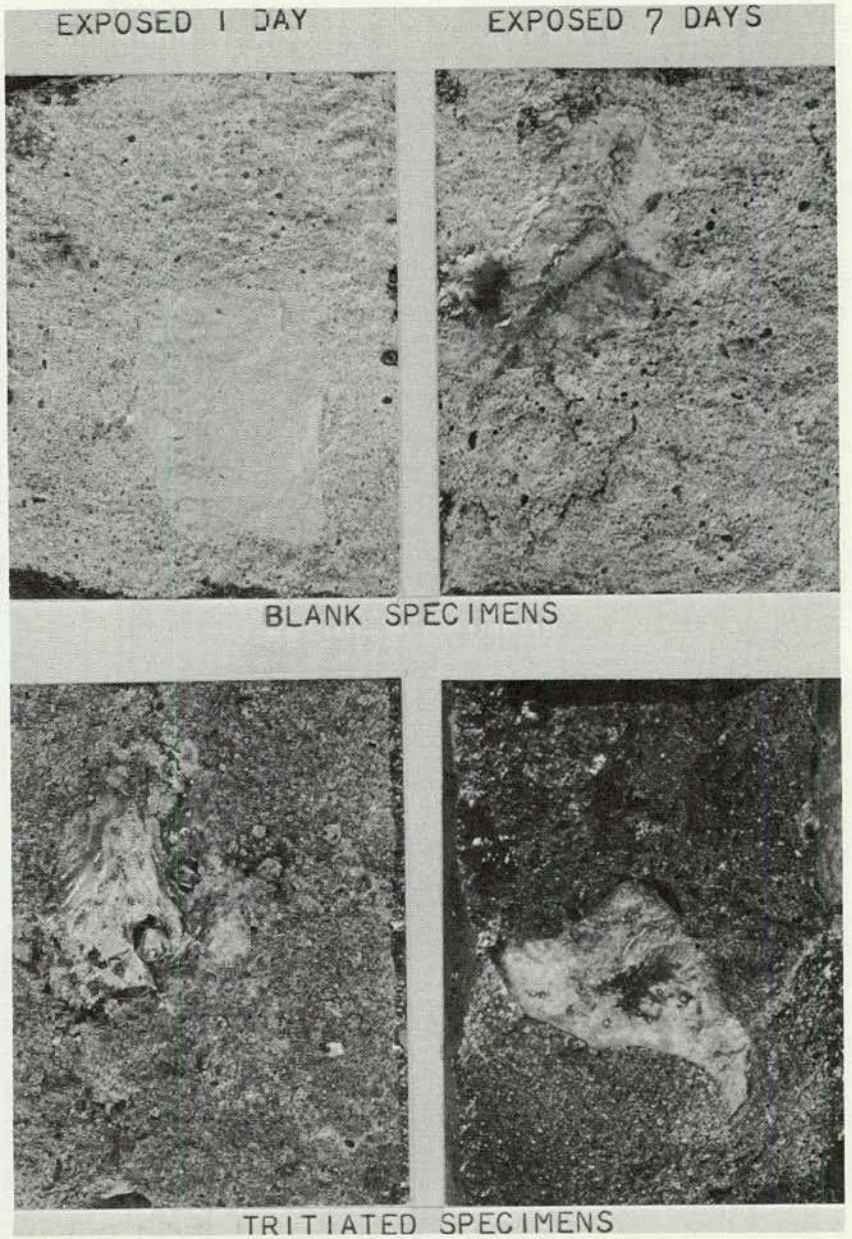

Figure 17. Specimens coated with impermeable coating.

emulsion. Preliminary tests of the emulsion in contact with the concrete did indeed produce artifacts on the emulsion.

Two alternatives seemed likely to alleviate this interference. Either an extremely thin impermeable coating or a scintillation medium could be interposed between the concrete and the emulsion. The impermeable coating, however thin, might have the disadvantage of reducing the intensity of the beta radiation available for exposing the emulsion, because only a few microns of solid material are capable of stopping the weak emissions. A scintillation medium is a material that emits electromagnetic radiations in the visible or ultraviolet region of the spectrum when bombarded by ionizing radiation, and these secondary light emissions then expose the emulsion (autoluminography).

Because neither the literature nor communication with persons engaged in nuclear tracer work shed light on the feasibility of either alternative, both were tested in the following experiments.

Experimental Work

Particles of a test aggregate were vacuum saturated with tritiated water (specific activity 20 mc per g), and each particle was encased in mortar in a mold 2 in. in diameter and 2½ in. long. Similar blank specimens were vacuum saturated with ordinary water. The design of the vacuum-saturating system is shown in Figure 13.

After sufficient curing time the specimens were broken by the tensile splitting test (ASTM C496-62T) to produce a fractured face through the aggregate and the paste. These faces were treated immediately with either a scintillation medium or an impermeable coating. The scintillation media tested were melted naphthalene, naphthalene dissolved in chloroform, and naphthalene and anthracene dissolved in benzene. The impermeable coating consisted of 0.25 percent clear fingernail polish (solid weight basis) dissolved in acetone.

In a darkroom the specimens were then coated with melted bulk photographic emulsion (Eastman Kodak NTB-3 nuclear tracking emulsion), and exposed in a light-proof box for 1 day and 7 days, after which they were developed.

Results

Figures 14 through 17 show the blank and the tritiated specimens with the various protective coatings, after 1-day and 7-day exposure. Although both exposure times gave excellent results, the density is naturally somewhat greater for the longer period. The blank specimens were totally free of artifacts. Dark areas around the edges of the specimens are a black "dope" used to seal the outside surfaces.

The results indicate that the autoradiographic technique is capable of locating tritium-labeled water in concrete, and that either a thin impermeable coating or autoluminography by scintillation media eliminates the problem of chemical artifacts. Of the scintillation media tested, naphthalene dissolved in chloroform was the most satisfactory.

Because this was a feasibility study of the method, no attempt was made to supply the environmental factors relevant to moisture migration. In view of the promise exhibited, further studies should be carried out using this technique to study the deterioration of concrete as it is affected by the presence and movement of water.

CHAPTER FOUR

AGGREGATE PARTICLE EXPANSION

The study of aggregate particle expansion here reported was undertaken to evaluate the hypothesis that unconfined freezing and thawing of aggregates under controlled rates and at predetermined degrees of saturation can produce laboratory measurements of dimension changes in the aggregate particles that will correlate with the frost resistance of concretes made with these aggregates.

BACKGROUND

Where the paste phase is of high quality and is adequately protected by entrained air, the destruction of concrete by freezing and thawing is solely a function of the nature of the coarse aggregate. This assumes that the air voids in the paste do not become critically saturated, but under most natural conditions of exposure and with an air content greater than 5 percent the assumption is reasonable. Inasmuch as the paste phase can be made virtually immune to natural frost action, examination of aggregates alone should be sufficient, or at least highly indicative, for laboratory prediction of frost resistance of concrete.

Earlier laboratory methods for testing aggregates, however, have revealed discouragingly poor relationships with field performance. These included magnesium or sodium sulfate tests to stimulate frost action, and unconfined freezing-and-thawing tests utilizing various saturating, freezing, and thawing procedures. In all cases aggregate deterioration was determined by breakdown of the aggregate particles as measured by sieve analysis before and after testing.

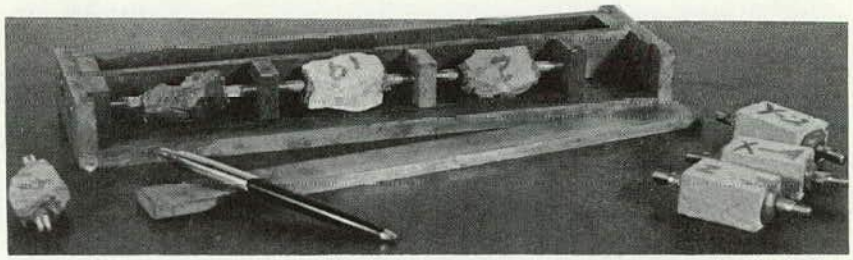

Figure 18. Method of installing gage studs on aggregate particle specimens.

Walker (*80*) reported in 1943 that the sulfate and unconfined freezing-and-thawing tests detect unsoundness in some aggregates, but not in others where field performance revealed unsoundness. Other investigators (*12, 35, 10, 92*) have also concluded that sulfate and unconfined freezing-and-thawing tests are not reliable indicators of frost resistance.

The sodium or magnesium sulfate tests are unsatisfactory measures of frost susceptibility because of the nature of the mechanism of destruction. The theory now most widely accepted for frost destruction of concrete postulates that the primary destructive force is hydraulic pressure generated by an advancing ice front in critically saturated pores. Because the destructive mechanism in the sulfate test is slower crystal growth within the pores, the destruction produced is primarily a function of pore size. But degradation by freezing is related to porosity, permeability, and degree of saturation, as well as pore size. It is conceivable, for example, that certain aggregate types displaying high permeability could perform poorly in the sulfate test and yet be essentially immune to frost destruction.

The anomalous conclusions reached in attempting to correlate the earlier unconfined freezing-and-thawing tests with field performance, or with freezing-and-thawing tests of concrete, can be explained by the method used to evaluate frost destruction. Because deterioration was determined on the basis of physical breakdown of the aggregate as measured by sieve analysis, the primary information gained from the unconfined test was the ability of the aggregate to accommodate elastically the stresses induced by freezing. The destruction of concrete, however, is a function of the strains produced in the aggregates. Some high strength aggregates capable of accommodating high internal stresses might induce strains in concrete of sufficient magnitude to destroy the paste matrix, yet the same aggregates might display little or no degradation in the unconfined tests. Conversely, a weak aggregate, or especially an aggregate possessing distinct planes of weakness, might fare badly in the unconfined test but fail to produce destructive strains in concrete.

TEST METHOD

In the present study, unconfined freezing-and-thawing tests were performed on vacuum-saturated aggregate particles known to have a wide range of field performance. Dilations during freezing were measured with transducers, and permanent length changes were measured with dial gages as well as transducers. To facilitate the length and dilation measurements, stainless-steel gage studs were cemented to the aggregate particles with epoxy resin. During the cementing process the gage studs were held in line by mortar bar molds, as shown in Figure 18. The brass and invar steel strain frames for the Powers test (Chapter Six) were employed, with slight modification, to support the specimens as shown in Figure 19. Figure 20 shows the dial-gage comparator used for measuring permanent length changes.

Initial length determinations were made after the specimens had been vacuum saturated at 15 mm Hg absolute for 1 hr and soaked 23 hr. The dial-gage comparator used for the length determinations held the specimens submerged in a 70 F water bath. The aggregate particles were then immediately installed in the strain frames and immersed in a kerosene cooling bath at 35 F. The temperature of the kerosene bath was lowered to 15 F at a rate of about 5 F per hour, and raised rapidly back to 35 F. During the single cooling-and-reheating event, length changes in specimens were continuously monitored by

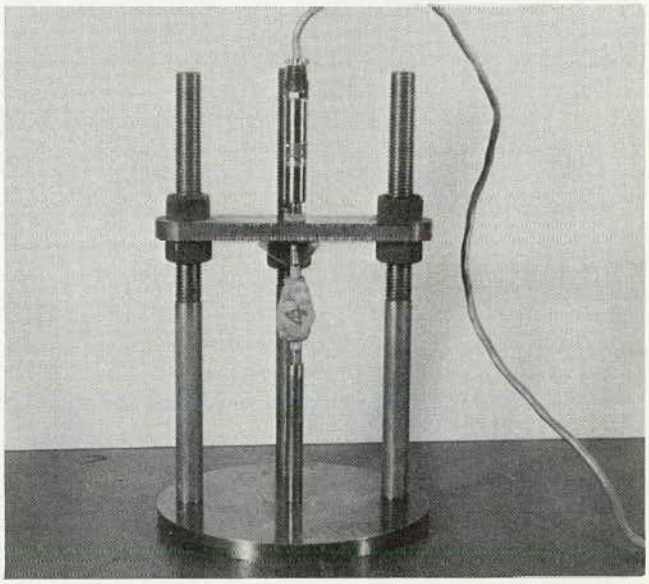

Figure 19. Strain-frame support for aggregate particle and transducer.

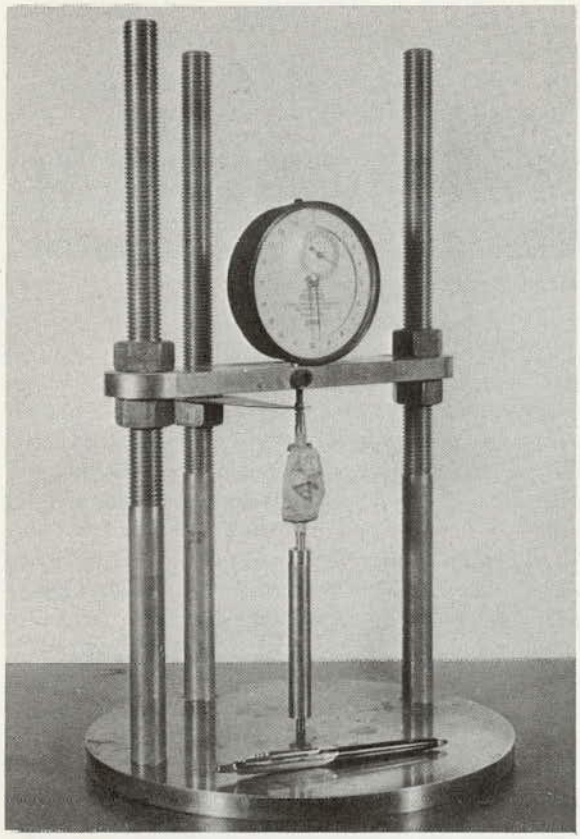

Figure 20. Dial-gage comparator and aggregate particle specimen.

transducers on the strain frames and automatically recorded on strip charts. Six specimens could be handled at a time with the equipment available. Dilations of the specimens were measured from the strip charts, as were permanent length changes. Following the test, the specimens were returned to the 70 F water bath for final length measurements.

Weights were also determined immediately before and after the test cycle. As the final step, the specimens were ovendried to constant weight and these weights were recorded.

From operations described the following data were obtained:

1. Permanent length change as determined by the dial-gage comparator readings.
2. Permanent length change as determined by transducer readings during the freeze-thaw cycle.
3. Percent of water contained prior to the freeze-thaw cycle.
4. Percent of water contained following the freeze-thaw cycle.
5. Amount of dilation during the freezing cycle.

In all, 23 sets of data were recorded, each set containing two to six specimens. The test data are summarized in Table E-4.

ANALYSIS OF DATA

The experimental design and data analyses were directed toward answering the following questions:

1. Can a dial-gage comparator determine permanent length change with sufficient accuracy as compared with determinations by more accurate but more expensive transducers?
2. Can permanent length-change readings alone differentiate the various aggregate types?
3. Do permanent length changes of unconfined aggregate particles correlate with the freeze-thaw performance of concrete made with the aggregates?

Dial Gages Versus Transducers

For the simplest and least costly method of measuring length change a dial-gage comparator would obviously be preferred to electronic apparatus. A statistical analysis of variance of the permanent length-change data revealed conclusively that no significant difference existed between the two methods of measuring permanent length changes (Table 13).

Permanent Length Change vs Aggregate Type

Table 13 also reveals that the aggregate type is a significant source of variation, indicating that permanent length change does vary among different aggregates.

Correlation of Aggregate Particle Data with Concrete Data

So far, it has been shown that permanent length change can be determined with sufficient accuracy with a dial-gage comparator, and that various aggregates display significantly different permanent length change after one cycle of freezing and thawing in the vacuum-saturated condition. If the permanent length change of the aggregate particles can be shown to correlate with measures of frost destruction of concretes made with the aggregates, a relatively simple test for determining frost resistance of concrete aggregates can be formulated. Such a correlation was attempted with the saturated concrete specimens from Phase II of the Powers test series (Chapter Six), which had been cured 13 days in limewater and three weeks in water at 35 F.

First-cycle total dilation was chosen as the measure of frost susceptibility for the concrete specimens, and average permanent length change as measured with the dial-gage comparator was used for the aggregates. The first attempt, utilizing all available data, failed to produce a significant correlation at the 95 percent significance level, but examination of the data revealed that two aggregates—Killins gravel (shale) and Rapid and Coralville limestone—were far out of line with the remaining data. Dropping these two aggregates from the correlation produced a significant correlation at 95 percent significance level. In general, therefore, the permanent length change of the aggregates should be a reliable measure of the frost resistance of concrete made with the aggregate.

TABLE 13

PERMANENT LENGTH CHANGE, ANALYSIS OF VARIANCE

SOURCE OF VARIATION	DEGREES OF FREEDOM	F RATIO	CRITICAL F RATIO[a]	SIGNIFICANCE[a]
Method of measuring	1	0.8167	3.84	None
Aggregate type	22	13.9635	1.55	Significant
Interaction	22	0.5308	1.61	None

[a] Significance level, 95 percent.

The two aggregates that failed to conform to the general pattern did not produce concrete dilations commensurate with the large permanent length changes observed in their unconfined state. One of these, Killins gravel (shale), was a very weak soft shale that probably lacked sufficient strength to exert dilating pressures on the confining paste matrix. The other, Rapid and Coralville limestone, was a soft clayey limestone, which probably failed to conform for the same reason.

The data for aggregate-particle permanent length change versus concrete dilation are shown in Figure 21. Figure 22, a plot of aggregate-particle permanent length change versus rapid freeze-thaw (ASTM C290) durability factors, gives further evidence of correlation between aggregate-particle and concrete data. Here again, Rapid and Coralville limestone failed to conform; rapid freeze-thaw tests were not run on the Killins gravel (shale) aggregate.

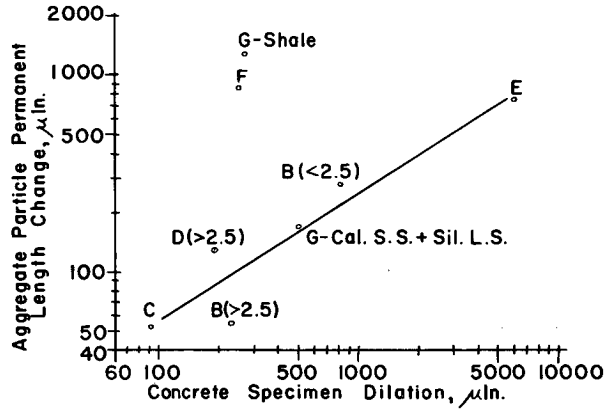

Figure 21. Aggregate particle permanent length change vs concrete specimen dilation.

DISCUSSION AND EVALUATION

The experimental data on permanent length change of aggregate particles strongly support the possibility of formulating a very simple test to evaluate aggregates with respect to the frost susceptibility of concrete. Although the experiment was not an unqualified success, in that two aggregates failed to follow the general correlation between permanent length change and concrete dilation, the two anomalous results were on the safe side; that is, the aggregate-particle test identified those aggregates as frost susceptible even though the first-cycle concrete dilation did not. Later dilations of the concrete specimens did, in fact, show that these aggregates were frost susceptible, tending to support the predictions of the aggregate tests.

Much more work is needed to verify the reliability and applicability of the aggregate-particle test. Future investigations of this method should be directed primarily toward expanding the range of aggregate types. All tests should consist of at least six replica specimens, and the particles should be carefully classified into narrow specific gravity and mineralogical groups. Because of the anisotropic behavior of many mineral aggregates, it would also be quite desirable, even necessary in some cases, to obtain the length measurements along orthogonal axes.

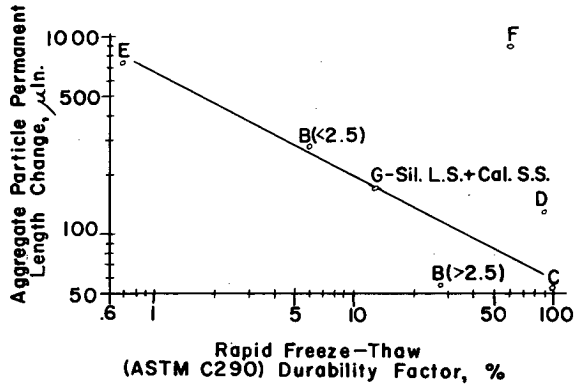

Figure 22. Aggregate particle permanent length change vs rapid freeze-thaw durability factor.

Average length changes for each mineralogical group and specific gravity fraction, combined on a weighted basis proportioned to the amount of each fraction in the raw aggregate, should provide a good indicator of the frost susceptibility of the aggregate.

CHAPTER FIVE

PETROGRAPHIC EVALUATION OF THE TEST AGGREGATES

Petrographic analyses were performed on representative test aggregates to explore the usefulness of petrography in evaluating freeze-thaw durability. Most of the data were obtained from thin sections of the aggregate particles and from macro observations of the concrete specimens before and after the freeze-thaw tests.

The test aggregates are considered individually in the following section. They are identified and more broadly described in Appendix C. General concepts are discussed at the end of the chapter.

PETROGRAPHIC ANALYSIS AND AGGREGATE PERFORMANCE

Aggregate A

Observation of thin sections of aggregate A revealed it to be dense igneous quartz with isolated liquid inclusions and discontinuous microfractures. No opal, chalcedony, or other materials that might be deleterious were recognized. Some limonite stain and very minor amounts of pyrite were present.

These findings suggest that aggregate A is nearly nonporous and relatively impermeable. The low porosity is verified by an average value for vacuum-saturated absorption of only 0.37 percent. But the average determined permeability, about 2×10^{-4} darcys, is higher than anticipated and is probably due to passage of water through the larger limonite-stained fractures rather than along the sutured grain boundaries and unweathered discontinuous microfractures. The low values obtained for the degree of vacuum saturation (averaging 47 percent) are attributed to the presence of 1 to 2 percent liquid inclusions, which increase the apparent value of the volume of voids and thus give anomalously low values for the degree of saturation (see sample calculation, Table B-1.)

The surfaces of the quartz particles were free of foreign material, except for minor amounts of limonite stain in some samples. It was thought, however, that the smooth surfaces and rounded shape of the particles might produce a poor bond with the cement paste. In subsequent freeze-thaw tests no deterioration of the bonding was noted, but mechanically broken samples of this concrete fractured around rather than through the quartz particles.

From this analysis, aggregate A was predicted to be durable to freeze-thaw conditions. Both its service record and an average durability factor of 96.7 after 300 freezing cycles support the prediction. The rapid freeze-thaw test results are tabulated in Appendix D.

Aggregate B

In aggregate B, chert fractions with both greater and less than 2.5 sp gr were present in sufficient quantitites for testing. Most particles of both fractions contained numerous microfractures and had weathered limonite-stained surfaces. In subsequent freeze-thaw tests, deterioration of the cement-aggregate bond was apparent, and many particles had separated from the paste in the ruptured concrete specimens.

The effect of the numerous voids in the fraction with less than 2.5 sp gr is difficult to evaluate without additional data. In thin section, some of these voids appear to be interconnected, forming permeable layers, but comparison of the permeability data shows that the values for both specific gravity fractions are similar, suggesting that the fractures and the grain boundaries are more permeable than the larger voids.

On the other hand, the larger values of water absorption of the lower specific gravity fraction relative to those of the higher fraction (average of 4.9 and 1.7 percent by weight, respectively, for vacuum saturation) indicate that the larger voids in the chert with less than 2.5 sp gr can become saturated and are not isolated. This combination of high porosity and moderate permeability (about 10^{-4} darcys) might produce high external pressures in the surrounding paste (77). The same would be true for the chert with higher specific gravity, but to a lesser degree.

In subsequent rapid freeze-thaw tests, the chert with less than 2.5 sp gr had a mean durability factor of only 6.0 and the chert with greater than 2.5 sp gr had a mean value of 27.0, based on 300 cycles.

Aggregate C

Petrographic examination of aggregate C revealed no characteristic that could be regarded as deleterious. This aggregate contained no voids visible with the petrographic microscope, and its average vacuum-saturated absorption was only 0.24 percent, unusually low for a limestone. Its permeability was too small to be measured with the equipment used in this program. The few limonite-stained fractures and stylolites observed in most of the particles were not regarded as important to freeze-thaw durability. The clean surfaces and angular particle shapes produced a very strong bond with the paste in the concrete test specimens.

As predicted by the petrographic determinations, aggregate C showed excellent resistance to freeze-thaw deterioration. It had the highest durability factor (98.1) of all the test aggregates.

Aggregate D

Aggregate D offered the petrographer an excellent opportunity to apply his skills to the prediction of freeze-thaw behavior. The limestone and dolomitic limestone with less

than 2.5 sp gr had the following characteristics that might at first be considered deleterious: (a) some particles were laminated; (b) most samples contained up to 1 percent pyrite and abundant interstitial and some surficial limonite; (c) all particles contained numerous interstitial voids, ranging up to 11 percent by volume in the most porous samples; (d) some particles contained chert lentils; (e) most particles contained continuous limonite-stained and calcite-healed fractures.

The lamination was a textural feature expressed only by abrupt changes in grain size normal to bedding, not by structural weaknesses such as schistocity or cleavage, and would not contribute to freeze-thaw susceptibility. The pyrite content was generally small and probably did not affect the test results, although prolonged exposure might produce discoloration or pop-outs. Although chert lentils were noted in thin section, none were found in the aggregates in the concrete specimens and their effect could not be seen. However, concrete with a coarse aggregate of chert extracted from this limestone had very poor freeze-thaw durability, suggesting that the chert lentils in the limestone might also be deleterious.

Except for the absence or scarcity of large interstitial voids, most of the limestone and dolomitic limestones with greater than 2.5 sp gr resembled the fraction with lower specific gravity. Both fractions contained fairly abundant continuous microfractures, which were expected to produce a relatively high permeability. Furthermore, the numerous voids could be expected to substantially increase the absorption and the permeability of the lower fraction. As seen in Appendices B and E, however, the measured permeabilities of the two fractions are similar, although the fraction with less than 2.5 sp gr is more than twice as absorptive. This would indicate that permeability is governed by the fractures.

It is also of interest to note here the large difference between the values for vacuum-saturated absorption and 24-hr immersion saturation. After 24-hr immersion, the degree of saturation is only about two-thirds and three-fourths, respectively, of that for vacuum saturation. In service and under rapid-freezing test conditions, the large voids in the fraction with less than 2.5 sp gr probably never attain or retain a harmful degree of saturation, and therefore are not deleterious. For this fraction, values of 98 to 99 percent were obtained for vacuum-saturated degree of saturation, but the smaller voids in the aggregate and in the cement paste would probably compete successfully with the large voids for water before freezing begins.

The 300-cycle durability factors were 89.6 for the fraction with greater than 2.50 sp gr and 88.9 for the lower fraction. These results appear to verify the statement of Swenson and Chaly (*70*): "Large voids in aggregates are drained by the smaller voids in the paste. . ."

Aggregate E

Nearly 90 percent of aggregate E consisted of weathered chert with less than 2.50 sp gr, and only that fraction was present in quantities sufficient for complete testing. Petrographic examination predicted poor freeze-thaw durability. Most particles had smooth limonite-stained surfaces, which in subsequent tests exhibited poor bond with the paste. In the concrete cylinders that were ruptured by freezing, most of the coarse aggregate was completely dislodged from the paste in the vicinity of the fractures.

The main reason for suspecting that this fraction would not be durable, however, was the presence of the dolomolds (see Appendix C), which constituted up to 9 percent by volume of most samples. These rhomb-shaped cavities were responsible for the high absorption (averaging 7.7 percent by weight for vacuum saturation). Unlike the voids in aggregate D, the dolomolds, for the most part, were isolated from the rest of the system. Apparently the only path for the water into and out of these voids was along a network of very fine microfractures that occurred in most samples, particularly in the chalcedony-rich parts. Except for the microfractures, the chert matrix surrounding the voids appeared in thin section to be very dense. Once the dolomolds were saturated, water could not readily be removed and a dangerous degree of saturation was probably retained. (High absorption values indicated that nearly complete saturation was possible.)

This chert had the lowest measured permeability of all the test aggregates. Upon freezing it would be expected to develop high internal pressures because of hydraulic pressure—that is, the critical-size effect (*77*). In actual service it has been classified as poor, and in this program nearly complete destruction (durability factor of only 0.7) occurred after five or six freeze-thaw cycles.

Aggregate F

Aggregate F was known to have poor resistance to frost action and was examined for this reason. The material tested had greater than 2.5 sp gr and ranged from relatively fresh lithographic limestone to fine- and medium-grained fresh and weathered dolomitic limestone and dolomite (see Appendix C). Studies of thin sections revealed that some varieties were laminated and some contained organic matter, pyrite, chalcedony, and limonite. None of these appeared to be deleterious in rapid freeze-thaw testing, but they would undoubtedly affect the overall performance under service conditions. Although the dolomite itself might be deleterious as the result of dedolomitization reactions, examination of the ruptured concrete specimens indicated that both the dolomite-poor and the dolomitic aggregates were susceptible to freeze-thaw damage. Some of the more dolomitic rocks were highly weathered and contained interstitial voids that were easily visible in thin section, but much of the fraction with less than 2.5 sp gr was very fine grained, and porosity and pore distribution could not be accurately determined in thin section. An average value of 4.60 percent by weight was obtained for vacuum-saturated absorption, even though the average degree of saturation was only about 80 percent.

Several factors appeared to be responsible for the susceptibility of this aggregate to freeze-thaw damage. In the ruptured test specimens the weathered and porous dolomites and dolomitic limestones showed a very poor bond with the paste. Any dilation of the particles destroyed the

bond and concentrated the stresses in the enclosing paste. In some of the concrete specimens fracturing was confined mostly to the paste, with some spalling of the aggregates occurring near the surface. Here, it would be worthwhile to determine the difference in the coefficients of thermal expansion of the paste and the aggregate. In addition, because of their very fine grain size some of the limestones and dolomitic limestones probably retain more interstitial water during freezing than does the cement paste. That concept has been favored for this particular aggregate (*34*) as well as for others (*64, 77, 38*).

In the test aggregate, several potentially dangerous characteristics were observed, but the effect of each appeared to be impossible to determine without a more selective freeze-thaw program. The need for narrower selection may be reflected in the wide range of durability factors (32.4 to 90.0) obtained for aggregate F.

Aggregate G

The sandstone-calcareous sandstone-arenaceous limestone fraction of aggregate G was tested because its durability was thought to be intermediate between that of the best limestones and the poor cherts. Petrographic analyses revealed this fraction to be a poorly indurated, weathered porous rock, which most petrographers would consider an unsound concrete aggregate.

A value of 7.94 percent by weight was obtained for vacuum-saturated water absorption on a single representative sample. There were no large voids to account for this high porosity, but small limonite-filled interstitial voids were abundant in all samples. Permeability data are lacking, but the values would probably be high.

Such a combination of porosity and permeability would be likely to permit movement of water from the aggregate under proper drainage conditions, but with poor drainage and rapid freezing the small size of the pores (as compared to those in aggregate D) would probably be sufficiently restrictive to make this weak aggregate fail. In the present study, the aggregate G sample had a durability factor of only 12.7.

DISCUSSION AND EVALUATION

Rigorous evaluation of concrete aggregates must include not only identification of their deleterious characteristics, but also an assessment of the possible contribution of each to failure under given conditions. In other words, it can only be achieved through a well-controlled selective testing program.

As demonstrated by this program and others, petrographic examination of concrete aggregates can be useful in determining the occurrence of deleterious features. Additional data, particularly those from pore studies, may be necessary to evaluate the possible effects of these features on the durability of the aggregates. As the results of more testing programs become available, petrographic examination can assume a more important role in aggregate evaluation.

In the study here reported, smooth weathered surfaces and high porosity appear to be responsible for freeze-thaw failures in aggregates B, E, F, and G, but as stated here and in numerous other reports, high porosity alone does not necessarily indicate an unsound rock. Although the fraction of aggregate D with less than 2.5 sp gr had an average value of water absorption more than twice as large as the fraction with greater than 2.5 sp gr, both had similar permeability and behaved similarly in the rapid freeze-thaw tests, suggesting that the larger pores do not retain a harmful degree of saturation. By determining the size, shape, and distribution of pores, petrographic analysis can aid in interpreting the relationship of porosity, absorption, permeability, and degree of saturation.

Petrography alone cannot disentangle and isolate all possible effects of the several potentially deleterious features that occur in most aggregates. After the characteristics directly related to freezing and thawing of water within concrete and aggregate have been determined, as well as those related to undesirable thermal expansion and chemical reactivity, petrography can be a valuable tool, perhaps the most valuable, for evaluating aggregate soundness.

CHAPTER SIX

THE POWERS TEST

The tests described in the previous chapters dealt with identification of frost-susceptible aggregate particles. This chapter reports a study of frost susceptibility of concrete incorporating the aggregates. The purpose was to evaluate a test method that would provide a link between the individual particle tests and the behavior of concrete under natural freezing conditions. The method proposed by Powers (*56*) was investigated because of its realistic approach to laboratory simulation of frost action in concrete.

POWERS' FREEZE-THAW METHOD

In view of his theories regarding the nature of frost destruction (see Chapter Two), Powers reasoned that the usual rapid freeze-thaw test methods could overestimate

the susceptibility of concrete to frost destruction, because unnaturally high freezing rates tend to produce excessive hydraulic pressures. On the other hand, owing to the absence of an extended period of low temperatures, the tests could underestimate potential frost damage caused by the growth of ice lenses. He further noted that existing methods failed to provide an opportunity for the specimens to experience the occasional drying periods usually encountered in the field.

Proposed Test Procedure

To circumvent those deficiencies, Powers proposed a new freeze-thaw test method. In the procedure he describes, the concrete specimens are cooled from room temperature to 0 F at a rate of approximately 5 F per hr, held at the low temperature for an extended period of time, and thawed in water at room temperature. The thawed specimens are stored in water for two weeks, and the cooling cycle is then repeated. During the cooling cycles continuous measurements are made with suitable strain measuring apparatus. The cycles are repeated until dilation occurs in a specimen, signifying the end of the period of frost resistance for that specimen. The specimens would contain sufficient entrained air to inhibit deleterious action of frost in the paste phase. His procedure for curing the specimens incorporates a two-week drying period.

Previous Applications

Tremper and Spellman (*75*) in 1961 reported the first use of the Powers test. The procedure they employed differed from Powers' only in minor respects. Aggregates selected by this method were used in 70 miles of concrete pavement traversing areas subject to severe winter conditions. The pavement has fared well through five winters, even though some of the aggregates would have been rejected by the rapid freeze-thaw tests. On the basis of Tremper and Spellman's work, the California Division of Highways adopted a slightly modified version of the Powers method as a standard test procedure for frost evaluation of concrete aggregates.

A second application of the Powers test was reported in 1963 by Wills et al. (*88*), whose equipment and methods varied slightly from both the Powers and California methods.

Aspects Requiring Clarification

The two laboratory evaluations cited indicate that the Powers test holds considerable promise, but they leave several important areas unclarified. Powers advised using the first occurrence of dilation as the criterion for the limit of frost resistance. Wills concluded that the first occurrence of either dilation or permanent length change signifies the start of destructive action. Tremper and Spellman suggested that an aggregate could be considered satisfactory if at least 65 percent of the specimens displayed less than 50 μin. per in. dilation and final length changes were less than 0.006 percent.

Powers did not specify strain measuring equipment for the proposed test. Tremper and Spellman obtained excellent results with linear-differential variable transformers (transducers). Wills and coworkers used dial gages, which are much less sensitive, and this might in part account for the difference in opinion regarding the most appropriate measure of frost destruction.

Other areas that were not clarified by the two previous investigations included the effects of aggregate conditioning, minor variations in air voids systems, low temperatures over extended periods, specimen conditioning, microcracking of the paste phase, and the ratio of specimen size to aggregate size. Also unexplored were the nature of the deterioration function when critically saturated concrete is subjected to additional cooling cycles, and laboratory-field correlations.

TEST METHOD

The research here described sought to resolve all areas of uncertainty in the Powers method except the establishment of laboratory-field correlations. A full account of the investigation is given by Cady (*13*).

Experimental Design

Owing to the space, equipment, and time limitations, the experimental work was conducted in two phases, as shown in Figures 23 and 24. Phase I was designed to provide information on the size ratio of specimen and aggregate, effects of minor (inherent) air-parameter variations, and effects of holding specimens at a low temperature for several hours; to evaluate the test equipment; and to determine the interrelations among test variables. Phase II was designed primarily to discover the most reliable indicators of frost damage, to evaluate the effect of a drying period on test results, and to examine the nature of the deterioration functions. It also included a study of microcracking during freeze-thaw cycles and its relation to frost damage.

Aggregates

The test aggregate comprised 50 percent of the coarse aggregate in each mixture and was confined to the ½-in. to ¾-in. and the ¾-in. to 1-in. size fractions. The rest of the coarse aggregate, evenly divided between the No. 4 to ⅜-in. and ⅜-in. to ½-in. size fractions, was either White Marsh gravel for tests of river-gravel-type aggregate, or Benner and Snyder limestone for tests of crushed-limestone-type aggregate. Because these aggregates are known to exhibit exceptionally high frost resistance, their presence could not significantly affect the test results. Moreover, according to the "critical size" concept it is the larger fractions that are most vulnerable to frost action. This procedure greatly simplified preparation of the coarse aggregates, because the need for specific gravity and petrographic fractionation of the smaller fractions was obviated.

One mix was an exception. In Phase II the specimens containing Paducah River gravel were composed of this aggregate only, split evenly into the four size fractions.

Immediately before they were incorporated into the mixtures, the coarse aggregates were vacuum saturated at

Aggregate	Replica Mixture[a]	Specimen Size (in.)	Specimen Number: Cycle R[b]	Specimen Number: Cycle S[c]
White Marsh gravel	1(5)	3 x 6	1 2 3	4 5 6
		4 x 8	1 2 3	4 5 6
	2(4)	3 x 6	1 2 3	4 5 6
		4 x 8	1 2 3	4 5 6
Paducah river gravel	1(6)	3 x 6	1 2 3	4 5 6
		4 x 8	1 2 3	4 5 6
	2(1)	3 x 6	1 2 3	4 5 6
		4 x 8	1 2 3	4 5 6
Eagle City and Maynes Creek limestone	1(2)	3 x 6	1 2 3	4 5 6
		4 x 8	1 2 3	4 5 6
	2(3)	3 x 6	1 2 3	4 5 6
		4 x 8	1 2 3	4 5 6

[a] Numbers in parentheses are random order of batch production. Curing procedure: 1 day in molds, 13 days in limewater, 7 days in air at 77 ± 2 F and 47 ± 2 percent relative humidity, and 14 days in water at 35 ± 2 F.
[b] Cooled at 5 F per hr to 15 F, then placed in 35 ± 2 F bath.
[c] Cooled at 5 F per hr to 15 F, held at 15 F for 20 hr, then placed in 35 ± 2 F bath.

Figure 23. Phase I experimental design.

15 mm Hg (absolute) for 1 hr and soaked an additional 23 hr.

The fine aggregate used throughout was a high-grade quartz river sand. The characteristics of this material are given in Table E-8.

Cement

A blend of three low-alkali Type I cements was used throughout both phases of the work. Table E-7 gives results of pertinent physical and chemical tests of each of the component cements and the composite test cement, which consisted of two parts each of cements B and C and one part of cement A. Low-alkali Type I cement was chosen to minimize the possibility of alkali-aggregate reaction, which could distort results of the freeze-thaw tests.

Mixture Design

The basic design criteria for all concrete mixtures made for both phases of the experiment were: Cement factor, 5½ sacks per cubic yard; slump, 3 ± ½ in.; air content, 6 ± 1 percent. Table 14 summarizes the characteristics of all the test mixtures.

Mixture designs were carried out in accordance with the American Concrete Institute method (ACI 613-54). To obtain the desired air content, neutralized Vinsol resin was used as an air-entraining agent, and air contents were checked during mixing by the gravimetric method (ASTM C-138).

The cement blend and the coarse and fine aggregates were mixed 30 sec in a 1½-cu ft drum mixer rotating at 24 rpm. Water was then added, and mixing proceeded for 1 min. This was followed by a 1-min rest period and 2 min of mixing before the concrete was discharged. The specimens were cast in lightly oiled steel molds and transferred to the fog room. After 24 hr the molds were

PRIMARY EXPERIMENT

Aggregate	Specimen[a] Number: Curing Proc. X[b]	Specimen[a] Number: Curing Proc. Y[b]
Benner and Snyder limestone	1 2 3	4 5 6
Eagle City and Maynes Cr. limestone, >2.50 sp gr	1 2 3	4 5 6
Rapid and Coralville limestone, >2.50 sp gr	1 2 3	4 5 6
Paducah river gravel, 100 percent	1 2 3	4 5 6
Meramec gravel:		
>2.50 sp gr	1 2 3	4 5 6
<2.50 sp gr	1 2 3	4 5 6
Killins heavy-media reject, <2.50 sp gr:		
Calcareous sandstone and arenaceous limestone	1 2 3	4 5 6
Shale	1 2 3	4 5 6

MICROCRACK STUDY

Aggregate	No. of Freeze-Thaw Cycles[c]	Specimen[a] Number
Paducah river gravel	1	1
	2	5
	3	6
	4	3
	5	2
	6	4

[a] All specimens 3 in. diameter by 6 in. long.
[b] Curing procedure X: 1 day in molds, 13 days in limewater, 7 days in air at 77 ± 2 F and 47 ± 2% R.H., and 14 days in water at 35 ± 2 F. Curing procedure Y: 1 day in molds, 13 days in limewater, and 21 days in water at 35 ± 2 F.
[c] Freeze-thaw cycle: Cool at 5 F per hr to 15 F, then place in 35 ± 1 F water bath.

Figure 24. Phase II experimental design.

removed, the specimens were numbered, and the curing procedures (Figs. 23 and 24) were initiated. Stainless-steel gage studs were cast or drilled into the ends of the specimens to facilitate length measurements.

EQUIPMENT DESIGN AND CALIBRATION

Cooling and Storing Facilities

A 35 F constant-temperature bath was used in the specimen conditioning processes and for specimen storage between cooling cycles. The desired temperature was maintained within ± 2 deg with a thermostatic system linked to a solenoid valve in the refrigerant inlet line. The bath temperature was monitored continuously with a recording gas bulb-type thermometer.

The cooling cycles were carried out in a refrigerated kerosene bath (Fig. 25) with thermostatic equipment similar to that in the constant-temperature bath. A propel-

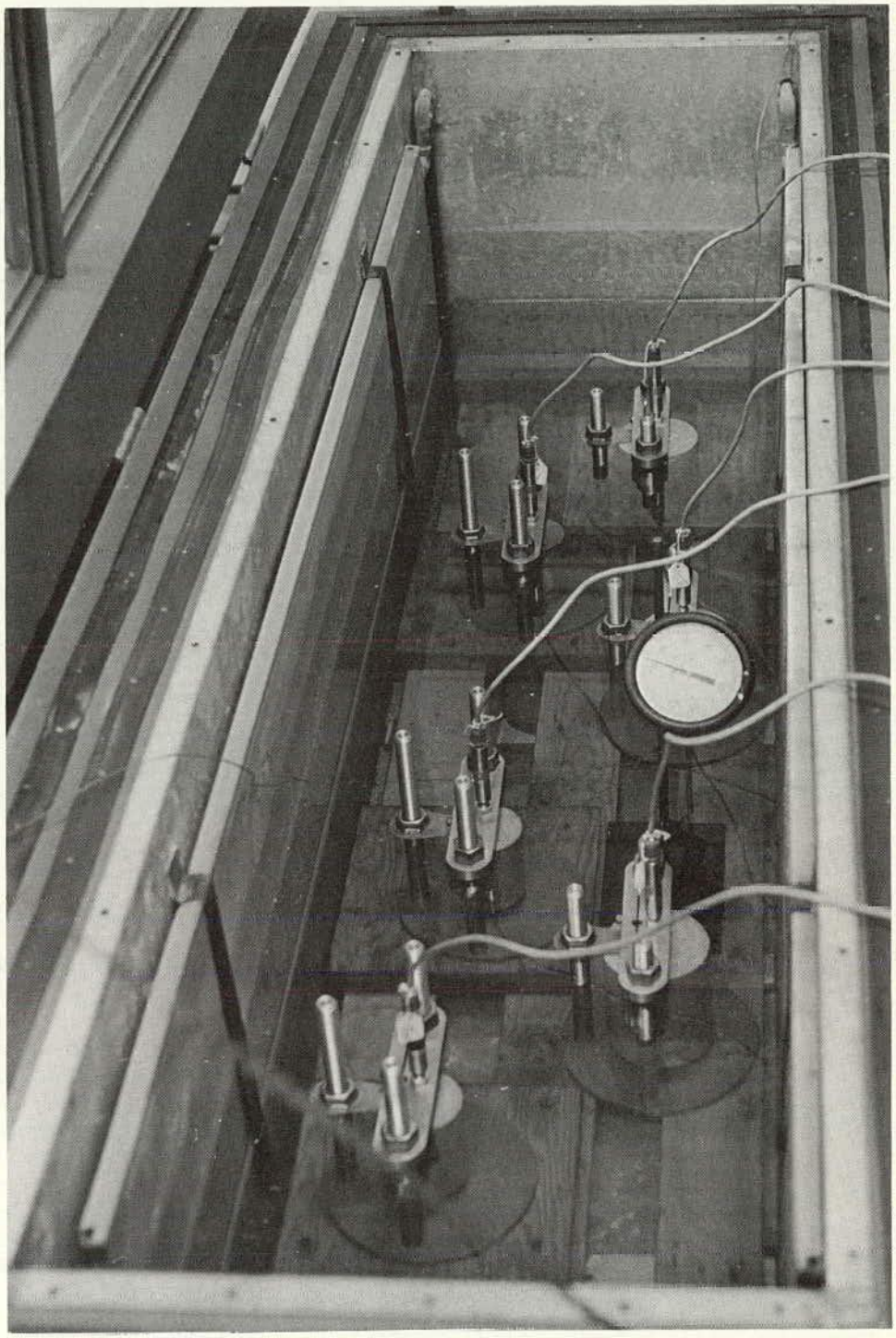

Figure 25. Cooling bath.

ler-type electric stirrer maintained temperature uniformity during the cooling process.

Instrumentation

The instrumentation used to provide a continuous record of length changes of the specimens during the cooling cycle was similar to that described by Tremper and Spellman (*75*). The basic installation (Fig. 26) consisted of strain frames for supporting the specimens, linear differential variable transformers (transducers) to detect length changes, and related instruments, and was capable of detecting length changes of 10^{-6} in. The related instrumentation (Fig. 27) consisted of an amplifier-indicator to supply transducer electrical input and provide scalar adjustment of the transducer output signal, a switching

TABLE 14

CONCRETE MIXTURE CHARACTERISTICS

AGGREGATE	MIX	SLUMP (IN.)	GRAV. AIR (%)	W/C RATIO
(*a*) PHASE I				
White Marsh gravel	1	2½	5.40	0.52
	2	3	5.39	0.51
Paducah River gravel	1	2¾	5.23	0.50
	2	3¼	6.63	0.57
Eagle City and Maynes Creek limestone	1	2½	6.61	0.55
	2	2¾	6.67	0.54
(*b*) PHASE II				
Benner and Snyder limestone		2¼	5.20	0.55
Eagle City and Maynes Cr. limestone, >2.50 sp gr		3	5.93	0.58
Rapid and Coralville limestone, >2.50 sp gr		3¼	6.47	0.59
Paducah river gravel [a]		3½	6.58	0.53
Meramec gravel, >2.50 sp gr		2½	6.37	0.54
Paducah river gravel, 100%		2¾	5.11	0.50
Meramec gravel, <2.50 sp gr		2¾	5.44	0.51
Killins gravel, calc. sandst. and aren. limestone		3	5.00	0.55
Killins gravel, shale		[b]	5.09	0.52

[a] Microcrack study.
[b] Mix too small to permit slump test.

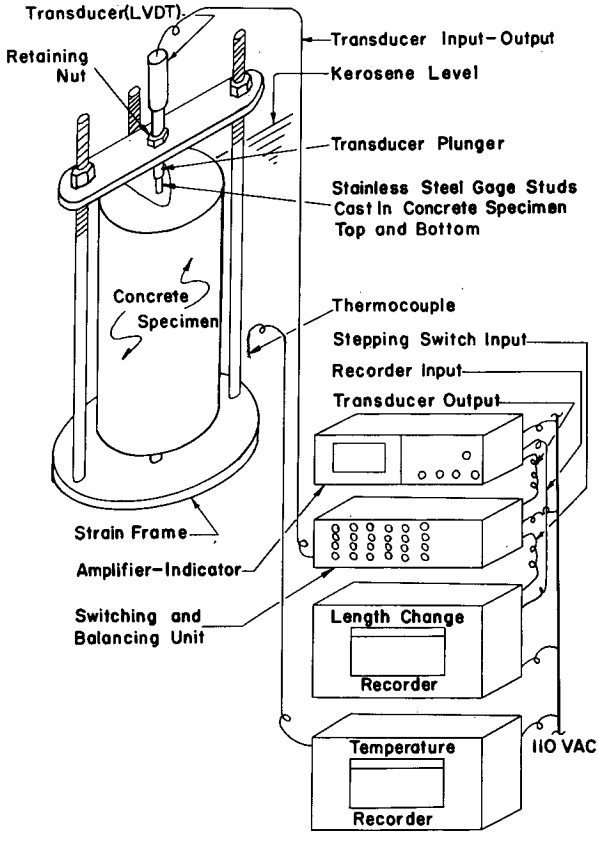

Figure 26. Length and temperature measuring system.

and balancing unit containing an individually calibrated balancing channel for each of the six transducers and a stepping switch to permit sequential reading of transducer outputs, a millivolt recorder containing six color-coded printing points to record the transducer outputs, and a recording potentiometer to provide a constant record of the kerosene-bath temperatures by means of a copper-constantan thermocouple. The millivolt recorder was the driver of the instrumentation train. As it stepped from point to point, it sent electrical impulses to the switching mechanism, which then activated the appropriate transducer channel.

Twelve strain frames were built to hold the specimens during the freezing cycles. Six of these were for specimens from 6 in. to 9 in. long and up to 4 in. in diameter. The remaining six were for specimens from 6 in. to 12 in. long and up to 6 in. in diameter. Figure 28 shows one of the smaller strain frames holding a 4 x 8-in. specimen. In this frame the bottom plate and yoke are ½-in. thick brass and the three threaded posts are ¾-in. Invar steel. The transducer is threaded into the yoke and tightened by means of a locknut.

Calibration of Strain-Measuring Facilities

The strain-measuring facilities were calibrated by obtaining length measurements while cooling material with known thermal-expansion properties. Invar steel was used for the reference material. A typical set of calibration curves and calculated calibration coefficients is shown in Figure 29.

ANALYTICAL DESIGN

Measured Variables

The length, weight, and dynamic modulus were determined for each specimen between the steps in the curing procedure and before and after every cooling cycle. Dilations and the temperatures of occurrence of dilations were obtained from the instrument charts for each specimen in every cooling cycle. Slopes of the cooling curves before and after dilation were also determined for the Phase I specimens. At the conclusion of the test cycles, air content and a spacing factor were determined for each of the Phase I specimens by linear traverse methods. These data are summarized in Tables E-7 and E-8.

Only the dilation variable requires explanation.

The Dilation Variable

As a critically saturated specimen is cooled below the normal freezing point of water, it contracts almost linearly until at some point a very rapid increase in length occurs. The rapid length change is not large, usually less than 25 μin. per in., and it occurs almost instantly. This phenomenon is termed the *first dilation,* and the temperature at which it occurs is called the *temperature of the first dilation.* Helmuth (*33*) has shown the first dilation to be the result of essentially instantaneous formation of dendritic ice in the interconnected capillaries of the concrete. The rapidity of the ice formation is attributed to

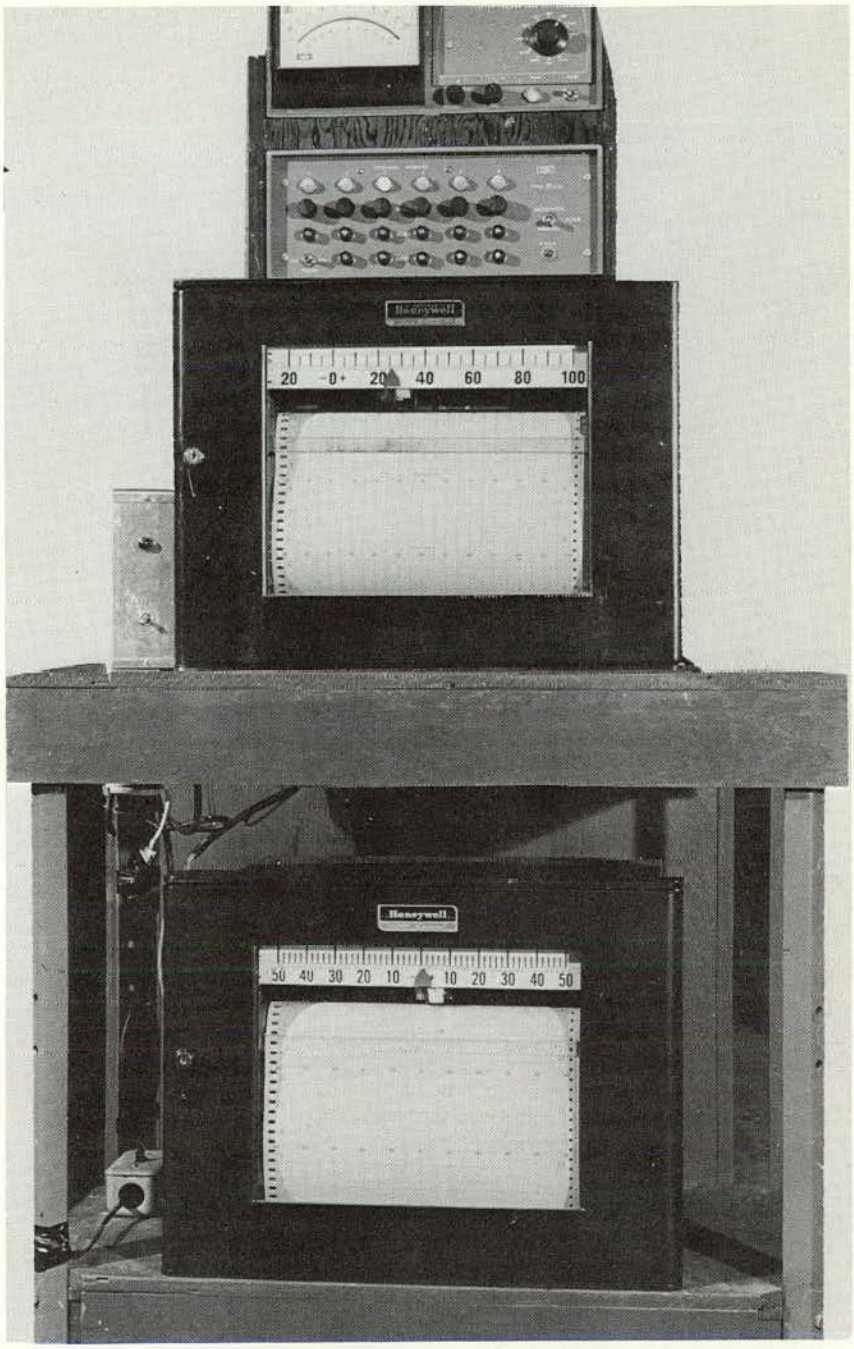

Figure 27. Length and temperature measuring instruments.

the fact that the water is supercooled. Dendritic ice propagation proceeds until all saturated voids larger than a critical size, determined by the temperature at which ice formation occurred, contain the fernlike growths.

Following the first dilation, the specimen continues to contract with decreasing temperature. If it is critically saturated, a second dilation, slower but more severe, occurs as the temperature decreases. According to Powers and Helmuth (*60*), the second dilation is caused by hydraulic pressure generated when the initial dendrites expand laterally and into ever smaller capillary pores. The second dilation continues with decreasing temperature until all freezable water has crystallized. At this point the specimen again starts to contract, but at a much greater rate than the initial contraction because of the high thermal coefficient of the ice in the pores and the stressed condition of the concrete.

As the number of cooling cycles for a given specimen increases, the first and second dilations move progressively closer together until they finally merge. At this point all

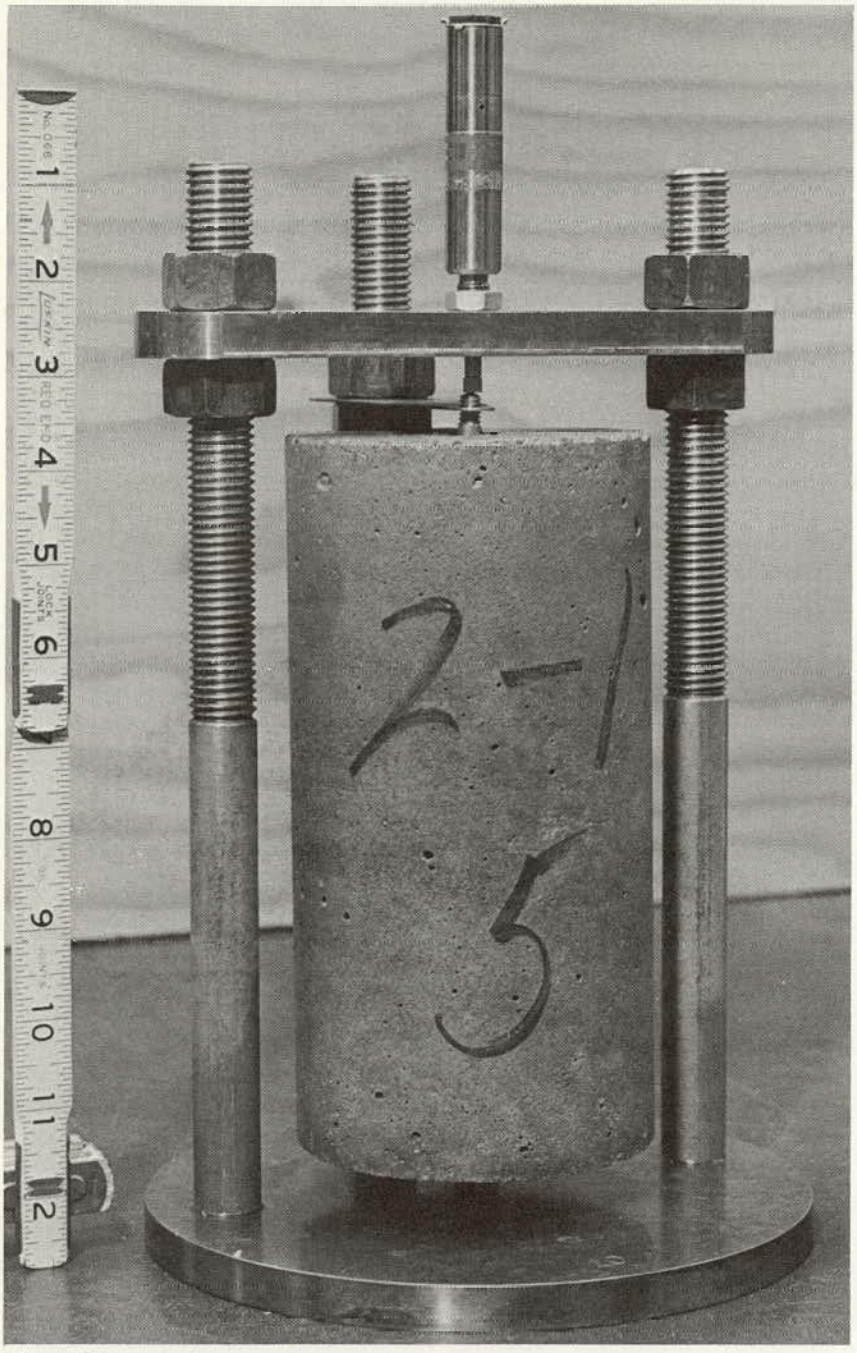

Figure 28. Strain frame with transducer (top).

penetrable voids are saturated, eliminating the pressure relief that accounts for the contraction between the first and second dilations in earlier cycles.

In the present research, second dilations were measured to the peak of the second dilation, from a straight-line continuation of the average slope of the length-change curve between the end of the first dilation and the beginning of the second dilation, or from a line parallel to the initial slope through the start of the second dilation. The temperature of the second dilation was taken to be the point at which the second dilation commenced.

The phenomena here described are well illustrated by the typical test chart shown in Fig. 30.

Correlation Analyses

All test variables from Phases I and II were subjected to symmetric correlation analyses, which served three purposes. First, the test methodology and results could be justified if those pairs of variables known to be related exhibited significant correlations in the analyses. Second, previously unknown relationships might evolve, as well as

correlations supporting or refuting previously unsubstantiated theory. Finally, correlation analysis would reveal, by association with known frost-damage indicators, which variables should be investigated further as measures of frost damage.

RESULTS AND DISCUSSION

The results of the correlation analyses for Phases I and II are shown in triangular matrix form in Figures 31 and 32.

Correlations with Existing Theory

Virtually all previously hypothesized and demonstrated relations among variables relevant to frost action in concrete were substantiated by the correlations. The increase in permanent length with increasing cycles observed by Powers (*57*) and Wills (*88*) was a notable exception. The absence of a significant correlation between these two variables may have resulted from difficulties experienced in obtaining sufficiently accurate length measurements with the dial-gage comparator.

Only one major conflict with existing theory was found in the correlations. This was an inverse relationship between the number of cooling cycles and the temperature of the first dilation, directly contradicting Helmuth's postulation (*33*) that the temperature at which the first dilation occurs is a random function. But the observed correlation can be explained on the basis of existing theory.

Assume that the air voids become progressively saturated under increasing freeze-thaw cycles. Until these voids are totally saturated, the moisture present is free surface moisture, and as such it freezes at or near the normal freezing point. The air-void ice, because of its lower free energy (entropy), attracts capillary water, which freezes upon contact with the ice. In the early cycles this would promote hydrostatic tension in the capillaries, favoring higher initial freezing temperatures. As the cooling cycles progress, increasing numbers of the air voids become filled and the water in them does not freeze near the normal freezing point. Hydrostatic tension due to entropy difference therefore decreases, and is replaced by hydraulic pressures associated with the volume change produced by crystallization of water. The overall increase in hydraulic pressure is conducive to lower freezing temperatures.

It can be concluded that the general agreement with previously established or hypothesized correlations validated the test method and analyses employed here.

New Correlations

Several previously unknown or unpublished correlations were revealed. Because interrelations among the variables produce a certain degree of redundancy, only the more important new correlations are described.

The slope of the length-temperature curve before dilation was shown to increase with progressive freeze-thaw cycles. This phenomenon has not been mentioned in the literature, and its occurrence is difficult to reconcile. One possible explanation, which ties in closely with the rationalization of the difference between Helmuth's theory and the observed data, is as follows:

Assume, as before, that air voids become progressively filled with water as freeze-thaw cycles progress. As the ice bodies formed in the air voids attract capillary water, owing to free energy differences, the air voids compete with the gel for capillary water during the cooling period and might even be able to extract water from the gel itself. During this period the gel is becoming less saturated because of its increased capacity for moisture absorption. Therefore, in addition to thermal shrinkage and drying shrinkage as the result of increased moisture capacity, additional shrinkage may possibly occur by attraction of gel water to air-void ice, or at least by retardation of the opposed swelling tendency through active competition for the available capillary water.

The observed correlation between first dilation and the slope of the length-temperature curve before dilation tends to support that theory for the correlation between cycle number and slope. In other words, the dilation increases as the amount of freezable water increases. If the increase in water occurs in air voids, as it almost surely

Channel No.	Transducer No.	Lead No.	Strain Frame No.	Invar Bar Length (in.)	Calib. Coeff. (μin./°F)*
1	276-A95	A-95	7	6	+1.2
2	443-A15	A-15	8	6	+3.8
3	443-A17	A-17	9	6	+3.1
4	443-A18	A-18	10	8	+3.4
5	443-A20	A-20	11	8	+6.3
6	443-A24	A-24	12	8	+1.0

* To be subtracted from specimen readings.

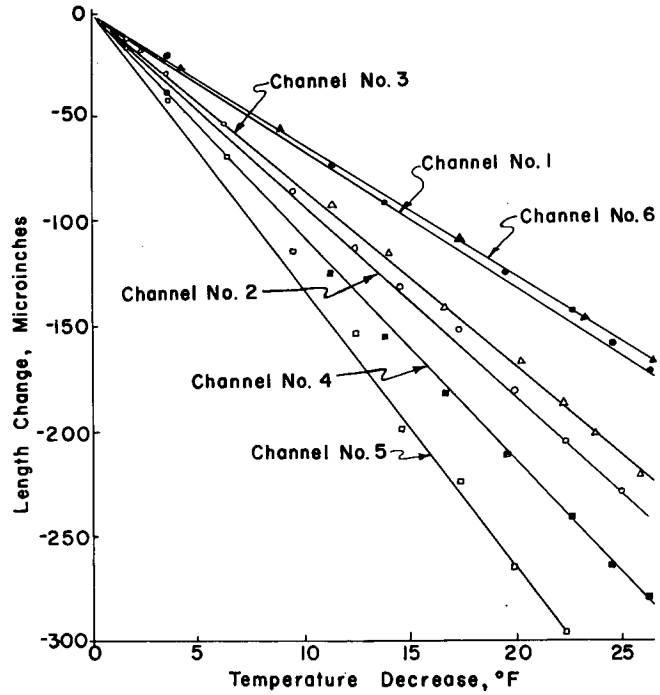

Figure 29. Strain frame and transducer calibrations.

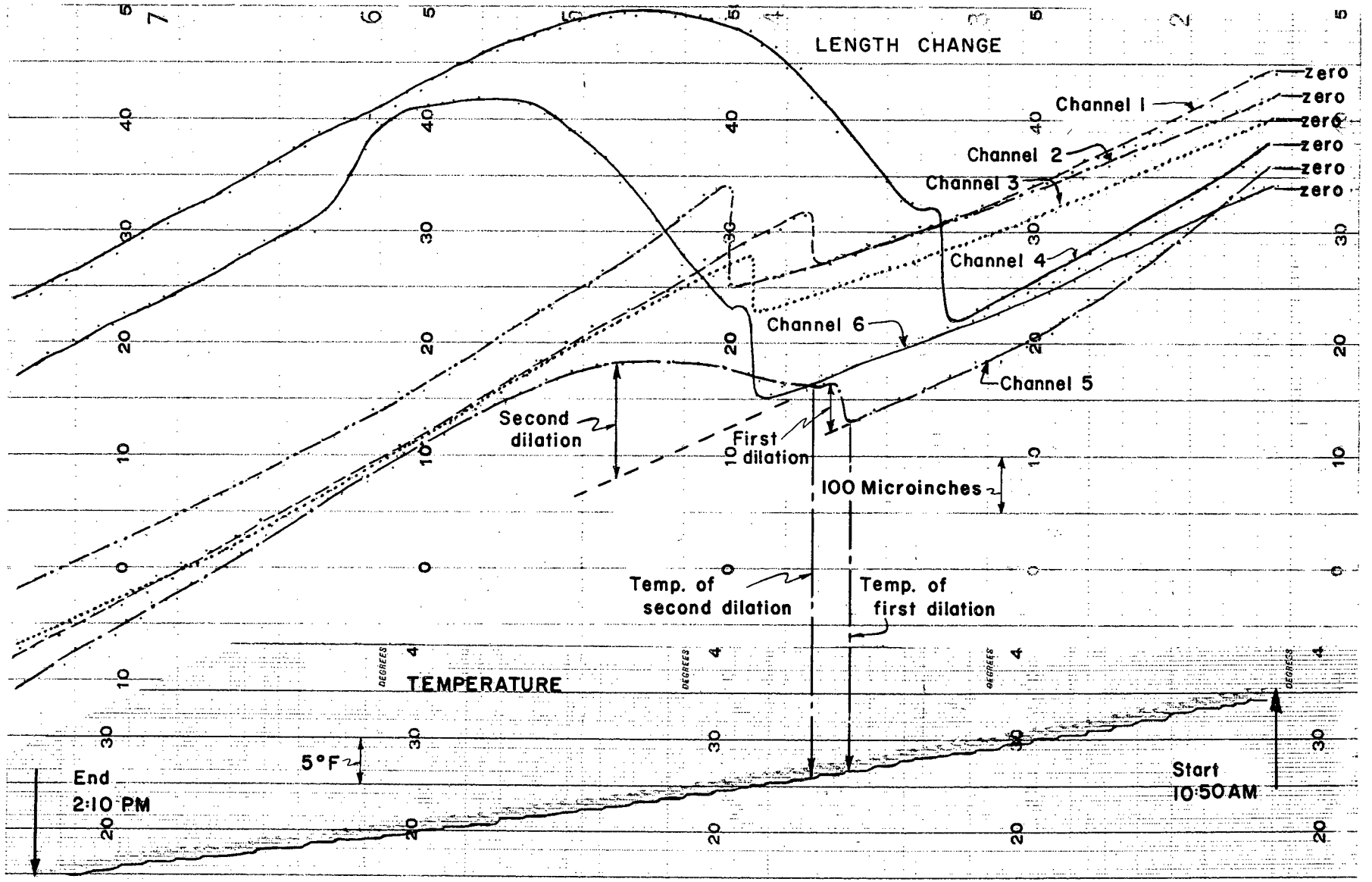

Figure 30. Typical length and temperature charts.

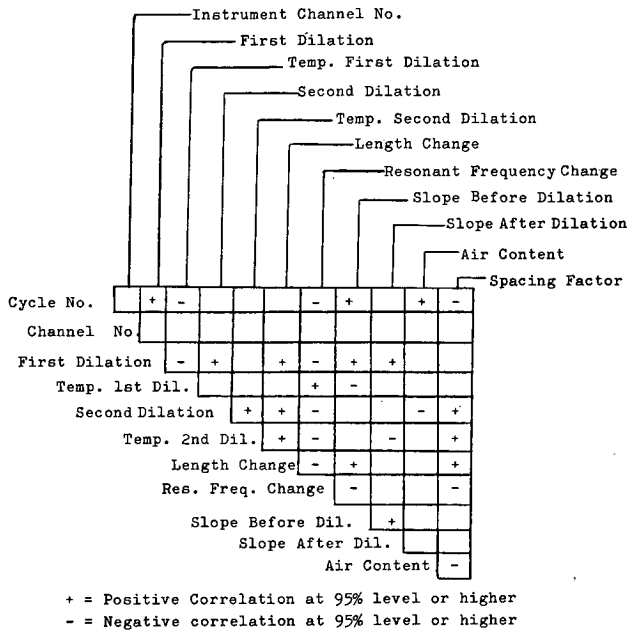

Figure 31. Correlation of test variables, Phase I.

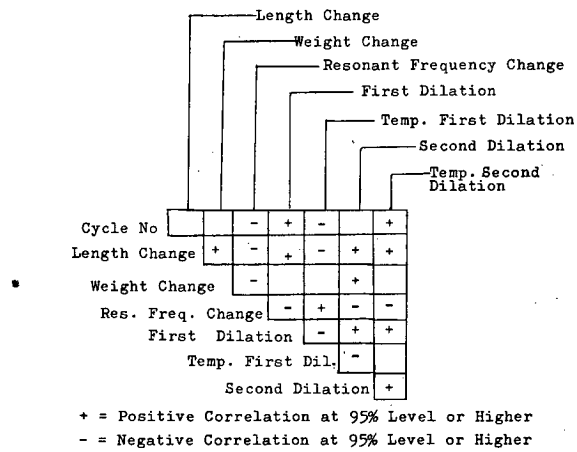

Figure 32. Correlation of test variables, Phase II.

must for soaked specimens, the conditions hypothesized for increasing the initial slope are present.

The negative correlation between first dilation and temperature of the first dilation is easily explained. As the temperature at which dilation occurs becomes lower, the degree of supercooling increases and the larger amount of dendritic ice, with its consequence of greater hydraulic pressures, produces greater dilation. The temperature of the second dilation was shown to increase with increasing second dilation, just the opposite of the negative correlation between temperature and amount of the first dilation. However, the two phenomena are basically different.

The first dilation results from the near-instantaneous formation of dendritic ice growths in the interconnected capillaries of the concrete, which include the penetrable pores of the aggregate particles. The second dilation results from hydraulic pressure generated by lateral growth of the dendrites. If the paste phase is protected by sufficient air voids, providing relief points for the hydraulic pressure, the second dilation is primarily a function of the coarse aggregate properties. Therefore, if the coarse aggregate particles are critically saturated and freezing produces excessive hydraulic pressure, a second dilation occurs. Otherwise, no second dilation will be observed.

Inasmuch as the second dilation, after its initial occurrence, increases rapidly in magnitude with each succeeding freeze-thaw cycle, it is evident that the coarse aggregate becomes more saturated with each succeeding cycle. This gain in saturation results from water being forced into the aggregate from the paste during the early stages of freezing, and from water absorbed during the soaking period between cycles. The consequence is earlier generation of disruptive hydraulic pressures, and the second dilations therefore occur at successively higher temperatures, with increasing magnitude of dilation. The test data revealed, however, that after the temperature of the second dilation reached approximately 25 F it remained relatively constant with succeeding cycles, even though the magnitude of the dilations continued to increase.

Three of the correlations shown in Figures 31 and 32 are considered to be invalid. The apparent correlations between cycle number and air content and between cycle number and air-void spacing are nonsensical. They merely reflect the fact that specimens with low air content (large spacing factors) failed during early cycles and were dropped from the test program. The third case is the negative correlation between the temperature of the second dilation and the slope after dilation.

This negative correlation conflicts with several other correlations. As the temperature of the second dilation increases, indicating increases in saturation, the slope after dilation would also be expected to increase owing to the high thermal coefficient of ice. A circumstance of the test probably explains the conflict. As the second dilation temperature increased and second dilations became very large, the end point of the test (15 F) was reached before dilation was completed and before the specimens had returned to normal contraction patterns. If the tests had been carried to some lower temperature, the final slopes might have been much greater and the correlation between slope and temperature of the second dilation might have been positive.

Measures of Frost Damage

Three proposed measures of frost damage were investigated—resonant frequency change, permanent length change, and dilations. Significant correlations were found between all possible pairs of these variables in both test phases. This suggests that they are mutually related and are therefore comparable in relating phenomena associated with any one measure.

Degradation in resonant frequency (relative sonic modulus) is a commonly accepted measure of frost destruction in concrete. Permanent length change, which is the end result of frost action, would appear to offer

TABLE 15

ANALYSIS OF VARIANCE, PHASE II DATA

VARIABLE	SOURCE OF VARIATION	CYCLE 1		CYCLE 2		CYCLE 4		CYCLE 8	
		F RATIO	SIGNIF-ICANCE[a]	F RATIO	SIGNIF-ICANCE[a]	F RATIO	SIGNIF-ICANCE[a]	F RATIO	SIGNIF-ICANCE[a]
Δ Length	Treatment	27.0615	95	55.9638	95	9.5650	95	6.4014	95
	Agg. type	17.0939	95	29.8373	95	1.8262	None	3.0943	None
	Interaction	11.1103	95	28.0722	95	1.7519	None	2.8854	None
Δ Weight	Treatment	0.0026	None	2.9919	None	5.0567	None	0.5915	None
	Agg. type	15.5022	95	9.2924	95	17.5254	95	29.0534	95
	Interaction	13.3201	95	5.2073	95	0.5764	None	1.4275	None
Δ Resonant freq.	Treatment	85.6333	95	48.2555	95	41.5328	95	8.3587	95
	Agg. type	41.3464	95	29.3821	95	6.1260	95	4.9253	95
	Interaction	39.2007	95	29.0582	95	4.0210	95	4.3041	95
Total dilations	Treatment	259.0035	95	76.9431	95	38.7579	95	59.7603	95
	Agg. type	142.4559	95	41.8167	95	5.9716	95	5.6378	95
	Interaction	141.5525	95	39.3494	95	5.1869	95	4.6763	95
Temp. at start of dilation	Treatment	13.7486	95	27.0336	95	1.5707	None	4.2374	None
	Agg. type	48.8797	95	56.4692	95	11.0473	95	3.2349	None
	Interaction	2.8360	95	2.0076	None	0.8494	None	1.9210	None

[a] 95 = Significance level of 95 percent or better.

a sensitive and accurate measure of frost action. Specimen length is strongly influenced, however, by temperature and moisture conditions, and this tends to make permanent length change measurements unreliable. These two measures of frost damage are static measures; that is, they are determined after the fact. Dilations during the cooling cycles are dynamic manifestations of the action of frost in concrete. Therefore, theoretically, dilations should be the most reliable measure of frost damage.

Analyses of variance performed on data from the first, second, fourth, and eighth cooling cycles of the Phase II specimens revealed that, of the three proposed measures of frost damage, total dilations (first dilation plus second dilation) provided the best discrimination among the aggregate types. Permanent length change failed to show significant differences in the later cycles. Change in resonant frequency revealed significant differences (95 percent confidence) among aggregate types in all cycles, but at lower significance levels than those given by total dilations. The analyses of variance are summarized in Table 15.

Deterioration Function

Permanent length change, total dilation, and resonant frequency data from Phase II were examined to determine whether any of these variables fit the mathematical model of specimen deterioration given by Powers (*56*):

$$D = A^n \tag{10}$$

in which

D = amount of permanent elongation;
A = a constant characteristic of the specimen; and
n = number of cycles after permanent elongation first appears.

To permit a linear regression of the cycle versus test parameter data, some manipulations of the mathematical model and the data were required. Reduced to logarithmic form, Eq. 10 becomes

$$\log D = n \log A \tag{11a}$$

or

$$n = (1/\log A) \log D \tag{11b}$$

in which A and n have the same connotation as before and D is the test parameter. The linear model expressed by Eq. 11*b* requires logarithms of the test parameters. Because zero and negative values occur in all of the test parameters, the following alterations were performed to make them amenable to use in Eq. 11*b*:

$$\Delta L' = \log (\Delta L + 1{,}650) \tag{12a}$$
$$\Delta RF' = \log (-\Delta RF + 350) \tag{12b}$$
$$D' = \log (\text{total dilation} + 10) \tag{12c}$$

Each of the adjusted test parameters for the 17 specimen sets was submitted to linear regression analysis. The results are summarized in Table 16. Again, using an entirely different approach, dilation is seen to be the most dependable indicator of concrete behavior in the Powers freeze-thaw tests. In view of these results, only total-dilation data are further discussed in relation to the deterioration function.

Because for all practical purposes D' = log total dilation, the following general equation may be written to represent the regression equations for total dilation:

$$\text{Total dilation} = (\text{antilog } M)^n (\text{antilog } I) \tag{13}$$

in which M and I are, respectively, the slope and intercept of the linear regression equation. Eq. 13 can be further reduced to

$$D = BA^n \tag{14}$$

TABLE 16

DETERIORATION FUNCTION CORRELATIONS, 17 CASES

PARAMETER	NUMBER OF RESULTS	
	95% SIG.	99% SIG.
$\Delta L'$	7	4
$\Delta RF'$	7	5
D'	14	13

in which A and B are constants for given aggregate-treatment combinations and are equal, respectively, to antilog M and antilog I.

When the aggregate types were arranged in order of decreasing durability factors as determined in the ASTM C290 rapid freeze-thaw test (see Appendix D) and compared with the A and B factors, it was found that B increased with decreasing durability factor for both types of specimen treatment, and that B was greater for the specimens that did not undergo a drying period than for those that did. The A factor was also generally greater for the specimens that did not undergo a drying period, but it was quite random with respect to relative frost resistance according to ASTM C290. These observations are shown in Table 17.

Using Eq. 14 and the A and B factors, theoretical eighth-cycle total dilations (microinches) were calculated. These results were arranged in the order of increasing dilations for each type of treatment and compared with the rating according to decreasing durability factors. The results are given in Table 18.

Except for the reversed positions of the Meramec <2.5 sp gr and the Killins aggregates in the "saturated" cases, the dilation results from the Powers method rated the aggregates in the same order as did the rapid freeze-thaw tests. It therefore appears that the rapid freeze-thaw method, which has been severely criticized in the literature (*34*) for alleged poor laboratory reproducibility and severity of test conditions, is equally capable of rating aggregates according to frost resistance, assuming that the rational approach of the Powers test closely approximates natural conditions. This supports the contention of Walker and McLaughlin (*79*) that rapid freeze-thaw tests are suitable for aggregate evaluations when used with care and by experienced personnel.

Comparison of Deterioration Function with Powers' Model

Powers observed that the increase in dilation with progressive cycles is initially a constant (*56*). After a number of cycles the dilation versus cycle number relationship becomes exponential. Apparently, the occurrence of the exponential relationship coincides with the attainment of a critical degree of saturation in the specimen. The number of cooling cycles that must be completed before the function becomes exponential depends on the protection afforded the paste phase by the entrained air, and on the characteristics of the coarse aggregate, the initial degree of saturation of the specimen, the water/cement ratio, and the cement content of the mixture.

In the regression of the experimental data to permit evaluation of the deterioration function, it was necessary to force all of the data into exponential form because in most cases the number of cycles was insufficient to provide enough data points to establish the pure exponential. The regression curves for the test data were therefore represented as continuous exponentials, whereas the actual curves consisted of an initial linear function to some "break" point, followed by an exponential. The difference is shown in Figure 33, which is a plot of dilation versus cycle number for a specimen of the saturated group containing Maynes Creek and Eagle City limestone (greater than 2.5 sp gr).

Because the total exponential approximation (curve B, Fig. 33) is related to the two functions comprising the actual data curve (curve A), the numerical value of B is dependent on the slope of the initial linear portion of curve A, the cycle number of the breakpoint, and the nature of the exponential portion of curve A. The first

TABLE 17

DURABILITY FACTOR (ASTM C290) VS REGRESSION PARAMETERS

AGGREGATE, ORDER OF DECREASING DURABILITY FACTOR	REGRESSION EQUATION PARAMETERS			
	DRIED		SATURATED	
	A	B	A	B
Benner and Snyder limestone	1.181	31.91	1.323	33.62
Eagle City and Maynes Cr. limestone, >2.5 sp gr	Corr. not significant		1.271	131.9
Rapid and Coralville limestone	1.127	63.02	1.218	235.9
Meramec gravel, >2.5 sp gr	Corr. not significant		1.283	214.9
Killins gravel, calc. sandstone and aren. limestone	1.124	63.14	1.341	556.0
Meramec gravel, <2.5 sp gr	1.214	99.11	1.185	1222.0
Paducah gravel	1.691	83.98	2.481	2199

TABLE 18

AGGREGATE DURABILITY RATINGS, ASTM C290 VS CALCULATED EIGHTH-CYCLE DILATIONS

AGGREGATE, ORDER OF DECREASING DURABILITY FACTOR	AGGREGATE, ORDER OF INCREASING EIGHTH-CYCLE DILATIONS	
	DRIED	SATURATED
Benner and Snyder limestone	Benner and Snyder	Benner and Snyder
Eagle City and Maynes Cr. limestone, >2.5 sp gr		Eagle City
Rapid and Coralville limestone	Rapid and Coralville	Rapid and Coralville
Meramec gravel, >2.5 sp gr		Meramec >2.5 sp gr
Killins gravel, calc. sandstone and aren. limestone	Killins	Meramec <2.5 sp gr
Meramec gravel, <2.5 sp gr	Meramec <2.5 sp gr	Killins
Paducah gravel	Paducah	Paducah

two of these three factors are critical with respect to frost destruction, because they define the limiting value of dilation signifying the end of frost resistance in the concrete. Although B is an artificially imposed quantity, it would be expected to emerge as a measure of frost resistance.

Empirical examination of the test data revealed that B was closely related to the dilations that occurred in the cycles that immediately followed the breakpoints in the actual data curves. That the correlation was better there than at the breakpoints was probably due to the influence of the exponential portions of the actual data curves. For this reason the first dilation value that deviated upward from the initial linear slope was designated as the critical dilation, D_c, in each case. The cycle numbers at which the critical dilations occurred were designated as the critical cycles, n'. Critical D_c and n' are shown in Fig. 33.

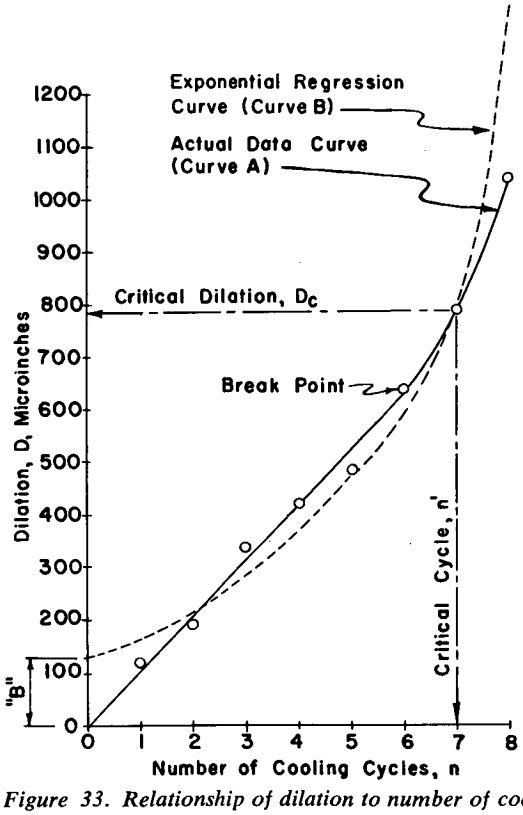

Figure 33. Relationship of dilation to number of cooling cycles.

Other factors being equal, the initial slope and the number of freeze-thaw cycles required to reach the critical point are dependent on the initial saturation condition and the aggregate type. If the cement factor is known to be constant and the water/cement ratio and the air-void spacing factor are assumed to be constant, then the specimens receiving a given curing treatment should produce B values dependent only on aggregate type. Because the correlations for the specimens that received no drying period were more significant than the correlations for those that were dried, and because most of the latter specimens failed to produce the exponential relationship in the specified eight cycles, the specimens with no drying period were selected for analysis. The values of D_c and n' obtained from plots

TABLE 19

D_c AND n' VALUES FOR TEST SPECIMENS WITH NO DRYING PERIOD

AGGREGATE	n'	D_c
Benner and Snyder limestone	8	328
Eagle City and Maynes Cr., >2.5 sp gr	7	773
Rapid and Coralville limestone	7	743
Meramec gravel, >2.5 sp gr	6	895
Killins gravel, shale	5	2,233
Killins gravel, calc. sandstone and aren. limestone	4	2,240
Meramec gravel, <2.5 sp gr	7	4,140
Paducah gravel	1	5,997

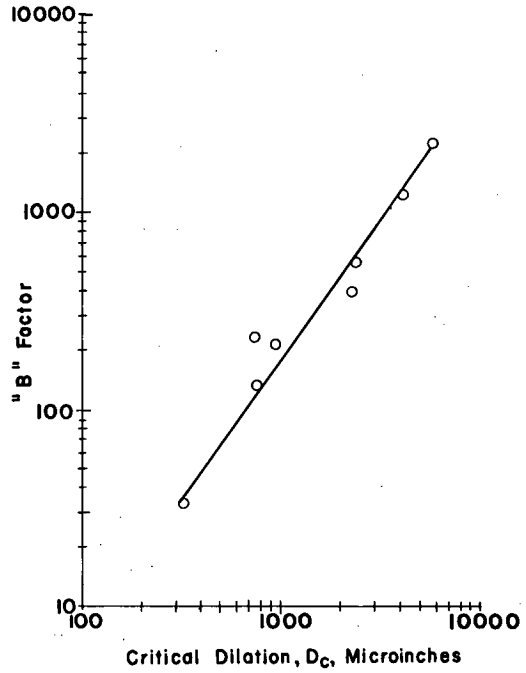

Figure 34. Relationship of B *factor to critical dilation for specimens with no drying period.*

of dilation vs cycle number for each aggregate are summarized in Table 19. The values of B obtained from the original regressions were then plotted against the observed values of D_c. Figure 34 presents rather convincing evidence that the B factor is a function of the critical dilation.

Further support for the postulated exponential nature of the decay function beyond critical dilation was gained by calculating the A factor from Eq. 14, using the values of n' and D_c from Table 19 and the B factors from the regressions. Comparison of the calculated values of the A factors with those obtained from the regressions (Table 20) showed generally quite good agreement.

The major conclusion from this analysis is that the dilation at any given cycle can be predicted by merely conducting freeze-thaw cycles until the change in dilation with each succeeding cycle starts to increase. This would be the terminal point of the test, because B can be estimated from Fig. 34 and A can be calculated from

$$A = (D_c / B)^{1/n'} \qquad (15)$$

The values of A and B so obtained can then be substituted in Eq. 14, thus completely defining the deterioration function for any given cycle number.

Significance of the A *Factor*

The rate of saturation of the air voids with succeeding cooling cycles was investigated using data from the Phase II specimens that did not undergo a drying period. It was assumed that at the start of the first freeze-thaw cycle the specimens were totally saturated except for the air voids, which were assumed to be totally dry. The degrees of saturation at the start of the first freeze-thaw cycle were then calculated from

TABLE 20

CALCULATED A FACTORS VERSUS REGRESSION A FACTORS FOR SPECIMENS WITH NO DRYING PERIOD

AGGREGATE	A FACTOR	
	CALCULATED	REGRESSION
Benner and Snyder limestone	1.330	1.323
Eagle City and Maynes Cr., >2.5 sp gr	1.288	1.271
Rapid and Coralville limestone	1.178	1.218
Meramec gravel, >2.5 sp gr	1.284	1.283
Killins gravel, shale	1.415	1.357
Killins gravel, calc. sandstone and aren. limestone	1.221	1.341
Meramec gravel, <2.5 sp gr	1.190	1.185
Paducah gravel	2.72	2.481

$$S_0 = 1.000 - P/100 \qquad (16)$$

in which S_0 is the degree of saturation before the first freeze-thaw cycle and P is the percentage of air in the concrete.

The degrees of saturation at the start of subsequent freeze-thaw cycles were calculated from

$$S_x = S_{x-1} + \Delta W/695 \qquad (17)$$

in which S_x is the degree of saturation prior to cycle x, S_{x-1} is the degree of saturation calculated for the previous cycle, ΔW is the specimen weight change in grams, and 695 is the specimen volume in cc.

Because the specimens were assumed to be saturated before the first cycle, except for the air voids, it was postulated that the rate of increase in degree of saturation was a direct indication of the rate of saturation of the air voids.

Regression equations were calculated for S_x vs x for each of the eight aggregate types used in Phase II. Degree of saturation, S_x, was selected as the dependent variable so that the linear regression coefficient would represent the rate of increase in degree of saturation. Correlation coefficients for the eight regressions revealed significant correlations, for all cases, at the 95 percent level or better.

A linear regression was then performed on the data for rate of saturation of air voids (dependent variable) vs the rate of change in log total dilation obtained from the deterioration-function analyses for the eight test aggregate series with no drying period. The regression revealed conclusively (better than 99 percent significance) that the rate of saturation of air voids varies directly with the rate of change in log total dilation. The rate of change in log total dilation is synonymous with log A, where A is identical to the A in Eq. 14. The rate of saturation of air voids, S, was therefore found to be related to log A by

$$S = 0.00825 \log A + 0.00021 \qquad (18)$$

Sources of Variability

An analysis of variance revealed that the replica mixtures in Phase I differed significantly, a matter which placed grave doubt on the dependability of the test. Inasmuch as the mixtures were prepared and treated in as nearly the same manner as possible and the aggregates were carefully fractioned, blended, and treated alike, it could only be concluded that some minor characteristic of the mixture must have produced the variation. Two mixture parameters, air-void spacing and water/cement ratio, seemed to be the only possible sources of the discrepancy.

The average air-void spacing factors for each of the Phase I mix batches are given in Table 21 (Table E-5 gives the individual specimen values.) It can be seen that all but one of the spacing factors were consistently near 0.0035 in. The first mixture containing Paducah gravel showed an average spacing factor 40 to 50 percent greater than the factors for the other five mixtures, and further examination of the test data revealed vast differences in the behavior of the two mixtures containing this aggregate. For example, of the 12 specimens for mix 1 containing Paducah gravel, 11 failed to complete eight cycles of testing, whereas only one of the 12 comparable specimens from mix 2 failed in testing. The air-void spacing factor could certainly have been responsible for the significant difference in mixtures discovered by the analysis of variance.

The water/cement ratio was found to vary between 0.50 and 0.56 (Table 14), but because this variation was not consistent with the observed variations in specimen behavior in the freeze-thaw tests, it was assumed to have a negligible effect on the test results.

The method of specimen treatment was also shown to be a significant source of variation. Two different curing procedures were used in Phase II, as shown in Figure 24. The analysis of variance summarized in Table 15 clearly indicates that the method of specimen treatment was a significant source of variation for all measures of frost damage. Detailed examination of the test data revealed that the one-week drying period incorporated in the first curing procedure increased the resistance to frost damage as much as twentyfold in some cases.

Three possible sources of variability were found to have negligible effect on the test results. These were the ratio of aggregate size to specimen length, extended periods of low temperatures in the cooling cycle, and the instrumentation and equipment used in the tests. The analysis of variance of the Phase I data showed that specimen size was not a significant source of variation. Because coarse aggregate of 1-in. maximum size was used in both the 6-in. and 8-in. specimens, it can be stated that the difference between the 1:6 and 1:8 ratios of aggregate size to specimen length had no significant effect on the test results.

The analysis of variance for Phase I brought to light that cycle type is not a significant source of variation. Holding one-half of the specimens at 15 F for 20 hr during about one-half of their freezing cycles (Fig. 23) had no effect on the dilations observed in subsequent cycles. In one of the theories on which Powers based his proposed test, he postulated that by a process similar to frost heave in soils, additional dilations could occur in critically saturated specimens held at low temperatures for a period of time, owing to the growth of ice lenses. If that postulation is valid, lower temperatures or longer periods of time must be required to produce this phenomenon.

TABLE 21

AIR-VOID SPACING FACTORS, PHASE I

AGGREGATE	MIX	AIR-VOID SPACING FACTOR[a] (IN.)
White Marsh gravel	1	0.00337
	2	0.00339
Paducah gravel	1	0.00511
	2	0.00352
Maynes Cr. and Eagle City limestone, <2.50 sp gr	1	0.00380
	2	0.00334

[a] Average of 12 specimens.

The nature and limitations of equipment for measuring test variables can profoundly affect the test results. The California Division of Highways study (*79*) used transducers to follow specimen dilation during freezing and a comparator to measure permanent length changes; Wills et al. (*88*) used dial gages for dilations and a strain gage for permanent length changes. The former study revealed dilations to be excellent indicators of frost damage, and the latter did not. In the present study transducers were used to measure dilations, with excellent results. In the first two cycles of Phase I, dial gages monitored length changes because the automatic recording equipment had not yet been set up. The lower sensitivity and the sluggishness of the dial gages completely obscured the important characteristics of the cooling curve.

The total absence of significant correlations between instrument channel number and any one of the other variables should also be noted. It indicates that the instrumentation did not significantly bias the test measurements.

MICROCRACK STUDY

Microcracking in the paste is the most significant form of cracking with respect to the failure of concrete. Hsu et al. (*36*) and Taylor and Broms (*72*) observed that the compressive strength of concrete is little affected until paste cracks develop and join interfacial cracks to form rupture surfaces through the concrete.

To examine the effects of frost action on microcrack development, an auxiliary study was conducted in conjunction with Phase II of the Powers-test investigation. The experimental design is given in Fig. 24.

Specimen Treatment

The six specimens for the microcrack study were 3 x 6-in. cylinders containing Paducah gravel, prepared in the same

manner as those for Phase II. One was subjected to one cycle of Powers-type freezing and thawing, the second to two cycles, and so on, the last specimen receiving six cycles. As each completed its prescribed number of cycles, is was stored in air at 77 ± 2 F and 47 ± 2 percent relative humidity.

When all of the cycling was finished, the middle section of each specimen was removed by cutting one quarter of the specimen length from each end with a diamond saw, perpendicular to the longitudinal axis. The removed section was ground and polished at both ends, and the polished faces were painted with a solution of red eosine dye in ethyl alcohol. Following a method similar to that employed by Hsu et al. (*36*), the dyed faces were then ground with 320-mesh silicon carbide in water until the surfaces appeared slightly pinkish. The specimens were allowed to dry for a few days in the same atmosphere as that used for storage, and then were examined under a stereoscopic microscope at 50× magnification. Microcracking was revealed as red traces of the eosine dye remaining after the grinding process.

Results and Discussion

To obtain a quantitative analysis of the amount of cracking, the two faces of each specimen were traversed at ½-in. intervals in two mutually perpendicular directions. The cracks were enumerated by a point-count method, and recorded in three categories—within aggregate particles, in the paste phase, and at the interface between paste and aggregate. The results of the microscopic examination are given in Table 22.

Quite probably, most of the cracking recorded for the aggregate existed in the aggregate before it was incorporated in the concrete. It is also probable that interfacial cracking observed in the one-cycle specimen existed before the specimen was subjected to the freeze-thaw cycle. Hsu and coworkers found that without the presence of external stress mechanisms, interface cracks can occur owing to shrinkage stresses during curing. As expected, however, interfacial cracking increased rather rapidly with increasing freeze-thaw cycles.

Table 22 shows that the number of cracks in the paste phase increases rapidly with progressive freezing and thawing. The increase is obviously not linear but more nearly exponential, and is very similar to the increase in dilation with progressive freeze-thaw cycles. By inference, therefore, the paste-phase microcracks appear to be direct manifestations of dilations that occurred during the freezing cycles.

TABLE 22

RESULTS OF MICROSCOPIC EXAMINATION OF MICROCRACK SPECIMENS

NUMBER OF FREEZE-THAW CYCLES	NUMBER OF CRACKS OBSERVED		
	AGGREGATE	PASTE	INTERFACE
1	29	3	70
2	31	17	70
3	31	44	85
4	34	56	90
5	47	94	153
6	43	174	164

CONCLUSIONS

The Powers-test experiments here reported support the following conclusions:

1. The instrumentation employed has a profound effect on the test results. Transducers provide the most sensitive and reliable means of monitoring dilations in concrete.

2. Total dilation is the best measure of frost action in concrete. Degradation in resonant frequency is also a good measure of frost action, but it is not as sensitive as dilation. Permanent length change is not acceptable as a measure of frost damage, because it is unduly influenced by extraneous conditions.

3. The temperature of the first dilation is not a random variable as hypothesized by Helmuth. It was found to vary inversely with the number of freeze-thaw cycles.

4. The extraneous sources of variability in the test method were the air-void spacing factor and specimen curing. Spacing factors should be limited to no more than 0.004 in. to minimize this source of variability. In the curing procedure, a one-week drying period greatly increased the resistance to frost damage.

5. No evidence was found to support Powers theory on "growth of ice bodies" in specimens held at low temperatures for extended periods. If the theory is valid, lower temperatures or longer periods of time are required for the evolution of this phenomenon.

6. For total dilation, the deterioration function follows the general equation $D = B\ A^n$, where D is the total dilation in microinches, A and B are constants for a given aggregate-treatment combination, and n is the number of freeze-thaw cycles. The constant B varies directly with the durability factor as determined by the rapid freeze-thaw method (ASTM C290). The deterioration function can be completely defined for any given aggregate-treatment-mix combination by conducting Powers freeze-thaw cycles until the change in dilation with cycle number starts to increase. This point is considered to be the test endpoint with regard to frost resistance.

7. The rate of saturation of the air voids during progressive freeze-thaw cycles varies with the type of coarse aggregate, and is related to the constant A in the deterioration function for saturated specimens.

8. Microcracking of the paste phase increases exponentially with increasing freeze-thaw cycles, in much the same manner as dilation.

CHAPTER SEVEN

GENERAL EVALUATION, TIME AND COST FACTORS, RECOMMENDATIONS

The primary objective of this research was to find a speedy, simple, and reliable test or battery of tests that would identify aggregates likely to be deleterious to concrete. Four areas were investigated, the experiments representing original ideas as well as extensions of existing methods: (1) aggregate-particle pore systems, (2) aggregate-particle expansion, (3) petrographic analysis, and (4) the Powers method of determining frost susceptibility.

Although an effort was made to select aggregates characterized by wide ranges of type and frost resistance, the number of aggregates tested was necessarily limited. Other aggregates may respond differently to the tests. Moreover, individual particles from the same lithological formation can exhibit statistical variations, within certain characteristic limits. For these reasons and because sampling and statistical techniques may vary, the same tests could yield significantly different results in other laboratories.

It should also be noted that although the Powers test is intended to simulate field conditions, no field tests were conducted in these studies and the performance of the test aggregates in the field cannot yet be inferred from the results of the laboratory experiments.

GENERAL EVALUATION

In point of the expressed objective, no one of the methods investigated combines all of the desired attributes. The aggregate-particle expansion test is speedy and simple, but it does not provide quantitative data for scientific analysis. Aggregate-pore studies, although more involved, do produce data that can be interpreted on a rational basis. If correlations between observed mineralogical structures and frost behavior have been otherwise established, the petrographic method, although also rather complex, is capable of yielding data that can be extrapolated to untested aggregates. None of the particle tests, however, can predict the response of the aggregates to variations in field conditions.

The Powers freeze-thaw test is capable of displaying the effects of variations in mixture, curing, and environment on mass aggregates. Although deleterious fractions of mass aggregates can be evaluated, Powers' method does not identify individual deleterious particles, and it is time-consuming.

Nevertheless, each of the four kinds of tests has its sphere of usefulness, and singly or in combination the tests can be serviceable in specific cases. Pore-system or particle-expansion studies of a new aggregate source can indicate potentially troublesome materials. The Powers test, with careful incorporation of mixture, curing, and environmental conditions similar to those anticipated in a given field area, can predict the probable degree of frost resistance. These examinations would indicate whether the concrete could be expected to perform satisfactorily, and if not, which materials should be removed or beneficiated to improve frost resistance. In the case of aggregates known to have poor frost resistance, studies of their pore characteristics or linear expansion properties can reveal the cause. With the required auxiliary information, petrographic analysis can predict frost susceptibility as reliably as the other two particle tests.

TIME AND COST FACTORS

Aggregate-Particle Pore Study

The pore characteristics of individual aggregate particles were determined by a permeability test designed during the project, and a porosity test. The time requirement for the permeability test is estimated to be 4 days minimum, including 3 days for specimen preparation. The porosity test requires approximately 3 days, but this time can be concurrent with the permeability tests. Computation and analysis time varies with the number of particles tested and the facilities available for computation.

The basic equipment for the permeability test was developed at a cost of about $500. For the standard laboratory equipment used in the porosity test, costs are readily available in manufacturers' catalogs.

Labor costs for the pore-systems tests may be broken down as follows:

	Man-Hours per Specimen	
Test	*Preparation*	*Testing*
Porosity	4	2
Permeability	2	1 to 6

Man-hours spent on permeability testing vary with the specimen.

Aggregate-Particle Expansion Study

The time requirement for testing the expansion of individual aggregate particles is about 3 days: specimen preparation, 2 days; testing, 1 day.

Equipment for the test includes facilities for vacuum saturation, a jig to hold the specimens while cementing gage points, a diamond saw to cut the specimens to the desired length, a drying oven, a cooling cabinet or bath, a constant-temperature bath, and a dial-gage comparator. The cost of these items can vary widely, depending on how elaborately the test system is designed. The minimum equipment cost is estimated to be about $1,000.

Labor for expansion testing is estimated to be about ½ man-hour per specimen.

Petrographic Analysis

Like the two previous studies, petrography examines individual aggregate particles. Preparation and examination time is about 2 days per specimen.

Petrographic analysis requires equipment for making thin sections of the aggregates, and a petrographic microscope. Photographic facilities for the microscope are desirable, although not absolutely necessary. The cost of the equipment, not including photographic facilities, is estimated to be about $2,500.

Labor per specimen is approximately 1 man-hour for preparation of thin sections and 3 man-hours for microscopic examination.

Powers Method

The Powers test method is the only one of the four that is applicable to mass aggregates. Specimen preparation time is 7 weeks, and test time will vary up to 16 weeks.

The equipment includes strain frames, strain-measuring devices, a cooling bath, a recording potentiometer, a comparator, a constant-temperature bath, and vacuum-saturation facilities. Also required are facilities for aggregate preparation, separation, and storage, and for concrete mixing, casting, and curing. The cost of equipment capable of handling six specimens per day (60 specimens per test, based on a 5-day work week) is estimated to be about $5,500.

Labor for each 6-specimen batch is estimated at 10 man-hours for specimen preparation and 6 man-hours per test cycle.

RECOMMENDATIONS

All of the tests reported here need further laboratory evaluation with a wider range of aggregate types, and the laboratory results should be correlated with field performance.

The pore-system studies should be extended to explore wider pressure ranges than were covered in this research. The relationship of pore systems to moisture migration should also be examined, because moisture movement is basic to the overall problem of frost destruction. The moisture-tracing technique developed in the course of this research and described in Chapter Three will greatly assist this work.

Later aggregate-particle expansion studies should include examination of volumetric expansion. In view of the anisotropy exhibited by many aggregate materials, the effects of particle orientation on linear expansion should be evaluated.

For petrographic evaluations, the major need is correlations of mineralogical structure with frost susceptibility.

The Powers method needs more study relative to the logical endpoint of the test. This means further investigation of the deterioration function, which is generally believed to indicate the attainment of critical conditions in concrete. Powers' theories concerning "growth of ice bodies" and "osmotic pressure" should be examined in more detail. Several observed phenomena basic to the nature of frost destruction, discussed in Chapter Six, likewise require further study.

APPENDIX A

BIBLIOGRAPHY

1. American Association of State Highway Officials, "Standard Method of Test for Specific Gravity of Soils, AASHO Designation: T100-60." *Standard Specifications for Highway Materials and Methods of Sampling and Testing,* Part II (1961), pp. 307-309.
2. American Concrete Institute, "Recommended Practice for Selecting Proportions for Concrete." ACI 613-54 (1959), pp. 49-64.
3. American Petroleum Institute, "Standard Procedure for Determining Permeability of Porous Media (Tentative)." API Code No. 27 (Oct. 1935).
4. American Society for Testing and Materials, "Standard Method of Test for Specific Gravity and Absorption of Coarse Aggregate, ASTM Designation: C127-59." *ASTM Standards,* Part 4 (1961), pp. 605-606.
5. American Society for Testing and Materials, "Tentative Method of Test for Resistance of Concrete Specimens to Rapid Freezing and Thawing in Water, ASTM Designation: C290-61T." *ASTM Standards,* Part 4 (1961), pp. 751-755.
6. Arnold, J. S., "An Improved Technic for Liquid Emulsion Autoradiography." *Proc. Soc. Exper. Biol. in Medicine,* Vol. 85, pp. 113-116 (1954).
7. Axon, E. O., "A Method of Estimating the Original Mix Composition of Hardened Concrete Using Physical Tests." *Proc. ASTM,* Vol. 62, pp. 1068-1080 (1962).
8. Black, N. W., *An Introductory Course in College Physics,* 3rd edition. Macmillan (1950).
9. Blanks, R. F., "Modern Concepts Applied to Concrete Aggregate." *Trans. ASCE,* Vol. 115, pp. 403-431 (1950).
10. Bloem, D. L., "Soundness and Deleterious Substances." *Spec. Tech. Publ.* 169, ASTM (1956), pp. 346-352.
11. Bloem, D. L., "Factors Affecting the Freezing and Thawing Resistance of Concrete Made with Chert Gravel." *HRB Record* No. 18 (1963), pp. 48-60.
12. Brink, R. H., "Rapid Freezing and Thawing Tests for Aggregates." *HRB Bull.* 201 (1958), pp. 15-23.
13. Cady, P. D., "Frost Action in Concrete and a Method for Evaluation." M.S. thesis, Dept. of Civil Engineering, The Pennsylvania State University (1964).
14. Calhoun, J. C., Jr., "The Flow of Some Pure Liquids Through Porous Media." M.S. thesis, Dept. of Petroleum and Natural Gas Engineering, The Pennsylvania State University (1941).
15. Calhoun, J. C., Jr., "An Investigation of the Flow of Homogeneous Fluids Through Porous Media." Ph.D. thesis, Dept. of Mineral Engineering, The Pennsylvania State University (1946).
16. Committee on Durability of Concrete, "Progress Report." *Proc. HRB,* Vol 24, pp. 174-202 (1944).
17. Coley, F. H., "A Study of Fluid Flow in Synthetic Porous Media." Ph.D. thesis, Dept. of Petroleum and Natural Gas Engineering, The Pennsylvania State University (1955).
18. Copeland, L. E., "Specific Volume of Evaporable Water in Hardened Portland Cement Pastes." *Jour. Am. Conc. Inst.,* Vol. 52, No. 8, pp. 863-874 (1956).
19. Copeland, L. E., and Hayes, J. C., "Porosity of Hardened Portland Cement Pastes." *Jour. Am. Conc. Inst.,* Vol. 27, No. 6, pp. 633-640 (1956).
20. Crumpton, C. F. Personal correspondence (Aug. 13, 1963).
21. Dolch, W. L., "Studies of Limestone Aggregates by Fluid-Flow Methods." *Proc. ASTM,* Vol. 59, pp. 1204-1215 (1959).
22. Dunagan, W. M., "Methods of Measuring the Passage of Water Through Concrete." *Proc. ASTM,* Vol. 39, pp. 866-881 (1939).
23. *Encyclopaedic Dictionary of Physics.* Pergamon Press (1961).
24. Fancher, G. H., Lewis, J. A., and Barnes, K. B., "Some Physical Aspects of Oil Sands." Bull. 12, Mineral Industries Exper. Sta., The Pennsylvania State University (1933), pp. 65-171.
25. Faul, A. F., and de Young, C. E., "Operation and Results with the Conrad Automatic Freezing Apparatus." Informal paper (unpubl.), conf. session on Performance of Concrete, Physical Aspects and Effect of Ice Control, HRB Annual Meeting, Jan. 8, 1963.
26. Foster, L. M., Gillespie, A. S., Jack, T. H., and Hill, W. W., "How to Study Hydrogen in Aluminum-Tritium Autoradiography." *Nucleonics,* Vol. 21, No. 4, pp. 53-55 (1963).
27. Franzen, M. H., "Aggregate Pore System Studies." M.S. thesis, Dept. of Civil Engineering, The Pennsylvania State University (1964).
28. Gomberg, H. J., "A New High Resolution System of Autoradiography." *Nucleonics,* Vol. 4, No. 4, pp. 28-44 (1951).
29. *Handbook of Chemistry and Physics,* 40th ed. Chemical Rubber Publishing Co. (1958).
30. Hansen, W. C., "Porosity of Hardened Portland Cement Paste." *Jour. Am. Conc. Inst.,* Vol. 60, No. 1, pp. 141-155 (1963).
31. Heid, J. G., "Permeability Studies of Porous Media." M.S. thesis, Dept. of Mineral Engineering, The Pennsylvania State University (1949).

32. HEID, J. G., MCMAHON, J. J., NIELSEN, R. F., and YUSTER, S. T., "Study of the Permeability of Rocks to Homogeneous Fluids." *Drilling and Production Practice, 1950,* Am. Petroleum Inst. (1951), pp. 230-246.

33. HELMUTH, R. A., "Capillary Size Restrictions on Ice Formation in Hardened Portland Cement Pastes." *Monograph 43,* Vol. II, Nat. Bur. Standards (1960), pp. 855-869.

34. "Report on Cooperative Freezing and Thawing Tests of Concrete." *HRB Spec. Report* 47 (1959).

35. HILTROP, C. L., and LEMISH, J., "Relationship of Pore-Size Distribution and Other Rock Properties to Serviceability of Some Carbonate Aggregates." *HRB Bull.* 239 (1960), pp. 1-23.

36. HSU, T. T. O., SLATE, F. O., STURMAN, G. M., and WINTER, G., "Microcracking of Plain Concrete and the Shape of the Stress-Strain Curve." *Proc. Am. Conc. Inst.,* Vol. 60, pp. 209-223 (1963).

37. JOFTES, D. L., "Liquid Emulsion Autoradiography with Tritium." *Laboratory Investigation,* Vol. 8, No. 1, pp. 131-138 (1959).

38. KENNEDY, T. B., and MATHER, K., "Correlation Between Laboratory Accelerated Freezing and Thawing and Weathering at Treat Island, Maine." *Jour. Am. Conc. Inst.,* Vol. 50, pp. 141-172 (1953).

39. KLINKENBERG, L. J., "The Permeability of Porous Media to Liquids and Gases." *Drilling and Production Practice, 1941,* Am. Petroleum Inst. (1942), pp. 200-213.

40. LARSON, T., CADY, P., FRANZEN, M., and REED, J., "A Critical Review of Literature Treating Methods of Identifying Aggregates Subject to Destructive Volume Change When Frozen in Concrete, and a Proposed Program of Research." *HRB Special Report* 80 (1964).

41. LEGG, F. E., JR., "Freeze-Thaw Durability of Michigan Concrete Coarse Aggregates." *HRB Bull.* 143 (1956), pp. 1-13.

42. LEMISH, J., RUSH, F. E., and HILTROP, C. L., "Relationship of Physical Properties of Some Lowa Carbonate Aggregates to Durability of Concrete." *HBR Bull.* 196 (1958), pp. 1-16.

43. LEWIS, D. W., DOLCH, W. L., and WOODS, K. B., "Porosity Determinations and the Significance of Pore Characteristics of Aggregate." *Proc. ASTM,* Vol. 53, pp. 949-962 (1953).

44. LEWIS, D. W., and VENTERS, E., "Deleterious Constituents of Indiana Gravels." *HRB Bull.* 94 (1954), pp. 1-10.

45. LITEHISER, R. R., "Effects of Deleterious Materials in Concrete." *Rock Products,* Vol. 41, pp. 39-40 (1938).

46. MANGER, G. E., "Porosity and Bulk Density of Sedimentary Rocks." *Contributions to Geochemistry,* Geol. Survey Bull. 1144-E (1963).

47. MCMAHON, J. J., "An Investigation of Air Permeabilities of Porous Media." M.S. thesis, Dept. of Mineral Engineering, The Pennsylvania State University (1949).

48. MUSKAT, M., *The Flow of Homogeneous Fluids Through Porous Media.* McGraw-Hill (1937).

49. MUSKAT, M., *Physical Principles of Oil Production.* McGraw-Hill (1949), pp. 123-138.

50. NERENST, P., "Frost Action in Concrete." *Monograph 43,* Vol. II, Nat. Bur. Standards (1960), pp. 807-834.

51. NORTON, P. F., and PLETTA, D. H., "The Permeability of Gravel Concrete." *Jour. Am. Conc. Inst.,* Vol. 27, pp. 1093-1132 (1931).

52. PENCE, E. A. Personal correspondence (Apr. 28, 1964).

53. PICKETT, G., "Flow of Moisture in Hardened Portland Cement During Freezing." *Proc. HRB,* Vol. 32, pp. 276-284 (1953).

54. POWERS, T. C., "A Working Hypothesis for Further Studies of Frost Resistance of Concrete." *Jour. Am. Conc. Inst.,* Vol. 16, No. 4, pp. 245-272 (1945).

55. POWERS, T. C., "The Nonevaporable Water Content of Hardened Portland Cement Paste—Its Significance for Concrete Research and Its Method of Determination." *Bull. ASTM* (May 1949), pp. 68-76.

56. POWERS, T. C., "Basic Considerations Pertaining to Freezing-and-Thawing Test." *Proc. ASTM,* Vol. 55, pp. 1132-1155 (1955).

57. POWERS, T. C. Personal correspondence (May 24, 1963).

58. POWERS, T. C., COPELAND, L. E., HAYES, J. C., and MANN, H. M., "Permeability of Portland Cement Paste." *Jour. Am. Conc. Inst.,* Vol. 26, No. 3, pp. 285-298 (1954).

59. POWERS, T. C., COPELAND, L. E., and MANN, H. M., "Capillary Continuity or Discontinuity in Cement Pastes." *Jour. Res. and Devel. Lab.,* Portland Cement Assn., Vol. 1, No. 2, pp. 38-48 (1959).

60. POWERS, T. C., and HELMUTH, R. A., "Theory of Volume Changes in Hardened Portland Cement Paste During Freezing." *Proc. HRB,* Vol. 32, pp. 285-297 (1953).

61. PRICE, W. L., "Ten Years of Progress in Gravel Beneficiation—1948-1958." *Circular* No. 71, Nat. Sand and Gravel Assn. (1958).

62. REAGEL, F. V., "Freezing and Thawing Tests of Concrete." *Proc. HRB,* Vol. 20, pp. 587-598 (1940).

63. REED, J. R., "Effect of a Downstream Obstruction on an Orifice Meter." M. S. thesis, Dept. of Civil Engineering, The Pennsylvania State University (1955), pp. 22-23.

64. RHOADES, R., and MIELENZ, R. C., "Petrography of Concrete Aggregates." *Jour. Am. Conc. Inst.,* Vol. 17, No. 6, pp. 581-600 (1946).

65. ROBERTSON, J. S., BOND, V. P., and CRONKITE, E. P., "Resolution and Spread of Images in Autoradiographs of Tritium-Labeled Cells." *Internat. Jour. Applied Radiation and Isotopes,* Vol. 7, pp. 33-73 (1959).

66. ROSE, W., and BRUCE, W. A., "Evaluation of Capillary Character in Petroleum Reservoir Rock." *Trans. Am. Inst. Mining and Metallurg. Eng.,* Vol. 186, pp. 127-142 (1949).

67. RUETTGERS, A., VIDAL, E. N., and WING, S. P., "An Investigation of the Permeability of Mass Concrete with Particular Reference to Boulder Dam." *Jour. Am. Conc. Inst.,* Vol. 6, pp. 382-416 (1935).

68. SWEET, H. S., "Research on Concrete Durability as Affected by Coarse Aggregates." *Proc. ASTM,* Vol. 48, pp. 988-1019 (1948).

69. SWEET, H. S., and WOODS, K. B., "A Study of Chert as a Deleterious Constituent in Aggregates." *Highway Res. Bull.* No. 2, Eng. Exper. Sta., Purdue Univ. (1942), pp. 43-44.

70. SWENSON, E. G., and CHALY, V., "Basis for Classifying Deleterious Characteristics of Concrete Aggregate Materials." *Jour. Am. Conc. Inst.,* Vol. 52, pp. 987-1002 (1956).

71. SYKES, W. A. Personal correspondence (Nov. 18, 1963).

72. TAYLOR, M. A., and BROMS, B. B., "Shear Bond Strength Between Coarse Aggregate and Cement Paste of Mortar." *Proc. Am. Conc. Inst.,* Vol. 61, pp. 939-957 (1964).

73. TRAUGH, C. E., "Some of the Limiting Aspects of the Validity of Darcy's Law." M. S. thesis, Dept. of Mineral Engineering, The Pennsylvania State University (1950).

74. TRAULWEILER, VON A., "Testing Frost Resistance of Stone by Means of the 'Nigrosin' Color Method after Hirschwald." *Strasse and Verkehr,* No. 23, pp. 269-371 (1943).

75. TREMPER, B., and SPELLMAN, D. L., "Tests for Freeze-Thaw Durability of Concrete Aggregates." *HRB Bull.* 305 (1961), pp. 28-50.

76. TYLER, I. L., and ERLIN, B., "A Proposed Simple Test Method for Determining the Permeability of Concrete." *Jour. Res. and Devel. Labs.,* Portland Cement Assn., Vol. 3, No. 3, pp. 2-7 (1961).

77. VERBECK, G., and LANDGREN, R., "Influence of Physical Characteristics of Aggregates on Frost Resistance of Concrete." *Proc. ASTM,* Vol. 60, pp. 1063-1079 (1960).

78. VOLK, W., *Applied Statistics for Engineers.* McGraw-Hill (1958), pp. 224-241.

79. WALKER, R. D., and MCLAUGHLIN, J. F., "Effect of Heavy Media Separation on Durability of Concrete Made with Indiana Gravels." *HRB Bull.* 143 (1956), pp. 14-26.

80. WALKER, S., "Soundness of Aggregates." *Report of Significance of Tests of Concrete and Concrete Aggregate,* ASTM (1943).

81. WASHBURN, E. W., "Porosity. I. Purpose of the Investigation; II. Porosity and the Mechanism of Absorption." *Jour. Am. Ceramic Soc.,* Vol. 4, pp. 916-922 (1921).

82. WASHBURN, E. W., and FOOTITT, F. F., "Porosity. III. Water as an Absorption Liquid." *Jour. Am. Ceramic Soc.,* Vol. 4, pp. 961-982 (1921).

83. WASHBURN, E. W., and BUNTING, E. N., "Porosity. IV. The Use of Petroleum Products as Absorption Liquids." *Jour. Am. Ceramic Soc.,* Vol. 4, pp. 983-989 (1921).

84. WASHBURN, E. W., and BUNTING, E. N., "Porosity. V. Recommended Procedures for Determining Porosity by Methods of Absorption." *Jour. Am. Ceramic Soc.,* Vol. 5, pp. 48-56 (1922).

85. WASHBURN, E. W., and BUNTING, E. N., "Porosity. VI. Determination of Porosity by the Method of Gas Expansion." *Jour. Am. Ceramic Soc.,* Vol. 5, pp. 112-129 (1922).

86. WASHBURN, E. W., and BUNTING, E. N., "Porosity. VII. The Determination of the Porosity of Highly Vitrified Bodies." *Jour. Am. Ceramic Soc.,* Vol. 5, pp. 527-537 (1922).

87. WILEY, G., and COULSON, D. C., "A Simple Test for Water Permeability of Concrete." *Jour. Am. Conc. Inst.,* Vol. 9, No. 1, pp. 65-75 (1937).

88. WILLS, M. H., JR., LEPPER, H. A., JR., GAYNOR, R. D., and WALKER, S., "Volume Change as a Measure of Freezing-and-Thawing Resistance of Concrete Made with Different Aggregates." *Proc. ASTM,* Vol. 63, pp. 949-965 (1963).

89. WING, S. P., "Discussion of a Paper by G. Wiley and D. C. Coulson: 'A Simple Test for Water Permeability of Concrete.'" *Jour. Am. Conc. Inst.,* Vol. 9, No. 1, pp. 76-1 to 76-4 (1937).

90. WITHEY, M. O., "Permeability and Absorption of Concrete." *Report on Significance of Tests of Concrete and Concrete Aggregates,* ASTM, 2nd ed. (1943), pp. 79-83.

91. WRAY, F. N., and LICHTEFELD, H. J., "The Influence of Test Methods on Moisture Absorption and Resistance of Coarse Aggregates to Freezing and Thawing." *Proc. ASTM,* Vol. 40, pp. 1007-1020 (1940).

92. WUERPEL, C. E., "Factors Affecting the Testing of Concrete Aggregate Durability." *Proc. ASTM,* Vol. 38, Part I, pp. 327-351 (1938).

APPENDIX B

PREPARATION, SEPARATION, AND PHYSICAL PROPERTIES OF TEST AGGREGATES

The procedures described here were used to separate and prepare the aggregates for testing, and to determine true and apparent specific gravity, absorption, degree of saturation, and dry and saturated surface-dry bulk densities. All tests and analyses to which they applied were conducted in accordance with ASTM or AASHO specifications, with AASHO specifications governing where a conflict existed between the two.

In the separating phase, the aggregates were classified according to size, specific gravity, and petrography. The objective was to distinguish in the petrographic classes those fractions above and below a specific gravity of 2.50, and to obtain for each fraction samples containing 50 percent by weight of material in each of two sizes—½ to ¾ in. and ¾ to 1 in.

The stages of these procedures are shown in Figure B-1.

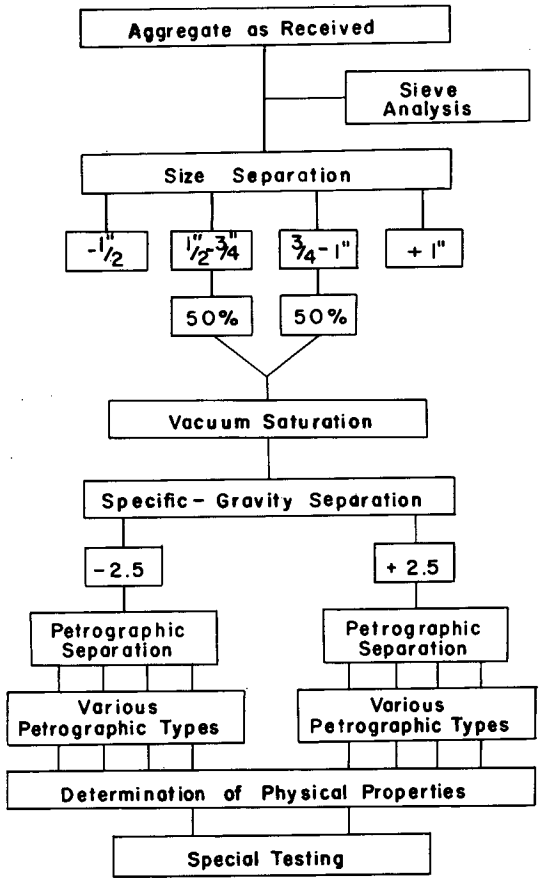

Figure B-1. Aggregate separation procedures.

SIEVE ANALYSIS AND SIZE SEPARATION

The sieve analyses were made on the material as received. Randomly selected fractions of each aggregate were run through a sample splitter and screened according to AASHO T27-60. The product was sampled 50 percent by weight in each of two sizes—½ to ¾ in. and ¾ to 1 in.

VACUUM SATURATION AND SPECIFIC GRAVITY SEPARATION

The size-sorted material was air-dried and subjected to a vacuum of 15 mm Hg (absolute) for 1 hr. Water was introduced into the vacuum chamber, and the aggregate was soaked 23 hr.

The heavy medium used in the separation was a mixture of tetrabromoethane (2.95 sp gr) and trichloroethylene (1.46 sp gr), producing a fluid with 2.50 sp gr. The surface-dried aggregate was placed in the fluid, and the float and sink were each removed, washed in acetone, and stored. The saturated condition of the particles prevented absorption of the heavy medium.

PETROGRAPHIC SEPARATION

Each of the two fractions from the specific gravity separation was separated into basic petrographic groups by simple techniques such as macroscopic examination and determinations of hardness and reactivity with acids. Detailed examinations (see Appendix C) were later made on particles considered to be representative of these fractions.

DETERMINATION OF DENSITY AND ABSORPTION PROPERTIES

A representative 3-kg sample was thoroughly washed, and ovendried to a constant weight at 212 to 230 F. The sample was then vacuum saturated at 15 mm Hg (absolute) for 5 min, and soaked for 24 hr. The saturated sample was surface-dried with an absorbent cloth, and weighed to the nearest 0.1 g both in air and in water. The sample was again ovendried to a constant weight at 212 to 230 F. The percentage of absorption was calculated from $[(SSD - D)/D]$ 100, where SSD is the saturated surface-dry weight and D is the ovendry weight. This procedure was repeated for 15-, 30-, and 60-min vacuum periods.

True specific gravity, apparent specific gravity, absorption, degree of saturation, dry bulk density, and saturated surface-dry bulk density were also determined for each sample, as given in Table B-1. On smaller-than-200-mesh

TABLE B-1

SAMPLE CALCULATION OF DENSITY AND ABSORPTION [a]

PROPERTY	IMMERSED 24 HR	VAC. SAT. 15 MIN
Ovendry weight, A (g)	3165.0	3166.2
Saturated surface-dry weight in water, C (g)	1968.8	1972.3
$A - C$	1196.2	1193.9
Apparent specific gravity, $S = A/(A - C)$	2.646	2.652
Saturated surface-dry weight in air, B (g)	3173.7	3178.6
$B - A$	8.7	12.4
Absorption, U (%) $= (B - A)/A \times 100$	0.27	0.39
Voids ratio $= UG/100 + (G - S)/S$	0.0212	0.0222
Degree of saturation $= UGS/(UGS + 100G - 100S)$	0.340	0.473
Bulk density, saturated surface-dry $= B/(B - C)$	2.646	2.650
Bulk density, dry $= A/(B - C)$	2.588	2.570

[a] White Marsh gravel: true sp gr, $G = 2.683$.

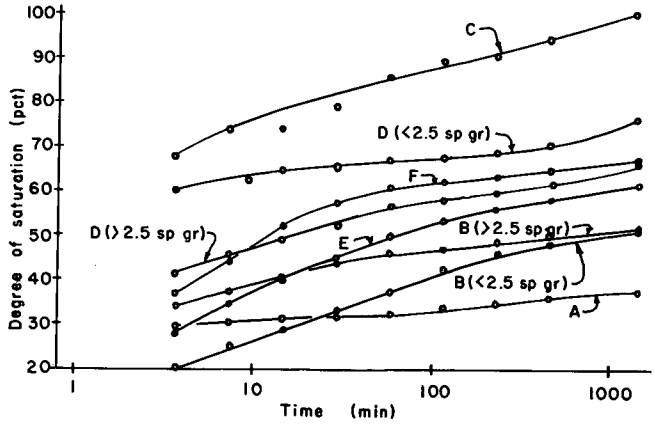

Figure B-2. Degree of saturation vs soaking time.

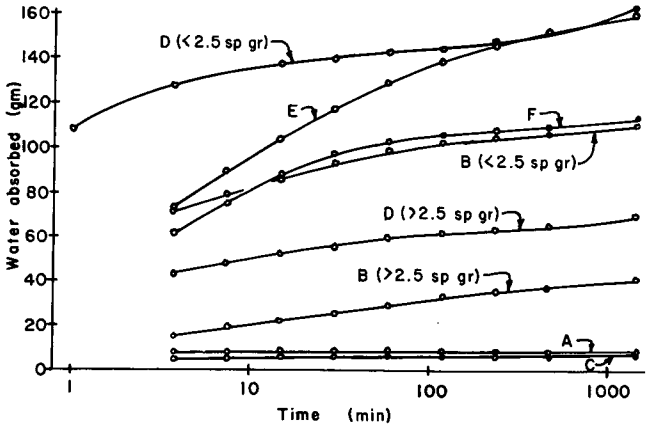

Figure B-3. Weight of water absorbed vs soaking time.

material the true specific gravity was determined by the pycnometer method. The other properties were determined as described in AASHO T85-60 (ASTM C127-59).

DEGREE OF SATURATION, AND ABSORPTION VS SOAKING TIME

The degree of saturation and the weight of water absorbed versus soaking time were determined from a single sample (approximately 3,150 g) of each test aggregate, the sample with the 24-hr absorption value nearest to the average value found in previous tests. Each sample was ovendried to constant weight and quickly immersed in an apparatus that permitted the weight of the sample in water to be determined. Readings were obtained at 3.75, 7.50, 15.0, 30.0, 60.0, 120, 240, 480 min and finally at 24 hr (a reading at 1 min was obtained for the Maynes Creek and Eagle City limestone fraction with less than 2.5 sp gr). The sample was again ovendried to constant weight. The degree of saturation was calculated as follows:

$$C_0 = A_f - A_f/x \qquad \text{(B-1)}$$

in which C_0 is the weight of ovendry sample at time zero, A_f is the final ovendry weight, and x is the average value for 24-hr-immersion dry bulk density.

$$B - A_f = C_n - C_0 \qquad \text{(B-2)}$$

in which B is the saturated surface-dry bulk density and C_n is the weight of the sample in water.

Then

$$\text{Bulk density (sat. surface-dry)} = B/(B - C_n) \qquad \text{(B-3)}$$

$$\text{Bulk density (dry)} = A_f/(B - C_n) \qquad \text{(B-4)}$$

$$\text{Apparent sp gr} = A_f/(A_f - C_n) \qquad \text{(B-5)}$$

$$\text{Absorp. of water (wt \%)} = (B - A_f)/A_f \qquad \text{(B-6)}$$

$$\frac{\text{Water vol.}}{\text{Solids vol.}} = \frac{V_w}{V_s} = \frac{\text{absorp.} \times \text{true sp gr}}{100} \qquad \text{(B-7)}$$

$$\frac{\text{Air vol.}}{\text{Solids vol.}} = \frac{V_a}{V_s} = \frac{\text{true sp gr—apparent sp gr}}{\text{apparent sp gr}} \qquad \text{(B-8)}$$

$$\text{Volume of voids} = V_v = V_w + V_a \qquad \text{(B-9)}$$

$$\text{Degree of saturation} = V_w/V_v \qquad \text{(B-10)}$$

Degree of saturation versus soaking time is shown in Figure B-2, and the weight of water absorbed is shown in Figure B-3. It is there apparent that the degree of saturation alone cannot be used to determine the resistance of an aggregate to freeze-thaw damage. Aggregates A and C had the lowest and highest values for degree of saturation, respectively, but both of these aggregates have good service records and were the most durable of all the aggregates tested in this program. A more useful function is the weight of water absorbed per given sample weight. In this case, aggregates A and C had the lowest values of all the test fractions.

APPENDIX C

PETROGRAPHIC DESCRIPTIONS OF TEST AGGREGATES

The following petrographic identifications describe the test fractions separated from the aggregate materials as received. These fractions do not necessarily represent a complete or accurate sampling of the source or the units from which they came.

Aggregate A: White Marsh gravel, Towson, Md.

This river gravel is subrounded to rounded, milky to colorless quartz (Fig. C-1). The grains have sutured boundaries and range from less than 0.05 mm to 2 cm in diameter. Some samples contain very minor amounts of pyrite, muscovite, and tourmaline. All samples contain an average of 1 to 2 percent liquid inclusions (up to 0.025 mm diameter) irregularly distributed or in stringers that cut grain boundaries. Microfractures occur in all samples, but they normally do not cross grain boundaries and they show no signs of weathering. Larger continuous limonite-stained fractures are present in some samples.

Aggregate B: Meramec gravel, Mo.

Oolitic chert and orthoquartzite, >2.5 sp gr. This fraction consists of two types, which are difficult to separate in hand specimens:

(1) This subfraction (Fig. C-2) is a subrounded yellow-brown orthoquartzite consisting of well-rounded quartz grains and lesser amounts of chert fragments, both with an average diameter of 0.4 mm. Each quartz grain consists of a single crystal fragment with numerous liquid and acicular solid inclusions. The chert is composed of microcrystalline quartz (average grain size <0.006 mm). Some fragments contain a quartz-grain core, but they are otherwise structureless. Most of the cementing material is iron-stained banded chalcedony with abundant limonite, particularly near the surfaces of particles. The layers of chalcedony are concentrically arranged around the quartz and chert grains, and the interstices are filled with authigenic anhedral quartz with an average diameter of 0.05 mm. The chalcedony contains numerous discontinuous microfractures, which normally do not cut grain boundaries.

(2) This subfraction (Fig. C-3) is a subrounded yellow-brown oolitic chert composed of about 30 percent concentrically banded microcrystalline quartz (average grain diameter <0.003 mm) oolites with quartz cement (average grain size 0.01 mm). Most samples contain about 1 percent interstitial chalcedony. Discontinuous microfractures are common in the quartz cement, but they normally do not cut grain boundaries.

Chert, >2.5 sp gr. This rock is subangular to subrounded, white to yellow-brown, dense, massive to laminated chert, composed of microcrystalline quartz with an average grain size <0.005 mm (Fig. C-4). All samples contain abundant interstitial limonite, and most have a smooth coating of weathered chert and limonite or chalcedony and limonite. Chalcedony is abundant, and some samples contain irregularly shaped, layered, limonite-stained masses up to 1 cm in diameter. Some contain interbedded orthoquartzite. All samples contain numerous microfractures, which are generally continuous across the particles.

Chert, <2.5 sp. gr. This material (Fig. C-5) is somewhat similar to the >2.5 sp gr chert except that it is more extensively weathered and contains numerous irregularly shaped voids filled or partly filled with limonite, vugs lined with quartz and limonite, and limonite-filled fractures. The voids and vugs average about 0.1 mm diameter and commonly are interconnected to form permeable layers.

Aggregate C: Black River group, Benner and Snyder limestones, Oak Hall Quarry, Oak Hall, Pa.

This rock (Fig. C-6) is an angular, dark gray, pelletiferous and fossiliferous, arenaceous limestone, mostly composed of internally structureless rounded aggregates of fine-grained calcite (average diameter 0.07 mm) with an equal amount of coarser-grained interstitial calcite (average diameter 0.02 mm). All samples contain 1 to 2 percent detrital quartz grains and up to 10 percent coarse-grained calcite (up to 1 mm diameter), most of which is pseudomorphic after fossil fragments. Most samples contain limonite-filled microfractures and stylolites and less than 1 percent interstitial limonite.

Aggregate D: Maynes Creek and Eagle City members of the Hampton formation, Le Grand Quarry, Le Grand, Iowa

Limestone and dolomitic limestone, <2.5 sp gr. This rock (Fig. C-7) is an angular to subangular, light to medium-dark brown and medium yellow-brown, massive to laminated limestone and dolomitic limestone with a wide range of grain sizes. The fine-grained (average grain size 0.05 mm) and medium-grained (average grain size 0.7 mm) varieties are by far the most abundant. The fine-grained is the more dolomitic and contains up to 40 percent euhedral calcite. Some samples contain lentils of coarse-grained calcite and stringers of chert. Pyrite, ranging up to 1 percent, and abundant interstitial and surficial limonite are commonly present. All samples contain minor amounts of detrital microcline and quartz. All the varieties of this fraction are weathered and contain up to 11 percent interstitial and intragranular voids with an average diameter of 0.05 mm in the fine-grained material, ranging up to 1 mm in the coarser-grained specimens. Most of these voids are filled or partly filled with limonite

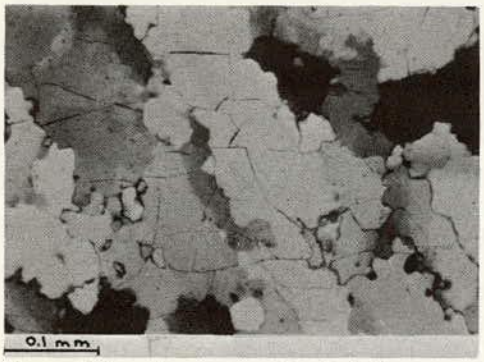

Figure C-1. Aggregate A, > 2.5 quartz, crossed nicols. Note sutured boundaries and discontinuous microfractures.

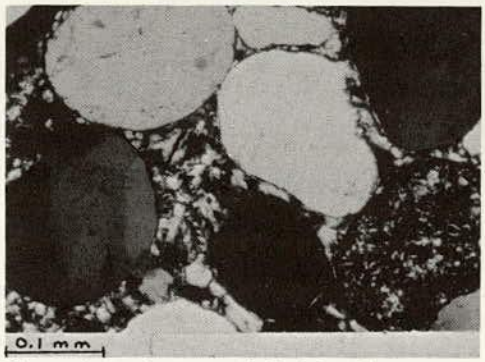

Figure C-2. Aggregate B, >2.5 orthoquartzite, crossed nicols. Note rounded quartz and chert grains in chalcedony cement.

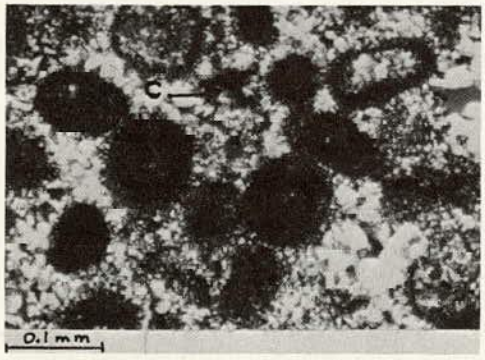

Figure C-3. Aggregate B, >2.5 oolitic chert, crossed nicols. Note oolites, quartz cement, and chalcedony (C).

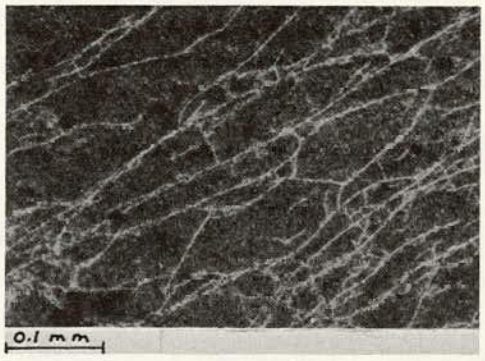

Figure C-4. Aggregate B, >2.5 chert, plain light. Note microfractures (limonite removed by leaching) and abundant interstitial limonite (dark).

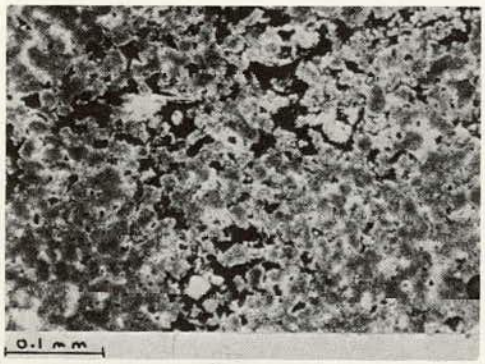

Figure C-5. Aggregate B, <2.5 chert, plain light. Note numerous voids (white), most of which are filled with limonite (black).

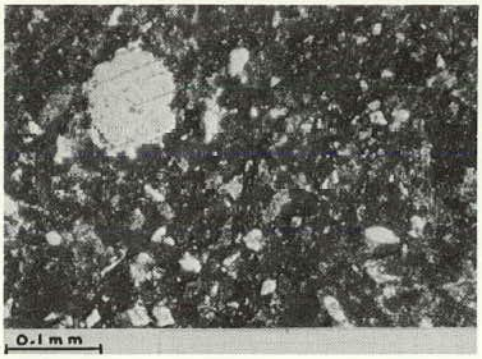

Figure C-6. Aggregate C, >2.5 limestone, crossed nicols. Note large calcite grain, quartz grains (white), limonite-stained fracture (black) in dark pelletiferous limestone.

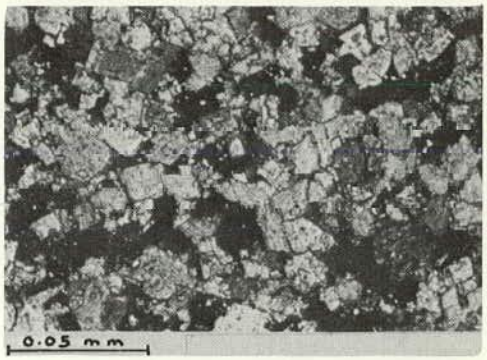

Figure C-7. Aggregate D, <2.5 dolomitic limestone, crossed nicols. Note numerous interstitial voids (black).

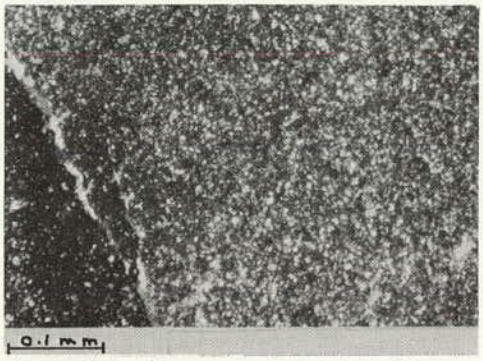

Figure C-8. Aggregate D, >2.5 dolomitic limestone, crossed nicols. Note dense structure and calcite-healed, limonite-stained fracture.

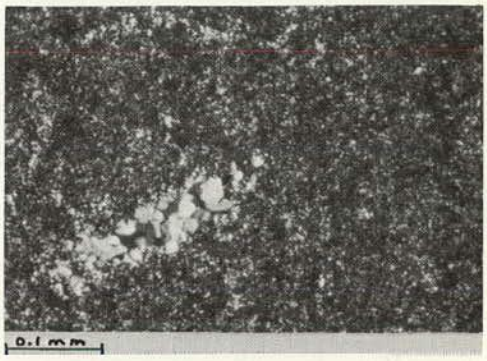

Figure C-9. Aggregate D, >2.5 chert, crossed nicols. Massive chert and lentil of coarser-grained quartz.

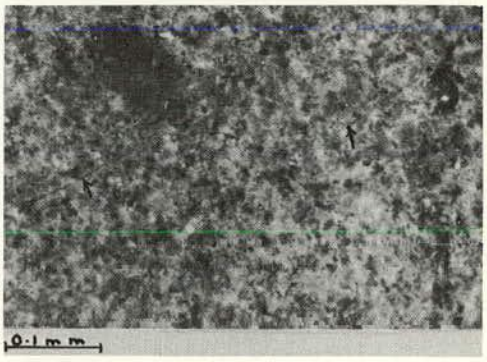

Figure C-10. Aggregate D, <2.5 chert, plain light. Weathered chert with abundant interstitial limonite and limonite-stained fracture (arrows).

Figure C-11. Aggregate E, <2.5 chert, plain light. Note dolomolds in massive chert (darker material is limonite).

Figure C-12. Aggregate E, <2.5 chert, plain light. Dolomolds in chert and chalcedony. Note numerous microfractures in the chalcedony.

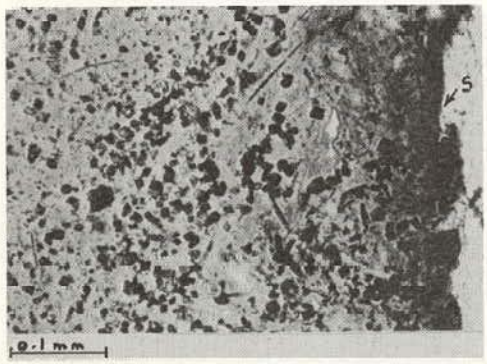

Figure C-13. Aggregate E, <2.5 chert, plain light. Interconnected limonite-filled dolomolds in chert, abundant limonite on surface (S) of particle.

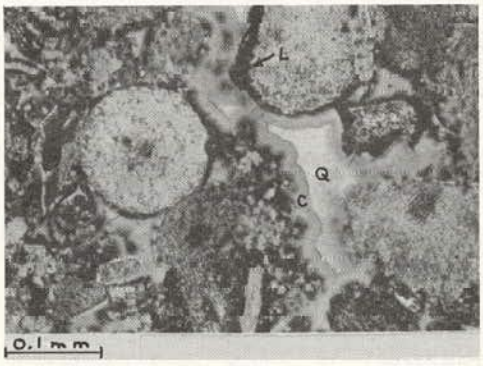

Figure C-14. Aggregate E, >2.5 chert, plain light. Rounded chert fragments in matrix of chalcedony (C), quartz (Q), and limonite (L).

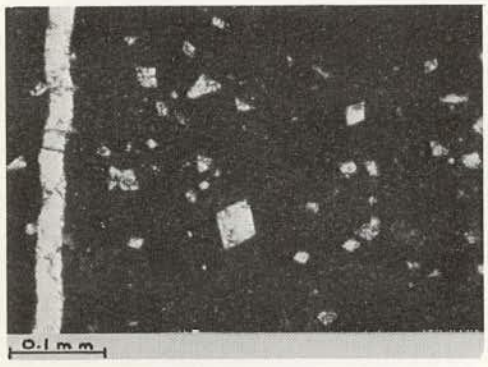

Figure C-15. Aggregate F, >2.5 lithographic limestone, plain light. Note dolomite rhombs and calcite healed fracture in dense, massive limestone.

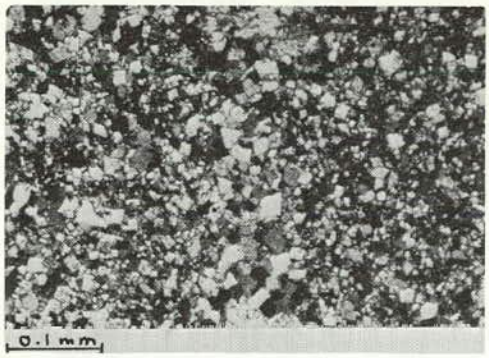

Figure C-16. Aggregate F, >2.5 dolomite, crossed nicols. Dense structure composed of euhedral dolomite and interstitial dolomite and calcite.

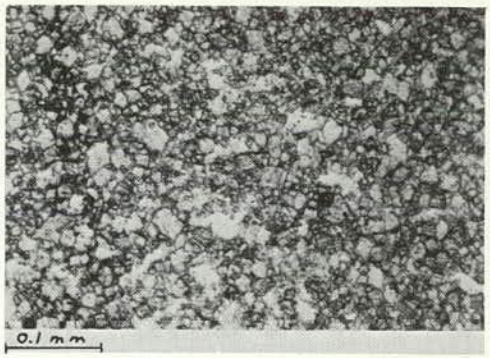

Figure C-17. Aggregate F, >2.5 weathered dolomite, plain light. Note dark interstitial limonite, limonite-stained fracture, and voids (V).

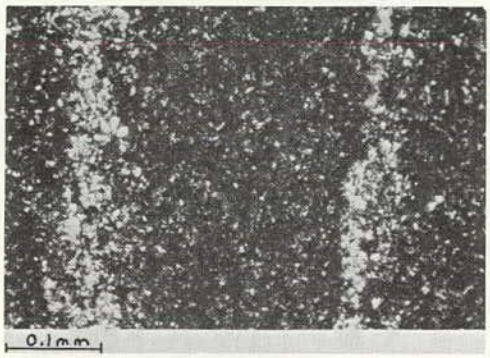

Figure C-18. Aggregate G, <2.5 arenaceous shale, plain light. Note two silt layers in dark carbonaceous shale.

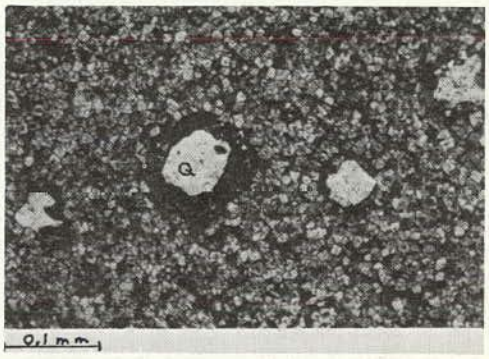

Figure C-19. Aggregate G, <2.5 arenaceous limestone, plain light. Quartz grains (Q) in poorly indurated limestone, abundant limonite in interstices and around quartz grains.

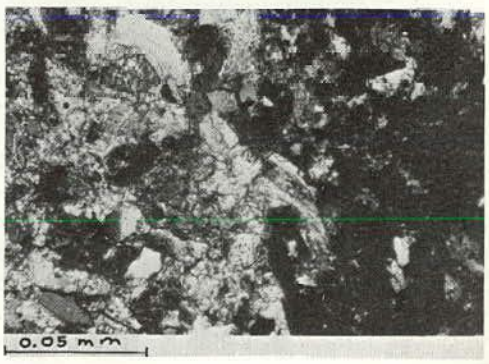

Figure C-20. Aggregate G, <2.5 calcareous sandstone, crossed nicols. At right, typical weathered, limonite-rich material with interstitial voids; at left, relatively fresh material resembling the >2.5 fraction.

and organic material. Limonite-stained and calcite-healed continuous microfractures are fairly abundant in most samples.

Limestone and dolomitic limestone, >2.5 sp gr. Most of this material is similar to the <2.5 sp gr material except for the scarcity or absence of interstitial voids (Fig. C-8). Some samples consist of a very fine-grained dense limestone (average grain size about 0.003 mm diameter) with about 20 percent fossil fragments. Some specimens of this fraction consist of dark circular fossil pellets with calcite cement, and resemble aggregate C.

Chert, >2.5 sp gr. This fraction (Fig. C-9) is an angular, dark yellow-brown to medium-light gray chert composed of faintly laminated to massive microcrystalline quartz (average grain size 0.003 mm diameter). Many samples contain lentils of quartz with an average grain diameter of 0.1 mm. Most samples are weathered and contain as much as 5 percent interstitial limonite. Calcite-healed fractures are common.

Chert, <2.5 sp gr. This fraction (Fig. C-10) is similar to the >2.5 sp gr chert except for the greater abundance of interstitial limonite and limonite-filled voids and fractures, ranging up to 9 percent limonite in some specimens.

Aggregate E: Paducah river gravel, Paducah, Ky.

Chert, <2.5 sp gr. This rock (Figs. C-11, C-12, C-13) is an angular, yellow-brown and white, massive to laminated chert consisting mostly of microcrystalline quartz (average grain size 0.006 mm diameter) and 0 to 20 percent fossil fragments composed of quartz grains with an average diameter of 0.06 mm. Most samples contain banded iron-stained chalcedony, which occurs as irregularly shaped masses up to 1 cm diameter or as interstitial cement, both commonly with quartz overgrowths. Most samples have a smooth weathered coating of limonite and chalcedony-rich chert. All contain 2 to 9 percent dolomolds (average diameter 0.5 mm), most of which are disseminated but commonly occur in continuous layers. Many of these rhomb-shaped cavities are filled or partly filled with limonite. All samples contain numerous microfractures, especially abundant in the chalcedony, which appear to be incipient desiccation fractures. Many of the dolomolds are interconnected by these microfractures.

Chert, >2.5 sp gr. Most of this chert (Fig. C-14) differs from the <2.5 sp gr fraction only in the amount of dolomolds, which never exceeds 2 percent in the >2.5 sp gr chert. Some consists of rounded chert fragments (average diameter 0.6 mm) with 0 to 5 percent silicified fossil fragments and iron-stained chalcedony cement concentrically banded around the chert grains. The chalcedony commonly has quartz overgrowths and is usually separated from the chert grains by a layer of limonite. Incipient microfractures are abundant in the chalcedony.

Miscellaneous, <2.5 sp gr. This fraction consists of minor amounts of extraneous coal, ferruginous sandstone, and siltstone.

Aggregate F: Cedar Valley formation, Rapid and Coralville members, Old Glory Quarry, Iowa

Limestone, dolomitic limestone, dolomite, >2.5 sp gr. This fraction may consist of five subfractions. A sample containing all of these has 12 percent insoluble residue:

(1) Angular, tan, massive to faintly laminated lithographic limestone (Fig. C-15) with an average grain size of about 0.002 mm, containing about 2 percent disseminated dolomite rhombs (average diameter 0.3 mm). Most samples contain some calcite-healed fractures and numerous continuous limonite-stained microfractures.

(2) Angular, tan to olive-brown dolomite (Fig. C-16) composed of euhedral dolomite rhombs (average diameter 0.03 mm), interstitial fine-grained calcite and dolomite, and minor amounts of detrital quartz and interstitial organic material. Some samples are laminated and have abrupt changes in grain size normal to the bedding planes.

(3) Angular, light gray to buff, laminated limestone with a range of grain sizes, changing abruptly across bedding planes, averaging from 0.05 to 1 mm in diameter. This rock has a fairly dense texture and contains minor amounts of detrital quartz, plagioclase, and pyrite.

(4) Angular, medium brown, fossiliferous limestone and dolomitic limestone composed of microcrystalline calcite (average grain size about 0.006 mm diameter), 0 to 20 percent euhedral dolomite up to 0.04 mm diameter, and 0 to 40 percent fossil fragments, many of which have been replaced by massive chalcedony and minor amounts of pyrite. Interstitial grains and lentils of organic material are abundant in some samples.

(5) Angular, tan to medium brown, laminated, weathered dolomite (Fig. C-17) composed of euhedral to subhedral dolomite (average grain size 0.05 mm diameter) and interstitial anhedral dolomite and calcite. This rock contains abundant layered limonite and networks of voids (up to 0.3 mm diameter), which parallel the bedding planes.

Chert, <2.5 sp gr. This rock is an angular medium-gray chert with a dense matrix of microcrystalline quartz and 5 to 15 percent euhedral dolomite having an average grain diameter of 0.05 mm. The matrix contains numerous fossil shells (average diameter 2 to 3 mm) composed of layered chalcedony. That the interior of some shells is filled with quartz over-growths and others are empty accounts for the low density.

Aggregate G: Killins gravel, float gravel from a heavy-medium separation, Killins Gravel Co., Ann Arbor, Mich.

Arenaceous shale, <2.5 sp gr. This fraction (Fig. C-18) is subrounded to rounded, dark gray to brownish-black fissile shale with thin (up to 0.1 mm) interbeds of silt (average grain size about 0.02 mm). All samples contain abundant carbonaceous material, mostly as opaque lamellae parallel to bedding planes. Minor amounts of fine-grained pyrite are disseminated throughout all samples. The clastic constituents are mostly quartz with muscovite, some potassium and sodium feldspars, and minor amounts of

chert fragments. Small interstitial voids are fairly abundant in the silt layers.

Sandstone, calcareous sandstone, arenaceous limestone, >2.5 sp gr. This fraction is a mixture of the following two groups:

(1) Subrounded, medium gray, massive arenaceous limestone composed of anhedral to subhedral calcite (average grain size 0.02 mm) with a minimum of about 1 percent detrital quartz (average grain size 0.01 mm). This rock is poorly indurated and contains up to about 9 percent interstitial limonite, especially abundant surrounding the quartz grains.

(2) Subrounded massive sandstone and calcareous sandstone consisting of quartz and minor amounts of microcline and plagioclase (average grain size 0.02 mm diameter), 0 to 40 percent interstitial calcite, and 0 to 8 percent muscovite and biotite (and chlorite). All samples contain abundant limonite.

Chert, >2.5 sp gr. This rock is a subangular, brown to white, dense, massive chert with abundant fossil fragments (up to 0.8 mm diameter) composed of chalcedony. Most samples contain up to 20 percent dolomite rhombs up to 0.1 mm diameter. Minor amounts of pyrite and 5 to 15 percent limonite occur in all samples. Most of the visible fractures are healed with microcrystalline quartz.

Chert, <2.5 sp gr. This chert is similar to the >2.5 sp gr chert except that it contains numerous limonite-stained voids in the chert and chalcedony, and to a lesser extent in the dolomite.

Quartz monzonite and arkose, >2.5 sp gr. These two fractions were separated together. They consist of the following types, the first being the more abundant:

(1) Subangular, medium gray, medium-grained quartz monzonite consisting of about 40 percent quartz and equal amounts of microcline and sericitized sodic plagioclase with accessory biotite, chlorite, and apatite. The texture is allotriomorphic granular.

(2) Subangular arkose containing 85 percent rounded quartz grains and 15 percent rounded microcline and some albite, both with an average grain size of about 0.2 mm. The cementing material is mostly microcrystalline quartz with some coarser-grained calcite.

Ferruginous sandstone, <2.5 sp gr. This fraction, relatively very minor in quantity, consists of weathered, poorly indurated, porous ferruginous sandstone.

Aggregate H: Gilmore City limestone, Alden Quarry, Iowa

Limestone, >2.5 sp gr. This rock is a subangular light-gray limestone containing about 40 percent rounded calcite fossil plates (average diameter 0.3 to 0.8 mm) with coarser-grained calcite cement. The fossil plates contain abundant opaque organic material.

Limestone, <2.5 sp gr. This fraction resembles the >2.5 sp gr limestone except for the presence of up to 10 percent voids (average diameter 0.07 mm) in the calcite cement. Usually these voids are interconnected and occur in layers.

APPENDIX D
RAPID FREEZE-THAW TESTS

All of the aggregate types used in the Powers-test studies except aggregate G (shale) were incorporated in concrete specimens and subjected to rapid freeze-thaw testing in accordance with ASTM C290-61T. Aggregate G (shale) was excluded because the quantity available was insufficient.

The concrete mixture proportions were the same as for the Powers-test specimens. Three prismatic specimens, 3x3x16 in., were made from each batch. For each specimen, changes in weight and in fundamental longitudinal resonant frequency were determined at frequent intervals. Testing was discontinued after a specimen had completed approximately 300 freeze-thaw cycles or when its relative sonic modulus, as defined in ASTM C290, had decreased to 60 percent.

Table D-1 summarizes the data obtained from the rapid freeze-thaw test.

TABLE D-1

RAPID FREEZE-THAW TEST RESULTS (ASTM C290)

MIXTURE VARIABLE						DURABILITY FACTOR (%)[a]	
AGGREGATE	AIR (%)	SLUMP (IN.)	SPECIMEN NO.	TERMINAL CYCLE	WEIGHT CHANGE (%)	100 CYC.	300 CYC.
A	5.88	2.25	1-5-A	300	−1.03	98.4	96.8
			1-5-B	300	−0.95	96.3	97.4
			1-5-C	300	−1.02	96.3	95.8
B, <2.50 sp gr	8.03	3.50	7-7-A	37	+0.64	21.1	7.0
			7-7-B	19	+0.64	16.0	4.0
			7-7-C	37	+0.73	21.1	7.0
B, >2.50 sp gr	5.88	2.75	7-8-A	192	−0.18	78.3	36.0
			7-8-B	240	−0.56	77.2	27.8
			7-8-C	98	+0.35	56.2	17.2
C	7.16	3	9-2-A	302	−0.11	97.8	99.5
			9-2-B	302	−0.11	95.9	95.4
			9-2-C	302	−0.11	98.9	99.5
D, LS <2.50 sp gr	8.88	3.50	5-3-A	302	−0.72	96.2	81.6
			5-3-B	302	−1.10	96.9	90.6
			5-3-C	302	−0.46	100.0	94.4
D, LS >2.50 sp gr	6.76	3.25	5-4-A	302	−0.62	97.7	94.9
			5-4-B	302	−0.70	96.6	88.8
			5-4-C	302	−0.88	96.6	85.2
D, chert <2.50 sp gr	5.52	2.25	5-10-A	12	+0.44	5.2	1.8
			5-10-B	6	+0.26	3.2	1.0
			5-10-C	6	+0.27	2.9	1.0
E, <2.50 sp gr	5.40	2.75	2-9-A	6	+0.36	2.1	0.7
			2-9-B	6	+0.52	2.3	0.8
			2-9-C	6	+0.45	2.2	0.7
F, >2.50 sp gr	6.47	3.25	5-A	302	−1.21	97.1	90.0
			5-B	302	−1.87	93.5	56.4
			5-C	166	−0.27	86.9	32.4
G, calc. SS + silty LS <2.50 sp gr	5.00	3	8-A	47	+0.36	27.2	9.4
			8-B	71	+0.45	34.4	12.0
			8-C	102	+0.18	50.6	16.8

[a] Based on minimum relative sonic modulus of 60 percent.

APPENDIX E
TEST DATA

TABLE E-1

POROSITY DATA FOR AGGREGATES

AGGREGATE TYPE	SAMPLE NO.	SPECIFIC GRAVITY		ABSORPTION	VOIDS RATIO	VOLUME VOIDS/ BULK VOLUME
		TRUE	APPARENT			
Gilmore City limestone, <2.50	1	2.688	2.564	3.80	0.1470	0.0930
	2	2.674	2.561	4.00	0.1537	0.0929
	3	2.677	2.559	4.04	0.1556	0.0936
	Avg.	2.680			0.1521	0.0932
Gilmore City limestone, >2.50	1	2.689	2.595	2.28	0.1122	0.0558
	2	2.747	2.592	2.16	0.1102	0.0526
	3	2.738	2.585	2.26	0.1158	0.0552
	Avg.	2.725			0.1127	0.0545
Maynes Creek and Eagle City limestone, <2.50	1	2.791	2.654	4.89	0.6259	0.1148
	2	2.780	2.644	4.99	0.6684	0.1165
	3	2.781	2.647	5.03	0.6576	0.1175
	Avg.	2.784			0.6506	0.1163
Maynes Creek and Eagle City limestone, >2.50	1	2.816	2.748	2.25	0.0858	0.0583
	2	2.807	2.727	2.25	0.0936	0.0579
	3	2.808	2.727	2.27	0.0942	0.0582
	Avg.	2.810			0.0912	0.0581
Paducah river gravel, <2.50	1	2.685	2.486	5.32	0.2201	0.1167
	2	2.677	2.473	5.40	0.2280	0.1178
	3	2.675	2.472	5.27	0.2249	0.1153
	Avg.	2.679			0.2243	0.1166
Paducah river gravel, >2.50	1	2.644	2.567	1.29	0.0609	0.0321
	2	2.634	2.575	1.29	0.0577	0.0322
	3	2.629	2.574	1.51	0.0639	0.0375
	Avg.	2.636			0.0608	0.0339
White Marsh gravel, >2.50	1	2.679	2.644	0.25	0.0207	0.0065
	2	2.676	2.646	0.27	0.0204	0.0072
	3	2.687	2.647	0.28	0.0203	0.0074
	Avg.	2.681			0.0205	0.0070
Benner and Snyder limestone, >2.50	1	2.733	2.721	0.23	0.0096	0.0063
	2	2.732	2.721	0.25	0.0101	0.0067
	3	2.724	2.722	0.28	0.0105	0.0075
	Avg.	2.730			0.0101	0.0068
Meramec gravel, <2.50	1	2.783	2.522	3.10	0.1893	0.0725
	2	2.788	2.519	3.24	0.1950	0.0755
	3	2.778	2.533	3.15	0.1864	0.0740
	Avg.	2.783			0.1902	0.0740
Meramec gravel, >2.50	1	2.691	2.606	1.29	0.0681	0.0326
	2	2.703	2.604	1.30	0.0692	0.0328
	3	2.684	2.606	1.26	0.0673	0.0317
	Avg.	2.693			0.0682	0.0324
Rapid and Coralville limestone, >2.50	1	2.903	2.771	3.92	0.1623	0.0980
	2	2.899	2.769	4.03	0.1662	0.1004
	3	2.914	2.773	3.93	0.1617	0.0983
	Avg.	2.905			0.1634	0.0989

TABLE E-2

MORTAR POROSITY DATA

CYLINDER NUMBER	OVENDRY WT, A (G)	WT. VAC. SAT. IN AIR, B (G)	WT. VAC. SAT. IN WATER, C (G)	$W_e = B - A$	$V_p = B - C$	VOIDS RATIO $= \frac{0.99W_e}{V_p - 0.99W_e}$
(a) SOAKED 14 DAYS						
1	1129.1	1308.0	692.9	178.9	615.1	0.4044
2	1099.0	1288.0	675.0	189.0	613.0	0.4393
3	1147.9	1322.1	704.2	174.2	617.9	0.3872
Avg.						0.4103
(b) SOAKED 76 DAYS						
1	1129.1	1315.0	702.2	185.9	612.8	0.4292
2	1099.0	1295.7	683.9	196.9	612.0	0.4674
3	1147.9	1328.5	713.5	180.6	615.0	0.4100
Avg.						0.4355

TABLE E-3

PERMEABILITY RESULTS

AGGREGATE	LEAST SQUARES PERMEABILITY (DARCYS)	NO. DATA POINTS	95 PERCENT CONFIDENCE RANGE (DARCYS)	CORRELATION COEFFICIENT	PROBABILITY OF CORRELATION (%)	PRESSURE RANGE (PSI)
Gilmore City limestone, <2.50						
No. 2 Test 1	4.664×10^{-4}	10	4.788×10^{-4} to 4.539×10^{-4}	0.9951	99.9 or more	15-65
No. 3A Test 1, 3	2.888×10^{-3}	15	4.313×10^{-3} to 1.463×10^{-3}	0.9981	99.9 or more	15-50
No. 3B Test 1	2.926×10^{-3}	11	3.853×10^{-3} to 1.998×10^{-3}	0.9915	99.9 or more	30-50
No. 4 Test 1	1.908×10^{-4}	9	1.984×10^{-4} to 1.831×10^{-4}	0.9899	99.9 or more	51-70
No. 6A Test 1	4.551×10^{-4}	11	4.740×10^{-4} to 4.363×10^{-4}	0.9923	99.9 or more	40-59
No. 6B Test 1	2.906×10^{-4}	7	3.169×10^{-4} to 2.643×10^{-4}	0.9933	99.9 or more	48-60
Avg.	1.202×10^{-3}					
Gilmore City limestone, >2.50						
No. 1A Test 1, 2, 3	1.941×10^{-3}	30	2.049×10^{-3} to 1.833×10^{-3}	0.8730	99.9 or more	15-72
No. 1B Test 1, 2	3.970×10^{-4}	25	4.071×10^{-4} to 3.869×10^{-4}	0.9724	99.9 or more	5-71
No. 2 Test 1	3.105×10^{-5}	11	3.485×10^{-5} to 2.725×10^{-5}	0.9741	99.9 or more	15-65
No. 4 Test 1	3.183×10^{-4}	11	3.402×10^{-4} to 2.963×10^{-4}	0.9656	99.9 or more	50-70
No. 5 Test 1	3.774×10^{-4}	11	3.869×10^{-4} to 3.680×10^{-4}	0.9959	99.9 or more	15-65
No. 6 Test 1	1.819×10^{-4}	11	1.907×10^{-4} to 1.731×10^{-4}	0.9626	99.9 or more	50-70
Avg.	5.411×10^{-4}					
Maynes Creek and Eagle City limestone, <2.50						
No. 1 Test 1, 2, 3	2.861×10^{-3}	35	3.021×10^{-3} to 2.741×10^{-3}	0.6003	99.9 or more	25-70
No. 2 Test 4	1.089×10^{-3}	12	1.150×10^{-3} to 1.028×10^{-3}	0.9371	99.9 or more	35-86
No. 3 Test 1	4.866×10^{-4}	11	4.952×10^{-4} to 4.780×10^{-4}	0.9960	99.9 or more	15-65
No. 4 Test 1	5.126×10^{-4}	12	5.259×10^{-4} to 4.993×10^{-4}	0.9922	99.9 or more	10-65
No. 5 Test 1	3.065×10^{-5}	12	3.201×10^{-5} to 2.929×10^{-5}	0.9945	99.9 or more	15-66
No. 6 Test 1, 2, 3[a]	-5.659×10^{-7}	18	-2.656×10^{-7} to -8.662×10^{-7}	0.8999	99.9 or more	54-86
No. 7 Test 1	2.600×10^{-4}	12	2.740×10^{-4} to 2.459×10^{-4}	0.9971	99.9 or more	25-66
Avg.	8.767×10^{-4}					
Maynes Creek and Eagle City limestone, >2.50						
No. 1 Test 5	8.814×10^{-4}	14	9.000×10^{-4} to 8.628×10^{-4}	0.9905	99.9 or more	10-71
No. 2 Test 1	7.952×10^{-6}	10	9.314×10^{-6} to 6.590×10^{-6}	0.9743	99.9 or more	50-70
No. 3 Test 1	7.755×10^{-4}	10	8.190×10^{-4} to 7.320×10^{-4}	0.9687	99.9 or more	30-50
No. 4 Test 1, 2[b]	1.956×10^{-7}	20	4.853×10^{-7} to 9.416×10^{-8}	0.3272	Less than 90.0	48-87
No. 6 Test 1, 2	3.507×10^{-3}	22	3.694×10^{-3} to 3.321×10^{-3}	0.8713	99.9 or more	25-86
No. 7 Test 1	4.954×10^{-4}	11	5.010×10^{-4} to 4.898×10^{-4}	0.9988	99.9 or more	16-65
Avg.	1.134×10^{-3}					

TABLE E-3—*Continued*

AGGREGATE	LEAST SQUARES PERMEABILITY (DARCYS)	NO. DATA POINTS	95 PERCENT CONFIDENCE RANGE (DARCYS)	CORRELATION COEFFICIENT	PROBABILITY OF CORRELATION (%)	PRESSURE RANGE (PSI)
Paducah river gravel, <2.50						
No. 1 Test 1	2.183×10^{-6}	10	2.863×10^{-6} to 1.504×10^{-6}	0.9648	99.9 or more	30-67
No. 2 Test 2	3.053×10^{-5}	13	3.272×10^{-6} to 2.835×10^{-5}	0.9897	99.9 or more	6-66
No. 3 Test 1, 2, 3	2.814×10^{-8}	17	2.140×10^{-7} to -1.577×10^{-7}	0.5487	95.0 or more	54-87
No. 4 Test 3[a]	-4.633×10^{-4}	9	-2.346×10^{-4} to -6.920×10^{-4}	0.9983	99.9 or more	36-76
No. 5 Test 1	5.159×10^{-6}	10	6.143×10^{-6} to 4.175×10^{-6}	0.9969	99.9 or more	50-69
No. 6 Test 1	3.396×10^{-9}	12	3.725×10^{-7} to -3.657×10^{-7}	0.9927	99.9 or more	10-65
Avg.	7.581×10^{-6}					
Paducah river gravel, >2.50						
No. 1 Test 3[a]	-2.586×10^{-7}	8	-1.318×10^{-7} to -3.853×10^{-7}	0.9485	99.9 or more	58-87
No. 3 Test 3[a]	-1.038×10^{-7}	10	1.063×10^{-8} to -2.183×10^{-7}	0.9003	99.9 or more	50-86
No. 5 Test 3	2.441×10^{-6}	12	3.010×10^{-6} to 1.872×10^{-6}	0.9714	99.9 or more	10-65
No. 6 Test 3	3.446×10^{-9}	10	8.201×10^{-8} to -7.511×10^{-8}	0.9703	99.9 or more	50-86
Avg.	1.222×10^{-6}					
White Marsh gravel, >2.50						
No. 1 Test 1, 2[a]	-4.673×10^{-8}	22	1.425×10^{-7} to -2.360×10^{-7}	0.5447	99.0 or more	25-85
No. 2 Test 2	7.802×10^{-4}	11	8.785×10^{-4} to 6.819×10^{-4}	0.7173	98.0 or more	21-70
No. 3 Test 1	Beyond limits of apparatus.					
No. 4 Test 1	5.455×10^{-5}	12	5.894×10^{-5} to 5.012×10^{-5}	0.9776	99.9 or more	34-54
No. 5 Test 1, 2[a]	5.347×10^{-7}	23	6.412×10^{-7} to 4.282×10^{-7}	−0.2346	Less than 90.0	30-87
No. 6 Test 3	9.928×10^{-7}	11	1.460×10^{-6} to 5.256×10^{-7}	0.8663	99.9 or more	15-65
Avg.	2.786×10^{-4}					
Benner and Snyder limestone, >2.50						
No. 2B Test 1	Beyond limits of apparatus.					
No. 5 Test 1[a]	-1.939×10^{-7}	10	-1.235×10^{-7} to -2.644×10^{-7}	0.9713	99.9 or more	49-86
No. 6 Test 1	Beyond limits of apparatus.					
Meramec gravel, <2.50						
No. 1 Test 4[a]	-4.728×10^{-8}	16	1.472×10^{-7} to -2.417×10^{-7}	0.9921	99.9 or more	11-86
No. 4 Test 4	4.829×10^{-7}	17	6.679×10^{-7} to 2.978×10^{-7}	0.9979	99.9 or more	6-87
No. 5 Test 1	5.443×10^{-4}	13	6.743×10^{-4} to 4.144×10^{-4}	0.9945	99.9 or more	5-65
No. 6 Test 1	9.310×10^{-7}	10	1.272×10^{-6} to 5.894×10^{-7}	0.9966	99.9 or more	21-65
No. 8 Test 2[a]	-4.333×10^{-7}	8	-3.469×10^{-7} to -5.196×10^{-7}	0.9926	99.9 or more	58-86
No. 9 Test 3[a]	-9.637×10^{-8}	9	1.523×10^{-7} to -3.451×10^{-7}	0.8854	99.0 or more	55-76
Avg.	1.819×10^{-4}					
Meramec gravel, >2.50						
No. 2 Test 1	8.751×10^{-5}	9	9.335×10^{-5} to 8.166×10^{-5}	0.9260	99.9 or more	20-60
No. 4 Test 1, 2, 3[a]	-1.931×10^{-7}	20	-4.209×10^{-8} to -3.440×10^{-7}	0.9617	99.9 or more	41-85
No. 5 Test 3[a]	-3.120×10^{-7}	10	-2.299×10^{-7} to -3.941×10^{-7}	0.9851	99.9 or more	51-86
No. 7 Test 4	1.911×10^{-7}	11	2.497×10^{-7} to 1.326×10^{-7}	0.9994	99.9 or more	34-85
No. 8 Test 1, 2, 3[a]	-3.256×10^{-7}	13	-2.296×10^{-7} to -4.215×10^{-7}	0.9683	99.9 or more	50-86
Avg.	4.385×10^{-5}					
Rapid and Coralville limestone, >2.50						
No. 1 Test 3	9.138×10^{-7}	12	1.323×10^{-6} to 5.043×10^{-7}	0.9965	99.9 or more	10-65
No. 2 Test 3	2.450×10^{-6}	13	3.264×10^{-6} to 1.637×10^{-6}	0.9933	99.9 or more	5-65
No. 3 Test 3	5.563×10^{-6}	12	6.548×10^{-6} to 4.578×10^{-6}	0.9930	99.9 or more	10-65
No. 4 Test 3	6.167×10^{-6}	12	7.436×10^{-6} to 4.898×10^{-6}	0.9892	99.9 or more	10-65
No. 5 Test 1	6.127×10^{-5}	10	6.360×10^{-5} to 5.894×10^{-5}	0.9986	99.9 or more	20-65
No. 6 Test 1	1.416×10^{-4}	10	1.508×10^{-4} to 1.325×10^{-4}	0.9914	99.9 or more	20-66
Avg.	3.633×10^{-5}					

[a] Negative results, not included in average.
[b] Single calcite crystal, not included in average.

TABLE E-4

SUMMARY OF AGGREGATE PARTICLE EXPANSION DATA

AGGREGATE	PERM. LENGTH CHANGE (μIN.)		WATER (%)		DILATION (μIN.)
	DIAL GAGE	TRANSDUCER	BEFORE F-T	AFTER F-T	
F, >2.50 sp gr	940	520	2.741	2.772	1330
	420	280	2.488	2.488	1105
	1080	620	2.766	2.794	1430
	640	270	4.097	4.068	1110
	1630	1380	4.842	4.871	2480
	580	110	2.924	3.010	770
E, >2.50 sp gr	—380	—30	2.168	2.229	140
	—150	—50	0.529	0.500	150
	—300	—130	1.805	1.837	0
	—210	—130	0.211	0.211	0
	—290	—140	2.125	2.183	50
	—280	—60	1.657	1.690	40
B, <2.50 sp gr	1800	1720	3.882	4.093	2360
	680	320	4.466	4.536	1060
	460	280	2.860	2.919	910
	520	330	5.502	5.502	1000
	890	490	4.630	4.665	1130
	460	140	2.895	2.858	850
H, <2.50 sp gr	390	910	3.879	3.837	1600
	980	270	5.217	5.247	900
	670	600	3.230	3.317	1550
	390	570	3.650	3.704	950
	290	—230	3.920	3.805	1580
	760	500	4.023	4.023	1050
H, >2.50 sp gr	220	190	3.052	3.027	530
	520	80	3.013	3.013	490
	50	160	2.395	2.476	560
	—110	180	1.128	1.160	490
	130	240	3.571	3.498	950
	—70	60	2.471	2.594	550
E, <2.50 sp gr	—450	720	8.399	8.202	920
	40	—90	1.961	1.961	70
	10	—70	5.816	5.694	220
	220	—140	2.358	2.389	80
	—370	—160	8.093	8.162	120
	—	—120	3.611	3.548	290
G, shale	1550	1540	7.162	7.292	2370
	1580	1060	7.630	7.674	1890
	1650	1390	6.663	6.727	2210
	1370	1120	6.926	6.985	2040
	540	1190	7.172	7.243	2160
	1030	890	6.694	6.767	1820
A	—70	0	0.462	0.446	220
	—170	—40	0.299	0.329	260
	—20	—120	0.156	0.156	40
	—220	—80	0.147	0.189	90
	—100	—80	0.209	0.261	90
	20	—140	0.232	0.255	40
B, >2.50 sp gr	190	200	1.718	1.718	960
	280	40	1.711	1.805	460
	100	—70	2.543	2.676	260
	—140	—70	1.096	1.238	140
	—100	—70	1.775	1.960	130
	0	—	1.974	1.900	80

TABLE E-4—*Continued*

AGGREGATE	PERM. LENGTH CHANGE (μIN.) DIAL GAGE	PERM. LENGTH CHANGE (μIN.) TRANSDUCER	WATER (%) BEFORE F-T	WATER (%) AFTER F-T	DILATION (μIN.)
D, >2.50 sp gr	70	20	1.278	1.156	290
	120	50	1.721	1.721	610
	—120	200	2.246	2.055	510
	550	200	1.791	1.875	1080
	210	120	3.172	3.144	390
	—50	—20	1.268	1.101	430
D, <2.5 sp gr	100	140	4.836	4.614	590
	800	360	5.201	5.170	950
	360	190	4.350	4.310	890
	290	120	3.944	3.908	930
	70	110	4.273	4.140	710
	150	50	4.168	4.014	550
G, calc. SS and silty LS	330	450	4.732	4.698	830
	150	400	5.415	5.312	1050
	—230	—260	5.396	5.439	720
	50	90	5.471	5.403	230
	330	190	3.813	3.781	590
	400	440	4.443	4.443	830
E, >2.5 sp gr	180	—30	0.806	0.849	160
	70	—80	1.896	1.783	90
	700	—140	0.701	0.668	20
E, 2.45-2.50 sp gr	25	—100	1.575	1.627	0
	100	—60	2.212	2.320	90
	300	—110	3.189	3.189	350
E, 2.40-2.45 sp gr	—130	60	2.295	2.359	170
	30	—30	3.374	3.374	240
	—100	—20	3.303	3.336	30
E, <2.40 sp gr	1400	2180	5.483	5.483	2700
	2370	2000	8.149	8.307	2500
	50	20	5.293	5.444	610
B, 2.45-2.50 sp gr	220	250	2.969	2.969	670
	240	290	2.575	2.605	920
	230	200	2.221	2.221	420
B, 2.40-2.45 sp gr	430	570	3.284	3.323	1170
	810	910	4.194	4.224	1580
	20	10	3.320	3.320	320
B, <2.40 sp gr	290	120	4.673	4.523	360
	180	460	4.862	4.819	1420
	250	150	4.033	4.033	710
H, 2.45-2.50 sp gr	—100	380	4.181	4.181	820
	—50	30	3.002	2.974	510
	—70	—10	3.947	4.008	480
H, 2.40-2.45 sp gr	30	220	4.740	4.619	620
	150	350	7.813	7.813	560
H, <2.40 sp gr	150	350	7.813	7.813	560
	530	710	5.607	5.607	910
C	180	—30	0.133	0.107	30
	20	—50	0.198	0.198	0
	—40	—80	0.217	0.163	30

TABLE E-5

POWERS TEST RESULTS, PHASE I

AGG. TYPE	SPEC. SIZE (IN.)	MIX NO.	SPEC. NO.	F-T CYCLES	CYCLES HELD AT LOW TEMP.	TOTAL DILATION LAST CYCLE (μIN.)	R. F. LOSS (%)	AIR (%)	SPACING FACTOR (IN.)	LENGTH CHANGE (μIN.)
A	3 x 6	1	1	8	—	120	Gain	6.3	0.00358	+1400
			2	8	—	135	Gain	6.1	0.00346	[a]
			3	8	—	90	0	6.9	0.00283	[a]
	4 x 8	1	1	8	—	60	Gain	5.3	0.00323	+1220
			2	8	—	230	0	6.1	0.00395	[a]
			3	8	—	100	Gain	5.5	0.00314	+1500
	3 x 6	1	4	8	3	200	Gain	6.2	0.00353	[a]
			5	8	3	340	Gain	5.4	0.00337	+2950
			6	8	3	440	Gain	6.8	0.00313	[a]
	4 x 8	1	4	8	3	220	Gain	7.1	0.00308	[a]
			5	8	3	160	1.0	8.5	0.00361	[a]
			6	8	3	95	Gain	5.6	0.00349	[a]
	3 x 6	2	1	8	—	140	Gain	7.5	0.00324	—110
			2	8	—	290	Gain	6.1	0.00309	[a]
			3	8	—	115	Gain	5.5	0.00322	+1750
	4 x 8	2	1	8	—	160	Gain	7.9	0.00266	[a]
			2	8	—	70	0	6.8	0.00423	+620
			3	8	—	120	Gain	5.5	0.00382	+250
	3 x 6	2	4	8	4	130	0.8	6.1	0.00329	+2680
			5	8	4	140	14.0	6.4	0.00345	+950
			6	8	4	100	16.6	6.1	0.00316	+300
	4 x 8	2	4	8	4	160	Gain	6.7	0.00357	+3550
			5	8	4	100	Gain	8.4	0.00361	[a]
			6	8	4	90	Gain	7.4	0.00331	[a]
E	3 x 6	1	1	6	—	1180	42.6	5.7	0.00512	+2200
			2	4	—	2550	42.4	3.5	0.00626	+2700
			3	4	—	1200	43.7	5.5	0.00458	+1090
	4 x 8	1	1	2	—	2430	Gain	5.2	0.00426	+2590
			2	2	—	3150	1.0	3.8	0.00492	+2210
			3	4	—	6200	54.0	3.5	0.00528	+7400
	3 x 6	1	4	8	3	200	37.5	4.4	0.00502	[a]
			5	6	3	1170	38.5	6.8	0.00556	[a]
			6	4	1	3000	69.3	7.7	0.00543	+6420
	4 x 8	1	4	4	1	4750	51.5	4.7	0.00461	+5950
			5	4	1	3480	55.0	3.9	0.00488	+4100
			6	5	2	3380	46.0	5.7	0.00543	[a]
	3 x 6	2	1	8	—	180	39.8	5.7	0.00388	—730
			2	8	—	220	34.4	7.7	0.00393	—400
			3	8	—	185	36.1	6.5	0.00415	—90
	4 x 8	2	1	8	—	535	0	5.0	0.00318	+20
			2	8	—	540	Gain	5.4	0.00375	—120
			3	8	—	210	Gain	6.3	0.00334	—1100
	3 x 6	2	4	8	4	160	39.2	7.7	0.00355	—590
			5	8	4	340	37.7	7.2	0.00375	—1550
			6	8	4	110	40.0	7.3	0.00439	—50
	4 x 8	2	4	2	2	3000	Gain	5.7	0.00271	+1550
			5	8	4	3480	18.9	7.2	0.00305	+3100
			6	8	4	200	Gain	8.5	0.00253	+150
D-1	3 x 6	1	1	8	—	140	Gain	7.8	0.00345	—1800
			2	8	—	110	Gain	8.4	0.00376	—1440
			3	8	—	110	Gain	7.7	0.00452	+1100
	4 x 8	1	1	8	—	130	Gain	6.3	0.00343	+350
			2	8	—	60	Gain	6.9	0.00367	+850
			3	8	—	125	Gain	6.5	0.00390	—500
	3 x 6	1	4	8	4	70	Gain	7.8	0.00374	0
			5	8	4	80	Gain	7.6	0.00373	—240
			6	8	4	80	Gain	6.3	0.00501	+560
	4 x 8	1	4	8	4	100	Gain	8.6	0.00384	—200
			5	8	4	150	Gain	6.4	0.00336	—280
			6	8	4	50	Gain	7.2	0.00315	+350
	3 x 6	2	1	8	—	150	Gain	6.5	0.00357	—700
			2	8	—	140	Gain	8.3	0.00353	[a]
			3	8	—	130	Gain	6.4	0.00315	+750
	4 x 8	2	1	8	—	110	Gain	5.5	0.00319	+390
			2	8	—	140	Gain	4.9	0.00405	+890
			3	8	—	130	Gain	6.3	0.00352	+4080
	3 x 6	2	4	8	4	110	Gain	6.9	0.00330	+730
			5	8	4	100	Gain	7.1	0.00308	—100
			6	8	4	280	0	9.3	0.00310	+1430
	4 x 8	2	4	8	4	120	Gain	8.1	0.00273	+120
			5	8	4	120	Gain	6.0	0.00336	—20
			6	8	4	115	Gain	7.0	0.00352	+700

[a] Faulty gage point.

TABLE E-6

POWERS TEST RESULTS, PHASE II

AGG. TYPE	SPEC. NO.	CURING PROC.	F-T CYCLES	WEIGHT CHANGE (G)	R. F. LOSS (%)	TOTAL DILATION LAST CYCLE (μIN.)	LENGTH CHANGE (μIN.)
C	1	Dried	8	+3.3	Gain	50	−30
	2	Dried	8	+3.1	Gain	140	−310
	3	Dried	8	+3.4	Gain	135	−610
	4	ND.	8	+3.4	1.2	230	−270
	5	ND.	8	+4.3	1.8	240	−300
	6	ND.	8	+4.2	0	515	−90
D-2	1	Dried	8	+4.7	6.8	370	+2160
	2	Dried	8	+5.0	0.6	60	−14940
	3	Dried	8	+5.0	0.6	220	+520
	4	ND.	8	+4.6	0	450	+790
	5	ND.	8	+5.2	5.5	1860	+3060
	6	ND.	8	+6.1	4.2	1040	+2060
F	1	Dried	8	+4.5	Gain	290	−570
	2	Dried	8	+4.7	Gain	250	+720
	3	Dried	8	+5.2	1.3	140	−230
	4	ND.	8	+4.8	0	1370	−2750
	5	ND.	8	+5.1	Gain	490	−3950
	6	ND.	8	+5.6	2.0	970	+620
E	1	Dried	1	+0.3	0	110	+90
	2	Dried	5	+4.6	1.9	100	−2780
	3	Dried	4	+4.8	0.6	140	−150
	4	Dried	6	+5.4	Gain	140	−90
	5	Dried	2	+1.9	Gain	120	−1010
	6	Dried	3	+3.3	Gain	165	−90
B-2	1	Dried	8	+3.8	Gain	70	+280
	2	Dried	8	+4.9	Gain	120	−5710
	3	Dried	8	+3.8	Gain	380	+2300
	4	ND.	8	+7.6	11.6	1150	+2520
	5	ND.	8	+6.4	11.0	700	+910
	6	ND.	8	+7.2	10.4	2120	+1720
E-100%	1	Dried	8	+10.7	60.1	3390	+5020
	2	Dried	7	+8.2	57.9	3100	+2990
	3	Dried	7	+10.2	57.2	3600	+4220
	4	ND.	2	+8.5	57.7	17360	+9010
	5	ND.	2	+8.3	56.6	16630	+8750
	6	ND.	2	+9.1	60.3	11240	+2520
B-1	1	Dried	8	+4.8	2.4	140	+110
	2	Dried	8	+5.1	12.7	1165	−1530
	3	Dried	8	+8.7	0.6	225	[a]
	4	ND.	6	+6.2	61.3	5340	+5600
	5	ND.	8	+6.5	16.5	1410	+3790
	6	ND.	8	+7.6	19.5	4760	+5430
G-1	1	Dried	8	+6.2	Gain	115	+980
	2	Dried	8	+6.3	Gain	65	−260
	3	Dried	8	+6.0	Gain	180	+210
	4	ND.	6	+8.5	19.2	4700	+4950
	5	ND.	7	+7.1	50.0	3220	+3270
	6	ND.	8	+7.0	13.8	3170	+4180
G-2	1	Dried	8	+4.9	2.1	480	+420
	2	Dried	8	+4.5	Gain	340	+300
	3	Dried	8	+5.1	0.7	380	+950
	4	ND.	8	+6.5	56.8	3050	+5080
	5	ND.	8	+5.7	53.2	3740	+6310
	6	ND.	8	+6.0	13.1	2460	+3640

[a] Faulty gage point.

TABLE E-7

CHEMICAL ANALYSES OF CEMENTS

TEST	CEMENT A	CEMENT B	CEMENT C	TEST CEMENT[a]
Physical:				
Setting time, Vicat	—	2:10	2:30	2:30
Fineness, 325 mesh	94.9	91.7	98.4	—
Autoclave expansion (%)	0.142	0.039	0.168	0.068
Flow	—	—	110	107
Compr. strength (psi):				
1 day	1518	1300	1650	—
3 days	—	2700	3580	—
7 days	—	3883	5220	4350
28 days	—	6000	7210	6642
Air (%)	7.96	—	8.5	10.9
Chemical (%):				
SiO_2	22.2	21.6	21.0	21.6
Al_2O_3	4.7	6.0	5.3	5.0
Fe_2O_3	2.1	3.5	2.4	2.8
CaO	64.1	64.6	64.0	64.1
MgO	3.4	1.0	3.6	2.4
SO_3	2.2	2.1	2.6	2.4
C_3S	—	48.0	54.0	52.3
C_2S	—	9.9	19.0	22.4
C_3A	—	—	10.0	8.5
C_4AF	—	—	7.0	8.5
K_2O	0.64	—	0.39	—
Na_2O	0.09	—	0.01	—
Alkali, as Na_2O	0.51	0.39	0.27	—
Ignition loss	0.97	1.00	1.00	1.45

[a] A composite of 2 parts cement B, 2 parts cement C, 1 part cement A.

TABLE E-8

PROPERTIES OF FINE AGGREGATE

PROPERTY	SAMPLE 1	SAMPLE 2	SAMPLE 3	AVG.
Passing (%):				
3/8 In.	100.0	100.0	100.0	100.0
No. 4	96.0	96.6	95.7	96.1
No. 8	77.9	79.6	78.6	78.7
No. 16	65.0	66.6	66.0	65.9
No. 30	48.0	49.2	48.7	48.6
No. 50	20.7	20.6	20.5	20.6
No. 100	3.2	2.9	2.9	3.0
No. 200	1.1	1.0	1.0	1.0
Spec. gravity:				
Bulk, SSD	2.634	2.629	—	2.632
Apparent	2.639	2.635	—	2.637
Absorption (%)	0.10	0.14	—	0.12
Fineness mod.	2.87	2.83	2.87	2.86

Previously published reports of the

NATIONAL COOPERATIVE HIGHWAY RESEARCH PROGRAM

are available from:

Highway Research Board
National Academy of Sciences
2101 Constitution Avenue
Washington, D.C. 20418

Inquiries concerning prices and quantity purchases should be directed to this address.

NCHRP Report No.	*Title*
—*	A Critical Review of Literature Treating Methods of Identifying Aggregates Subject to Destructive Volume Change When Frozen in Concrete and a Proposed Program of Research—Intermediate Report 81 pp. $1.80
1	Evaluation of Methods of Replacement of Deteriorated Concrete in Structures 56 pp. $2.80
2	An Introduction to Guidelines for Satellite Studies of Pavement Performance 19 pp. $1.80
2A	Guidelines for Satellite Studies of Pavement Performance 85 pp. + 9 figs., 26 tables, 4 app. $3.00
3	Improved Criteria for Traffic Signals at Individual Intersections—Interim Report 36 pp. $1.60
4	Non-Chemical Methods of Snow and Ice Control on Highway Structures 74 pp. $3.20
5	Effects of Different Methods of Stockpiling Aggregates—Interim Report 48 pp. $2.00
6	Means of Locating and Communicating with Disabled Vehicles—Interim Report 56 pp. $3.20
7	Comparison of Different Methods of Measuring Pavement—Interim Report 29 pp. $1.80
8	Synthetic Aggregates for Highway Construction 13 pp. $1.00
9	Traffic Surveillance and Means of Communicating with Drivers—Interim Report 28 pp. $1.60
10	Theoretical Analysis of Structural Behavior of Road Test Flexible Pavements 31 pp. $2.80
11	Effect of Control Devices on Traffic Operations—Interim Report 107 pp. $5.80
12	Identification of Aggregates Causing Poor Concrete Performance When Frozen—Interim Report 47 pp. $3.00
13	Running Cost of Motor Vehicles as Affected by Highway Design—Interim Report 43 pp. $2.80
14	Density and Moisture Content Measurements by Nuclear Methods—Interim Report 32 pp. $3.00
15	Identification of Concrete Aggregates Exhibiting Frost Susceptibility—Interim Report 66 pp. $4.00

* Highway Research Board Special Report 80.

THE NATIONAL ACADEMY OF SCIENCES — NATIONAL RESEARCH COUNCIL is a private, nonprofit organization of scientists, dedicated to the furtherance of science and to its use for the general welfare. The Academy itself was established in 1863 under a congressional charter signed by President Lincoln. Empowered to provide for all activities appropriate to academies of science, it was also required by its charter to act as an adviser to the federal government in scientific matters. This provision accounts for the close ties that have always existed between the Academy and the government, although the Academy is not a governmental agency.

The National Research Council was established by the Academy in 1916, at the request of President Wilson, to enable scientists generally to associate their efforts with those of the limited membership of the Academy in service to the nation, to society, and to science at home and abroad. Members of the National Research Council receive their appointments from the president of the Academy. They include representatives nominated by the major scientific and technical societies, representatives of the federal government, and a number of members at large. In addition, several thousand scientists and engineers take part in the activities of the research council through membership on its various boards and committees.

Receiving funds from both public and private sources, by contribution, grant, or contract, the Academy and its Research Council thus work to stimulate research and its applications, to survey the broad possibilities of science, to promote effective utilization of the scientific and technical resources of the country, to serve the government, and to further the general interests of science.

The Highway Research Board was organized November 11, 1920, as an agency of the Division of Engineering and Industrial Research, one of the eight functional divisions of the National Research Council. The Board is a cooperative organization of the highway technologists of America operating under the auspices of the Academy-Council and with the support of the several highway departments, the Bureau of Public Roads, and many other organizations interested in the development of highway transportation. The purposes of the Board are to encourage research and to provide a national clearinghouse and correlation service for research activities and information on highway administration and technology.